

# UC San Diego

## UC San Diego Electronic Theses and Dissertations

### Title

Strongly correlated electron behavior in As-based and thin film Sb-based filled skutterudites

### Permalink

<https://escholarship.org/uc/item/0tm2q66r>

### Author

Baumbach, Ryan Eagle

### Publication Date

2009

Peer reviewed|Thesis/dissertation

UNIVERSITY OF CALIFORNIA, SAN DIEGO

Strongly correlated electron behavior in As-based and thin film Sb-based filled  
skutterudites

A dissertation submitted in partial satisfaction of the  
requirements for the degree Doctor of Philosophy  
in  
Physics

by

Ryan Eagle Baumbach

Committee in charge:

Professor M. Brian Maple, Chair  
Professor Michael M. Fogler  
Professor Sungho Jin  
Professor Clifford Kubiak  
Professor Sunil Sinha

2009

Copyright  
Ryan Eagle Baumbach, 2009  
All rights reserved.

The dissertation of Ryan Eagle Baumbach is approved,  
and it is acceptable in quality and form for publication  
on microfilm:

---

---

---

---

---

---

Chair

University of California, San Diego

2009

For her nearly inexhaustible support, understanding, and grace during a particularly difficult year, this dissertation is dedicated to my loving wife, Amber.

I was also inspired by the resilience and inscrutable joy which my daughter expressed every day, even under difficult circumstances. Thank you Madeleine.

*317 is a prime, not because we think so,  
or because our minds are shaped in one way rather than another,  
but because it is so,  
because mathematical reality is built that way.*

– Godfrey Hardy

*Even if you're on the right track,  
you'll get run over if you just sit there.*

– Will Rogers

*We have a lot of fish to fry.*

– M. Brian Maple

*If we knew what it was we were doing,  
it would not be called research, would it?*

– Albert Einstein

## TABLE OF CONTENTS

	Signature Page . . . . .	iii
	Dedication . . . . .	iv
	Epigraph . . . . .	v
	Table of Contents . . . . .	vi
	List of Figures . . . . .	viii
	List of Tables . . . . .	xii
	Acknowledgements . . . . .	xiii
	Vita, Publications, and Fields of Study . . . . .	xvi
	Abstract . . . . .	xix
I	Introduction . . . . .	1
	A. Correlated electron behavior . . . . .	1
	1. Fermi Liquid . . . . .	1
	2. Magnetic $d$ - and $f$ - electron ions . . . . .	3
	3. Dilute $d$ - and $f$ -electron ions in a Fermi sea . . . . .	5
	4. Concentrated $d$ - and $f$ -electron ions in a Fermi sea . . . . .	10
	5. Quantum criticality . . . . .	14
	B. Filled skutterudites . . . . .	16
	1. Ce-based filled skutterudites . . . . .	17
	2. CeRu <sub>4</sub> As <sub>12</sub> . . . . .	19
	3. CeOs <sub>4</sub> As <sub>12</sub> . . . . .	20
	C. Thin film filled skutterudites . . . . .	22
	D. Concluding remarks . . . . .	23
	Bibliography . . . . .	29
II	Sample Preparation . . . . .	36
	A. Flux growth of As-based filled skutterudites . . . . .	36
	B. Pulsed laser deposition of filled skutterudites . . . . .	40
	1. PrFe <sub>4</sub> Sb <sub>12</sub> growth experiment . . . . .	42
	Bibliography . . . . .	53
III	Non-Fermi liquid behavior in the filled skutterudite compound CeRu <sub>4</sub> As <sub>12</sub> . . . . .	56
	A. Introduction . . . . .	56
	B. Experimental Details . . . . .	57
	C. Results . . . . .	58

	D. Discussion . . . . .	62
	E. Summary . . . . .	68
	Bibliography . . . . .	75
IV	The filled skutterudite $\text{CeOs}_4\text{As}_{12}$ : a hybridization gap semiconductor . . . . .	79
	A. Introduction . . . . .	79
	B. Experimental Details . . . . .	80
	C. Results . . . . .	81
	D. Discussion . . . . .	84
	E. Summary . . . . .	90
	Bibliography . . . . .	97
V	A metal insulator transition in $\text{YbFe}_4\text{Sb}_{12}$ granular thin films . . . . .	101
	A. Introduction . . . . .	101
	B. Experimental Details . . . . .	102
	C. Results . . . . .	103
	D. Analysis . . . . .	105
	E. Discussion . . . . .	107
	F. Summary . . . . .	108
	Bibliography . . . . .	115

## LIST OF FIGURES

- Figure I.1: The Doniach phase diagram, where the temperatures  $T_K \propto \exp(-1/|\mathcal{J}|N(E_F))$  and  $T_{RKKY} \propto \mathcal{J}^2 N(E_F)$  are plotted vs the exchange interaction  $|\mathcal{J}|N(E_F)$  [33], illustrating a hypothetical competition between the RKKY and Kondo interactions. The actual ordering temperature (bold line) initially increases with increasing  $|\mathcal{J}|N(E_F)$ , as the strength of the RKKY interaction increases. However, as the strength of the Kondo interaction becomes comparable to that of the RKKY interaction, the actual magnetic ordering temperature is suppressed, by comparison to the value expected according to the RKKY interaction, and then driven towards  $T = 0$  at  $|\mathcal{J}_c|N(E_F)$ . Thus, for small  $|\mathcal{J}|N(E_F)$ , the RKKY interaction is strongest, yielding a magnetic ground state. For large values of  $|\mathcal{J}|N(E_F)$ , the Kondo interaction is dominant, leading to a paramagnetic (sometimes Fermi liquid) ground state. For real systems,  $|\mathcal{J}|N(E_F)$  is tuned by parameters such as chemical substitution  $x$ , pressure  $P$ , and magnetic field  $H$ . 24
- Figure I.2: Filled skutterudites have the chemical formula  $MT_4X_{12}$  and crystallize in the cubic space group  $\text{Im}\bar{3}$  with two formula units per unit cell. The lattice constant  $a$  is large  $\sim 7.8\text{-}9.3 \text{ \AA}$ . The rare earth position is  $(0, 0, 0)$ , the transition metal position is  $(0.25, 0.25, 0.25)$  and the pnictogen position is  $(0, y, z)$  where the parameters  $y \sim 0.35$  and  $z \sim 0.16$  are variable depending on the particular chemical composition. . . . . 25
- Figure I.3: A grid summarizing the physical behavior observed for  $\text{CeT}_4\text{X}_{12}$ . More than half of these compounds are weakly magnetic semiconductors where the gap size is correlated with the lattice constant. The remaining As-based members of the series are weakly magnetic and show strongly correlated electron behavior. The remaining Sb-based members are similar to their As analogues, except that they show magnetic behavior similar similar to that expected for  $\text{Ce}^{3+}$  ions. . . . . 26
- Figure I.4: Magnetic susceptibility  $M/H = \chi(T)$  for the Ce-based filled skutterudites showing that for the P and As-based versions, strong hybridization between the Ce ions and the conduction electron ions results in weakly magnetic or nonmagnetic behavior below room  $T$ . For the Sb-based versions, the magnetic susceptibility is similar to that expected for  $\text{Ce}^{3+}$  ions for  $T > 100 \text{ K}$ , where the development of a Kondo coherent state appears to suppress  $\chi(T)$ . The straight line is the expected  $\chi(T)$  for  $\text{Ce}^{3+}$  ions according to Hund's rules. [58, 59, 106, 107, 108, 109, 110, 111]. . 27

Figure I.5:	Electrical resistivity for the Ce-based filled skutterudites showing that, for more than half of these compounds, the transport behavior is semiconducting where the energy gap size decreases with increasing lattice constant. The remaining members of the series exhibit poor metal behavior, with non-Fermi liquid behavior appearing at low $T$ for $\text{CeRu}_4\text{As}_{12}$ and $\text{CeRu}_4\text{Sb}_{12}$ and a Kondo coherent state for $\text{CeFe}_4\text{Sb}_{12}$ . [57, 106, 108, 112] . . . . .	28
Figure II.1:	A schematic of the high pressure cell that was used to synthesize the As-based filled skutterudites. . . . .	45
Figure II.2:	As shown for these $\text{PrOs}_4\text{As}_{12}$ specimens, the characteristic form of the filled skutterudite arsenide single crystals is a regular bi-pyramid with summits cut out along the [100] planes. The crystal in the lower left corner is oriented such that the [111] direction points out of the page. The central crystal shows interesting macro-defects. . . . .	46
Figure II.3:	(a) The arsenic rich part of the Cd - As phase diagram [6] relevant to the flux compositions used for growing crystals of the lanthanide filled skutterudite arsenides. (b) A diagram of the two chamber quartz ampoule used for estimation of the vapor pressure of $\text{CdAs}_2$ as described in the text. . . . .	47
Figure II.4:	The schematic for a high vacuum chamber for deposition of thin films using the pulsed laser deposition technique. The main components are the gas flow system, the heater block, the target rotator and the target. . . . .	48
Figure II.5:	X-ray diffraction pattern for $\text{PrFe}_4\text{Sb}_{12}$ grown on various substrates. For clarity, the substrate peaks were removed from the figure. The following abbreviations for substrate names are used : yttria stabilized zirconia (YSZ) and strontium titanate (STO). . . . .	50
Figure II.6:	Scanning electron microscope secondary electron image of a thin film of $\text{PrFe}_4\text{Sb}_{12}$ grown on a strontium titanate substrate under conditions reported for 111705. . . . .	51
Figure II.7:	Electrical resistivity $\rho$ vs temperature $T$ data for thin films grown on several different substrates compared to data for single crystals [16]. . . . .	52
Figure III.1:	Electrical resistivity $\rho$ vs temperature $T$ for $\text{CeRu}_4\text{As}_{12}$ . Inset : log - log plot of $\rho - \rho_0$ vs $T$ between 65 mK and 10 K, where $\rho_0$ is the residual resistivity. The data can be described by the expression $\rho(T) = \rho_0 + AT^n$ where $\rho_0 = 136 \mu\Omega\text{cm}$ , $A = 19.0 \mu\Omega\text{cmK}^{-n}$ and $n = 1.4$ (straight line in the figure). . . . .	70

Figure III.2:	Magnetic susceptibility $\chi$ vs temperature $T$ for $\text{CeRu}_4\text{As}_{12}$ between 2 K and 300 K. The magnetic susceptibility is defined as $\chi = M/H$ , where $M$ is the magnetization and $H$ is the magnetic field, and was measured in fields of 10 kOe (filled circles) and 50 kOe (unfilled circles). For $2 \text{ K} < T < 10 \text{ K}$ , $\chi(T)$ measured in a 10 kOe field is described by either a power law (curve a) or a logarithmic (curve b) function (see text).	71
Figure III.3:	Total magnetic susceptibility $\chi$ and intrinsic susceptibility $\chi_{lin}$ (see text) vs temperature $T$ for $\text{CeRu}_4\text{As}_{12}$ between 2 K and 300 K. Inset: Magnetization $M$ vs applied field $H$ at $T = 2 \text{ K}$ . The total magnetization $M$ is treated as a sum of a linear intrinsic magnetization $M_{lin}$ and an impurity Brillouin function $M_{imp}$ .	72
Figure III.4:	Specific heat $C$ divided by temperature $T$ vs $T$ for $\text{CeRu}_4\text{As}_{12}$ . For $T < 2.6 \text{ K}$ , an upturn is observed which persists to 650 mK. The divergence conforms to a weak power law (curve a) or logarithmic function (curve b) (see text). It should be noted that a small feature is observed with a maximum at 2.4 K which appears to be related to an impurity phase. Shown in the inset is a plot of $C/T$ vs $T^2$ between 0.5 K and 10 K. The straight line is a fit of Eqn. III.4 which yields $\gamma = 26 \text{ mJ/mol K}^2$ and $\theta_D = 156 \text{ K}$ .	73
Figure III.5:	Thermoelectric power $S$ vs temperature $T$ for two different crystals of $\text{CeRu}_4\text{As}_{12}$ from the same batch. Inset (i) shows $S$ vs $T$ between 0.47 K and 10 K while inset (ii) displays $S/T$ vs $T$ between 0.47 K and 4 K.	74
Figure IV.1:	Electrical resistivity $\rho$ vs temperature $T$ data for $\text{LaOs}_4\text{As}_{12}$ [17] and $\text{CeOs}_4\text{As}_{12}$ for $T = 65 \text{ mK} - 300 \text{ K}$ . Right inset close up: The zero field $\rho(T)$ data for $\text{CeOs}_4\text{As}_{12}$ are not described well by an Arrhenius equation which would be appropriate for a simple single gap semiconductor. Instead, the data are described by a three gap expression (Eqn. IV.4). Left inset close up: $\rho(T)$ data for $\text{CeOs}_4\text{As}_{12}$ for $T = 65 \text{ mK} - 300 \text{ K}$ and magnetic fields (a) 0 T, (b) 0.3 T, (c) 0.5 T, (d) 0.7 T, (e) 1.0 T, (f) 1.5 T, (g) 2.0 T, (h) 3.0 T, (i) 5.0 T, (j) 7.0 T, and (k) 9.0 T.	93
Figure IV.2:	Magnetic susceptibility $M/H = \chi$ vs temperature $T$ data for $\text{CeOs}_4\text{As}_{12}$ and $\text{LaOs}_4\text{As}_{12}$ for $T = 1.9 \text{ K} - 300 \text{ K}$ and $H = 500 \text{ Oe}$ . Also shown is the intrinsic magnetic susceptibility $\chi_{int}(T)$ , as defined in the text, for which a Curie - Weiss (CW) impurity contribution has been subtracted. Inset close up: The low $T$ fits to $\chi(T)$ are described by Eqns. IV.6, IV.7, and IV.8.	94

Figure IV.3:	Specific heat divided by temperature $C(T)/T$ vs temperature squared $T^2$ data for $\text{CeOs}_4\text{As}_{12}$ for $T = 650 \text{ mK} - 18 \text{ K}$ and in magnetic fields of 0 and 5 T. Inset close up: $C(T)/T$ vs $T^2$ data for $T = 650 \text{ mK} - 10 \text{ K}$ and in magnetic fields of 0 and 5 T. The straight lines are the fits to the data as described in the text by Eqn. IV.1. . . . .	95
Figure IV.4:	Thermoelectric power $S$ vs temperature $T$ for $\text{CeOs}_4\text{As}_{12}$ and $\text{LaOs}_4\text{As}_{12}$ for $T = 0.5 \text{ K} - 300 \text{ K}$ . Near 300 K, $S(T)$ for $\text{CeOs}_4\text{As}_{12}$ is positive and one order of magnitude larger than that for metallic $\text{LaOs}_4\text{As}_{12}$ . Left inset close up: $S$ vs $1/T$ is used in the text to identify an energy gap. Right inset close up: $S/T$ vs $T$ is used to characterize the charge carrier density at low $T$ , as discussed in the text. . . . .	96
Figure V.1:	X-ray diffraction data for a $\text{YbFe}_4\text{Sb}_{12}$ film ( $t = 6000 \text{ \AA}$ ) grown on an MgO substrate. Filled skutterudite peaks are apparent and show the film is polycrystalline. The inset displays the main peak width at half maximum. . . . .	111
Figure V.2:	SEM images for samples “a”, “d”, “g”, and “h”, show some of the different topologies found for thin film specimens of $\text{YbFe}_4\text{Sb}_{12}$ . It is assumed that dark spots are voids in the film and grey and white spots are filled. To quantify the topological variation, the ratio of the empty space surface area to the total surface area ( $V/A$ ) is defined. The dark spots were traced by hand and the software package ImageJ [9] was used to measure their surface area. The results, summarized in Table I, show that $V/A$ decreases systematically for samples “a”-“h”. . . . .	112
Figure V.3:	(i,ii) Electrical resistivity vs temperature for samples “a” - “h” illustrating the smooth evolution from the insulating to metallic state. (inset) Residual resistivity at $T = 3 \text{ K}$ vs void density ( $V/A$ ) for various samples. The correlation between the electronic state and $V/A$ is evident as residual resistivity increases logarithmically with $V/A$ . . . . .	113
Figure V.4:	Linear fits to $\ln W$ vs $\ln T$ at low temperatures for samples “a” - “e” show that samples “a” and “b” conform to a stretched exponential function (Eqn. V.3a) while samples “c” - “e” are described by a power law function (Eqn. V.2a). . . . .	114

## LIST OF TABLES

<p>Table II.1: Growth conditions for <math>\text{PrFe}_4\text{Sb}_{12}</math> thin films. <math>T_{abl}</math> is the temperature of the substrates during film growth. <math>P_{laser}</math> is the laser energy density calculated using a beam size at the target of <math>2 \text{ mm} \times 1 \text{ mm}</math>. <math>t_{anneal}(\text{min})/T(^{\circ}\text{C})</math> gives the anneal duration in minutes and temperature in <math>^{\circ}\text{C}</math>. . . . .</p>	49
<p>Table III.1: Atomic coordinates, displacement parameters, and occupancy factors for <math>\text{CeRu}_4\text{As}_{12}</math>. <math>U_{eq}</math> is defined as one-third of the trace of the orthogonalized <math>U_{ij}</math> tensor. . . . .</p>	69
<p>Table IV.1: Crystal structure data for <math>\text{LaOs}_4\text{As}_{12}</math> and <math>\text{CeOs}_4\text{As}_{12}</math>. The atomic coordinates <math>x</math>, <math>y</math>, and <math>z = 0.25</math> for <math>T</math> atoms and 0 for <math>M</math> atoms. The listed quantities are the following; <math>a</math> (<math>\text{\AA}</math>) is the unit cell parameter, <math>x</math>, <math>y</math>, and <math>z</math> are the atomic coordinates for the As atoms, <math>O</math> are the occupancy factors for the <math>T</math>, As, and <math>M</math> atoms, <math>l_{M,T:As}</math> (<math>\text{\AA}</math>) are the chemical bond lengths <math>M</math> - As and <math>T</math> - As, <math>D</math> (<math>\text{\AA}^2 \times 10^3</math>) are the displacement parameters for atoms <math>T</math>, As, <math>M</math>, and <math>R1/wR2</math> are the final discrepancy factors in <math>\%</math>. . . . .</p>	92
<p>Table V.1: Summary of results. <math>V/A</math> is the void surface area to total surface area ratio calculated from SEM images as defined above, <math>t</math> (<math>\text{\AA}</math>) is the film thickness, <math>A</math> is the coefficient for the power law fit Eqn. V.2a where the error is <math>\sim 0.01A</math>, <math>\beta</math> is the power law exponent described in Eqn. V.2a where the error is <math>\sim 0.005</math>, <math>\rho_0</math> is the coefficient for the stretched exponential fit Eqn. V.3a where the error is <math>\sim 0.25\rho_0</math>, <math>x</math> is the power of the stretched exponential as described in Eqn. V.3a where the error is <math>\sim 0.05</math>, <math>T_1</math> is the fit parameter described in Eqn. V.3a where the error is <math>\sim 10 \text{ K}</math>, and <math>T_{\Delta}</math> is the gap size as defined in Eqn. V.3a when <math>x = 1</math> with error <math>\sim 5 \text{ K}</math>. . . . .</p>	110

## ACKNOWLEDGEMENTS

Many people have contributed to this thesis and the magnitude of their assistance and support can not be overstated. First, I would like to thank my thesis advisor, Professor M. Brian Maple, whose influence has fundamentally informed my approach to scientific research. I feel profoundly fortunate to have worked in such a productive and stimulating research environment as his laboratory, here at the University of California, San Diego. It is also important to mention my undergraduate thesis advisor, Professor Frank “Bud” Bridges at the University of California, Santa Cruz, who gave me my first opportunity to perform basic experimental research, at the Stanford Synchrotron Radiation Laboratories. During that time I developed several of my guiding ideas concerning condensed matter research.

I would also like to thank the members of the Maple group who have been both scientific collaborators and friends during my time as a graduate student. In particular; Ben Taylor for introducing me to the pulsed laser deposition technique and being a steady force for consistency and quality in the lab, N. Butch for being a persistent skeptic and crusader for high scientific standards, J. Hamlin for initiating an extremely stimulating year of research into the Fe- $Pn$  high  $T_c$  compounds and being an energetic research partner, J. P. Paglione for providing an example for how much fun research can be, P.-C. Ho for introducing me to the metallic flux growth technique for filled skutterudites in addition to dilution refrigerator technology, D. Zocco for performing enlightening high pressure experiments, T. Sayles and L. Shu for performing specific heat measurements, C. McElroy for being an extremely tolerant office-mate, E. Gonzalez and K. Huang for their excellent work in materials preparation and also for their consistently entertaining activities, and K. Chan for being of immense help in the production of thin films. I would also like to thank my research collaborators, Professor Z. Henkie, R. Wawryk, T. Cichorek, and A. Pietraszko, at the Institute for Low Temperature and Structural Research at the Polish Academy of Sciences in Wroclaw Poland, not only for their excellence in

our research collaborations, but also for hosting me during my visit in 2007. I also want to thank A. Slebarski for the interesting conversations regarding correlated electron physics. Additionally, I should acknowledge the administrative support that was provided by A. Morris, C. Rosado, and G. Doran, whose efforts made it possible to think about research more often than administrative activities.

It also goes without saying that, in large part, this thesis work was made possible by the generous contributions of my parents and Amber's parents. I am extremely fortunate to have been given the opportunity to focus on research during times when other issues could easily have overwhelmed any scientific undertaking. I hope that someday I can repay the immense investment that they have made in my career. I also hope that I can repay my large debt to my family by promoting the aspirations of my daughter, Madeleine, and any other future children. I hope that someday she will take the same enjoyment and inspiration from learning as I have. Finally, the most credit goes to my wife, Amber, who tolerated my absence during long work hours and constantly motivated me to do my best.

Parts of the text and data of Chapter II are reprints of material that appears in "Crystal growth and properties of the filled skutterudite arsenides," Z. Henkie, M. B. Maple, A. Pietraszko, R. Wawryk, T. Cichorek, R. E. Baumbach, W. M. Yuhasz, and P.-C. Ho, *J. Phys. Soc. Jpn. Suppl. A* 77, 128 (2008) and "Pulsed Laser Deposition of  $\text{PrFe}_4\text{Sb}_{12}$  Thin Films," R. E. Baumbach, W. M. Yuhasz, and M. B. Maple, *Appl. Phys. A* 84, 227-229 (2006). The text and data of Chapter III is a reprint of material that appears in "Non Fermi liquid behavior in the filled skutterudite compound  $\text{CeRu}_4\text{As}_{12}$ ," R. E. Baumbach, P.-C. Ho, T. A. Sayles, M. B. Maple, R. Wawryk, T. Cichorek, A. Pietraszko, and Z. Henkie, *J. Phys.: Condens. Matter* 20, 075110 (2008). The text and data of Chapter IV is a reprint of material that appears in "The filled skutterudite  $\text{CeOs}_4\text{As}_{12}$ : a hybridization gap semiconductor," R. E. Baumbach, P.-C. Ho, T. A. Sayles, M. B. Maple, R. Wawryk, T. Cichorek, T. Pietraszko, and Z. Henkie, *Proc. Natl. Acad. Sci.* 105, 17307 (2008). The text and data of Chapter V is a reprint of material that appears

in “A metal insulator transition in  $\text{YbFe}_4\text{Sb}_{12}$  thin films,” R. E. Baumbach, W. M. Yuhasz, and M. B. Maple, *Thin Solid Films* 516, 3378 (2008). The dissertation author is the primary investigator and author of these articles except the first, for which Z. Henkie and M. B. Maple are the primary investigators.

The crystal growth work reported in this thesis was supported by the U. S. Department of Energy (DOE) under research Grant DE FG02-04ER46105 and crystal growth equipment was sponsored by the U. S. DOE through Grant DE FG02-04ER46178. Low temperature measurements were funded by the National Science Foundation (NSF) under Grant 0802478. Research performed in Poland by Z. Henkie was supported by the Polish Committee for Scientific Research Grant No. 1 P03B 073 27 and the Polish Ministry of Science and Higher Education Grant No. NN 202 4129 33.

## VITA

- 2002 Bachelor of Science in Physics with Honors,  
University of California, Santa Cruz
- 2002–2006 Teaching Assistant, Department of Physics  
University of California, San Diego
- 2002–2008 Graduate Research Assistant, University of California,  
San Diego  
Advisor: M. Brian Maple
- 2004 Master of Science, Physics  
University of California, San Diego
- 2009 Doctor of Philosophy, Physics  
University of California, San Diego

## PUBLICATIONS

- R. E. Baumbach, J. J. Hamlin, L. Shu, N. Crisosto, D. A. Zocco, and M. B. Maple, “Superconductivity in  $LnFePO$  ( $Ln = La, Pr, \text{ and } Nd$ ) single crystals,” submitted to the New Journal of Physics (2008).
- M. M. Qazilbash, J. J. Hamlin, R. E. Baumbach, M. B. Maple, and D. N. Basov, “Charge dynamics in the normal state of the iron oxypnictide superconductor  $LaFePO$ ,” submitted to Phys. Rev. Lett. (2008).
- R. E. Baumbach and M. B. Maple, “Filled skutterudites: magnetic and electrical properties,” submitted to Encyclopedia of Materials: Science and Technology (2008).
- B. Nowak, O. Zogal, A. Pietraszko, R. E. Baumbach, M. B. Maple, and Z. Henkie, “Enhanced spin fluctuation in the As-based filled skutterudite  $LaFe_4As_{12}$ ,” in preparation (2008).
- J. J. Hamlin, R. E. Baumbach, D. A. Zocco, T. A. Sayles, and M. B. Maple, “Superconductivity in single crystals of  $LaFePO$ ,” J. Phys.: Condens. Matter 20, 365220 (2008).
- D. A. Zocco, J. J. Hamlin, R. E. Baumbach, M. B. Maple, M. A. McGuire, A. S. Sefat, B. C. Sales, R. Jin, D. Mandrus, J. R. Jeffries, S. T. Weir, Y. K. Vohra, “Effect of pressure on the superconducting critical temperature of  $La[O_{0.89}F_{0.11}]FeAs$  and  $Ce[O_{0.88}F_{0.12}]FeAs$ ,” Physica C 468, 2229 (2008).
- R. E. Baumbach, P.-C. Ho, T. A. Sayles, M. B. Maple, R. Wawryk, T. Cichorek, T. Pietraszko, and Z. Henkie, “The filled skutterudite  $CeOs_4As_{12}$ : a hybridization gap semiconductor,” Proc. Natl. Acad. Sci. 105, 17307 (2008).

- R. E. Baumbach, P.-C. Ho, T. A. Sayles, M. B. Maple, R. Wawryk, T. Cichorek, A Pietraszko, and Z. Henkie, "Non Fermi liquid behavior in the filled skutterudite compound  $\text{CeRu}_4\text{As}_{12}$ ," *J. Phys.: Condens. Matter* 20, 075110 (2008).
- Z. Henkie, M. B. Maple, A. Pietraszko, R. Wawryk, T. Cichorek, R. E. Baumbach, W. M. Yuhasz, and P.-C. Ho, "Crystal growth and properties of the filled skutterudite arsenides," *J. Phys. Soc. Jpn. Suppl. A* 77, 128 (2008).
- M. B. Maple, Z. Henkie, R. E. Baumbach, T. A. Sales, N. P. Butch, P.-C. Ho, T. Yanagisawa, W. M. Yuhasz, R. Wawryk, T. Cichorek, and A. Pietraszko, "Correlated electron phenomena in Ce- and Pr-based filled skutterudite arsenides and antimonides," *J. Phys. Soc. Jpn. Suppl. A* 77, 7 (2008).
- R. E. Baumbach, W. M. Yuhasz, and M. B. Maple, "A metal insulator transition in  $\text{YbFe}_4\text{Sb}_{12}$  thin films," *Thin Solid Films* 516, 3378 (2008).
- R. E. Baumbach, W. M. Yuhasz, M. B. Maple, "Metal insulator transition in disordered  $\text{YbFe}_4\text{Sb}_{12}$  thin films," *Physica B* 403, 800 (2008).
- B. J. Taylor, R. E. Baumbach, T. A. Sayles, and M. B. Maple, "Critical dynamic vortex fluctuations amidst a nascent peak effect in granular  $\text{CeRu}_2$  thin films," *J. Phys.: Condens. Matter* 20, 335214 (2008).
- A. Slebarski, M. B. Maple, R. Baumbach, and T. Sayles, "Interplay between spin - glass and non - Fermi - liquid behavior in  $\text{CeNi}_{1-x}\text{Rh}_x\text{Sn}$ ," *Phys. Rev. B* 77, 245133 (2008).
- D. E. MacLaughlin, M. S. Rose, J. E. Anderson, O. O. Bernal, R. H. Heffner, G. J. Nieuwenhuys, R. E. Baumbach, N. P. Butch, and M. B. Maple, "Effect of annealing on glassy dynamics and non-Fermi liquid behavior in  $\text{UCu}_4\text{Pd}$ ," *Physica B* 374-375, 177-179 (2006).
- R. E. Baumbach, W. M. Yuhasz, and M. B. Maple, "Pulsed Laser Deposition of  $\text{PrFe}_4\text{Sb}_{12}$  Thin Films," *Appl. Phys. A* 84, 227-229 (2006).
- R. Baumbach, F. Bridges, L. Downward, D. Cao, P. Chesler, and B. Sales, "Off-center phonon scattering sites in  $\text{Eu}_8\text{Ga}_{16}\text{Ge}_{30}$  and  $\text{Sr}_8\text{Ga}_{16}\text{Ge}_{30}$ ," *Phys. Rev. B* 71, 024202 (2005).
- F. Bridges, R. Baumbach, D. Cao, P. Chesler, M. Anderson, and B. Sales, "Probing phonon scattering sites in the thermoelectric clathrate  $\text{Eu}_8\text{Ga}_{16}\text{Ge}_{30}$ ," *Radiation effects and defects in solids* 158, 343 (2003).

## FIELDS OF STUDY

Major Field: Physics

Studies in strongly correlated electron materials

M. Brian Maple, Bernd T. Matthias Professor of Physics,  
University of California, San Diego

## ABSTRACT OF THE DISSERTATION

Strongly correlated electron behavior in As-based and thin film Sb-based filled  
skutterudites

by

Ryan Eagle Baumbach

Doctor of Philosophy in Physics

University of California, San Diego, 2009

Professor M. Brian Maple, Chair

Results for two categories of filled skutterudites that have previously received limited attention are presented: (1) single crystals of the As-based filled skutterudites and (2) thin films of the the Sb-based filled skutterudites. We show that the compounds  $CeT_4As_{12}$  ( $T = Ru, Os$ ) exhibit non-Fermi liquid and Kondo insulator behavior, respectively. The phenomena seen in these materials is discussed in terms of strong hybridization between the localized  $f$ -electron states and the conduction electron states, with various perturbing factors. Results for thin films of the compounds  $PrFe_4Sb_{12}$  and  $YbFe_4Sb_{12}$ , which were synthesized by the pulsed laser deposition technique, are also presented. Measurements of the  $PrFe_4Sb_{12}$  specimens indicate that the films are single phase and exhibit behavior that is comparable to that seen in bulk specimens. To explore the affect of film thickness,  $YbFe_4Sb_{12}$  specimens were synthesized where  $t$  was varied from 6000 to 300 Å. Thick films ( $t > 1000$  Å) show electrical transport behavior similar to that seen for bulk specimens. A metal to insulator transition is observed for thin films ( $t < 1000$  Å) which is correlated with film topology.

# I

## Introduction

### I.A Correlated electron behavior

#### I.A.1 Fermi Liquid

The term “free-electron gas” refers to a quantum many body system composed of non-interacting electrons. Electrons are spin 1/2 particles, i.e. fermions, and, therefore, obey the Pauli exclusion principle. For  $T = 0$ , they fill the momentum states  $p = \hbar k$  up to the highest occupied level, the Fermi energy  $E_F = \hbar^2 k_F^2 / 2m_e$ , for which  $\hbar$  is Planck’s constant,  $k_F = (3\pi^2 N/V)^{1/3}$  is the Fermi wave vector, and  $m_e$  is the bare electron mass. Specifically, the density of states for a free-electron gas is given by the expression,

$$N(E) = \frac{m_e}{\hbar^3 \pi^2} \sqrt{2mE} \quad (\text{I.1})$$

According to this theory, the specific heat divided by temperature  $C(T)/T$ , magnetic susceptibility  $\chi(T)$ , and electrical resistivity  $\rho(T)$  are described at low temperatures by the expressions,

$$\frac{C(T)}{T} = \frac{\pi^2 k_B^2}{3} N(E_F) = \gamma_0 \quad (\text{I.2a})$$

$$\chi(T) = \mu_B^2 N(E_F) = \chi_0 \quad (\text{I.2b})$$

$$\rho(T) = AT^2 \quad (\text{I.2c})$$

where  $k_B$  is the Boltzmann constant,  $N(E_F)$  is the electronic density of states at the Fermi energy, and  $\mu_B$  is the Bohr magneton [1, 2]. Although the free-electron gas model provides a reasonable starting point for describing the behavior of electrons in a solid, it does not fully characterize even simple metals, such as the alkali metals, alkaline earths, and the so-called “noble metals” (Cu, Ag, Au), because electron-electron and electron-phonon interactions affect their physical properties.

To describe a Fermi sea with weak interactions, Landau proposed the well known Fermi liquid theory [3, 4, 5], which was originally developed to characterize  $^3\text{He}$ , but also does remarkably well describing the low  $T$  physical properties of regular metals [6]. In this picture, electron-electron interactions can be taken into account by replacing individual electrons with “quasiparticles” with slightly enhanced masses  $m^*$ , for which the excitation spectrum can be mapped onto that of a free-electron gas. The quasiparticle is thought of as an electron that is “dressed” by interactions with the other electrons in the system. According to this theory,  $C(T)/T$ ,  $\chi(T)$ , and  $\rho(T)$  are given by,

$$C(T)/T = \frac{m^*}{m_e} \gamma_0 = \gamma \quad (\text{I.3a})$$

$$\chi(T) = \frac{m^*}{m_e} \frac{\chi_0}{1 + F_0^a} \quad (\text{I.3b})$$

$$\rho(T) = AT^2 \quad (\text{I.3c})$$

where  $F_0^a$  is a Landau parameter and  $\sqrt{A} \propto m^*$ . For regular metals,  $m^*/m_e \sim 1-10$  and  $\gamma_0 \sim 1-10$  mJ/mol-K<sup>2</sup>.

For most materials, the effects of lattice vibrations, i.e. phonons, become dominant with increasing  $T$ , enhancing quantities such as  $C(T)/T$  and  $\rho(T)$ . According to Debye’s model, which assumes that vibrational energy is quantized in a solid and can be described by plane waves in a box, the lattice term for the specific heat is given by  $C(T)/T = \beta T^2$  where  $\beta = r1944(T^3/\Theta_D)^3$  J/mol-K for  $T < \Theta_D/10$  [7]. In Debye’s expression,  $r$  is the number of atoms per molecule and  $\Theta_D$  is the Debye temperature, which is proportional to the cutoff frequency

for phonon modes. For typical metallic systems  $\Theta_D$  is of the order of hundreds of kelvin. This extremely simplified model is remarkably successful in describing a wide range of systems, despite the complicated phonon spectra that exist for most real materials. For electrical resistivity, the effects of phonons can be accounted for by considering Matthiessen's rule, which states that  $\rho(T)$  is a linear sum of the different scattering processes including: the Fermi liquid term ( $AT^2$ ), the nonmagnetic impurity scattering term ( $\rho_0$ ), and the electron-phonon scattering  $\rho_{e,p}(T)$  term, which is usually a complicated function due to the complexity of phonon spectra. Thus, for regular metals,  $\rho(T)$ , and  $C(T)/T$  are given by linear sums of the Fermi liquid and lattice terms and yield the expressions,

$$C(T)/T = \gamma + \beta T^2 \quad (\text{I.4a})$$

$$\rho(T) = \rho_0 + \rho_{e,p}(T) + AT^2 \quad (\text{I.4b})$$

The  $T^2$  term in  $\rho(T)$  is usually too small to measure since  $A$  is proportional to the square of the quasiparticle mass and the impurity and lattice terms are large by comparison. As a result, its physical existence was not unambiguously identified until the observation of heavy fermion behavior.

### I.A.2 Magnetic $d$ - and $f$ - electron ions

In addition to the intrinsic itinerant electron magnetism found in metals, magnetism also arises from localized unpaired electron spins in partially filled  $d$ - or  $f$ -electron orbitals, as found in transition metal, rare earth, and actinide elements [1, 2, 8]. For these elements, the effective magnetic moment of an isolated ion is given by the expression,

$$\mu_{eff} = g_J \mu_B \sqrt{J(J+1)} \quad (\text{I.5a})$$

where  $J$  is the total angular momentum,  $\mu_B$  is the Bohr magneton, and  $g_J$  is the Landé  $g$ -factor given by,

$$g_J = \frac{3}{2} + \frac{S(S+1) - L(L+1)}{2J(J+1)} \quad (\text{I.6a})$$

The quantity  $J$  is determined according to Hund's rules, which describe the way in which electrons populate the available states in the local atomic shells. Hund's rules state that the electrons are arranged to (1) maximize their spin angular momentum  $S$ , and thereby reduce the repulsive Coulomb energy, (2) maximize the orbital angular momentum  $L$  and thereby satisfy the Pauli exclusion principle and coordinate the rotation of the electrons to minimize the Coulomb repulsion energy, and finally (3) the value of  $J$  is given by  $J = |L - S|$  if the shell is less than half full and  $J = L + S$  if it is more than half full. The third rule represents an attempt to minimize the spin-orbit energy. It is important to note that, for transition metals, the orbital angular momentum may be quenched as the result of crystalline electric field effects, yielding  $J$  values that are smaller than those predicted by Hund's rules and also giving  $g_J = 2$ .

A wide variety of types of magnetic behaviors can arise for both  $d$ - and  $f$ -electron systems, the simplest examples being paramagnetism, antiferromagnetism, and ferromagnetism [8]. At high enough temperatures, thermal excitations are stronger than spin exchange interactions, leading to random spin orientations for the magnetic ions in a crystalline lattice. This situation is referred to as the paramagnetic state and is characterized by a linear response in magnetization  $M$  to a small magnetic field,  $M = \chi H$ . For larger  $H$ , the magnetization evolves according to the well-known Brillouin function where  $M$  saturates to a constant value for  $\mu_B H \gg k_B T$ . The temperature dependence of the magnetic susceptibility is given by the Curie-Weiss law,

$$\chi(T) = \frac{C}{T - \Theta_{CW}} \quad (\text{I.7})$$

where  $C = N_A \mu_{eff}^2 / 3k_B$  and  $\Theta_{CW}$  is the Curie-Weiss temperature, which indicates whether the spin interactions are antiferromagnetic ( $\Theta_{CW} < 0$ ) or ferromagnetic ( $\Theta_{CW} > 0$ ). As temperature is decreased, magnetic ordering may occur if the magnetic interactions overwhelm the thermal excitations, causing adjacent spins to align in opposite directions below the Néel temperature  $T_N$  for antiferromag-

nets and in the same direction below the Curie temperature  $T_C$  for ferromagnets. In some cases, the spin interaction may not be strong enough to cause magnetic ordering, even at very low temperatures, causing the Curie-Weiss behavior to extend to  $T = 0$ . It should also be emphasized that there are several other types of complicated magnetic states including helical and spiral structures, spin glass ordering, ferrimagnetism, metamagnetism, itinerant electron ferromagnetism, etc.

### I.A.3 Dilute $d$ - and $f$ -electron ions in a Fermi sea

The  $d$ - and  $f$ -electrons of transition metal, lanthanide, and actinide elements can also interact with the conduction electrons of a host material, giving rise to several interesting types of correlated electron phenomena. In the 1930s, measurements revealed the first indications of these types of behaviors as low temperature minima in the electrical resistivity of basic metals, such as Cu, Ag, and Au [9, 10]. This behavior was eventually identified with the presence of dilute concentrations of  $d$ -electron impurities that were dissolved into metallic host materials, as for the systems CuFe, CuMn, and others. Later (1960s), it was shown that similar effects occur for lanthanide solutes in dilute alloy systems such as LaCe and YCe [11]. Over the past few decades, intense research has revealed that the lanthanides with two available valence states (Pr, Sm, Eu, Tm, and Yb) and some actinides also show similar behaviors.

An explanation of this behavior eluded the scientific community until 1964, when J. Kondo proposed the (now well-known) Kondo Hamiltonian. The Kondo Hamiltonian describes the interaction between the conduction electron and magnetic impurity electron spins according to the expression,

$$H = -2\mathcal{J}\mathbf{S} \cdot \mathbf{s} \quad (\text{I.8a})$$

where  $\mathcal{J}$  is negative and characterizes the strength of the antiferromagnetic spin exchange interaction,  $\mathbf{S}$  is the impurity ion spin, and  $\mathbf{s}$  is the conduction electron spin density at the impurity site [12]. For lanthanide ions, the strong spin-orbit

coupling may sometimes modify this expression, yielding the Hamiltonian,

$$H = -2\mathcal{J}(g_J - 1)\mathbf{J} \cdot \mathbf{s} \quad (\text{I.9})$$

where  $g_J$  is the Landé  $g$ -factor and  $\mathbf{J}$  is the total angular momentum, according to Hund's rules [13]. Around the same time (1965), it also was shown that the bound state described by the Kondo Hamiltonian appears in the electronic density of states as a sharp feature at the Fermi energy [14, 15]. This peak, sometimes called the ‘‘Abrikosov-Suhl’’ resonance, has important implications for a variety of physical situations, even beyond typical Kondo systems. For instance, any system which exhibits such a resonance at  $E_F$ , regardless of its origin, can exhibit ‘‘Kondo-like’’ properties.

The original calculations by Kondo, which were made using perturbation theory up to third order in  $\mathcal{J}$  (second order in perturbation theory), yield an expression for electrical resistivity for  $T \gg T_K$  given by,

$$\rho_K(T) = A|\mathcal{J}|^2 S(S+1)[1 - \mathcal{J}N_c(E_F)\log(D/k_B T)] \quad (\text{I.10a})$$

where  $N_c(E_F)$  is the electronic density of states for the conduction electron band at the Fermi energy and  $D$  is a cut-off that roughly corresponds to the conduction electron band width. This result explains the minimum in  $\rho(T)$  as a being due to a linear combination of the phonon term  $\rho_{e,p}(T)$ , which decreases with decreasing  $T$ , and the Kondo term  $\rho_K(T)$ , which increases with decreasing  $T$ . This calculation also yields a value for the Kondo temperature given by,

$$T_K \sim T_F \exp[-1/N_c(E_F)|\mathcal{J}|] \quad (\text{I.11a})$$

where  $T_F$  is the Fermi temperature. It is apparent that although the Kondo model describes some of the features of a dilute alloy system with  $d$ - or  $f$ -electron ion solutes, there is a divergence in the predicted physical properties at  $T = T_K$ , making the Kondo Hamiltonian unphysical for  $T < T_K$ . In other words, the simple perturbation treatment of the Kondo Hamiltonian does not describe the bound state

which emerges for  $T \ll T_K$ . The limitations of this expression appear prominently in experimental results for which the low  $T$  electrical resistivity saturates towards a constant value, i.e. the “unitary limit”, and the ground state is a Fermi liquid.

This apparent disagreement between theory and experiment remained an open issue for several years and attracted numerous theoretical treatments. For instance, both Abrikosov and Suhl developed mathematical techniques to sum all higher terms in the perturbation series (1965) and found that those terms also make logarithmic contributions to  $\rho(T)$ , making it clear that perturbation theory could not completely describe the low  $T$  behavior [16]. A possible solution to this problem was proposed in 1975 when Wilson applied renormalization group theory to the Kondo problem [17, 18] and showed that at low  $T$ ,  $\mathcal{J}$  approaches infinity and the magnetic impurities and conduction electrons form a spin singlet bound state, resulting in a nonmagnetic Fermi liquid ground state. Calculations were later made in the context of the  $n$ -channel Kondo model which predicted that, for  $T \ll T_K$ ,  $\rho(T)$  is given by the expression [19, 20],

$$\rho_K(T) = \rho_K(1 - c(T/T_K))^2 \quad (\text{I.12})$$

Thus, for  $T \gg T_K$ , the magnetic impurities behave as weakly interacting magnetic moments that are described by Curie-Weiss behavior with a negative  $\Theta_{CW} \sim (3-4)T_K$ . For  $T \ll T_K$ , the magnetic moments are screened by the divergent antiferromagnetic interaction with the conduction electrons, leading to a nonmagnetic many body singlet ground state. In this picture, the temperatures near  $T_K$  are interpreted as a crossover regime separating local moment behavior at high  $T$  and nonmagnetic behavior for low  $T$ .

A topic closely related to the Kondo model is the valence fluctuation picture [23], which was originally introduced to account for the nearly  $T$ -independent Pauli-like magnetic behavior below a characteristic temperature  $T_{vf}$  as observed for the systems,  $\alpha$ -Ce [21], SmS in its collapsed “gold” phase [22, 23, 24], SmB<sub>6</sub> [25], and others. For these types of systems, it appears that the bounding states for the

rare earth ions,  $4f^n(5d6s)^m$  and  $4f^{n-1}(5d6s)^{m+1}$ , are nearly degenerate in energy and, as a result, it is favorable for the rare earth ions to acquire an additional degree of freedom by entering an intermediate valence state. The nearly degenerate  $f$ -electron states promote fluctuations between the available electronic configurations at a frequency  $\omega_{vf} \approx k_B T_{vf}/\hbar$ , where  $T_{vf}$  separates magnetic behavior at high temperatures  $T \gg T_{vf}$  and nonmagnetic behavior at low temperatures  $T \ll T_{vf}$ . In this picture, the magnetic susceptibility is given by the expression,

$$\chi(T) \approx \frac{n_{4f^n} \mu_{eff}^2(4f^n) + n_{4f^{n-1}} \mu_{eff}^2(4f^{n-1})}{3k_B(T + T_{vf})} \quad (\text{I.13a})$$

where  $n_{4f^n}$  and  $n_{4f^{n-1}} = 1 - n_{4f^n}$  are the fraction of electrons in the nearly degenerate states and  $\mu_{eff}^2(4f^n)$  and  $\mu_{eff}^2(4f^{n-1})$  are the square of their effective magnetic moments, according to Hund's rules. As  $T$  approaches 0 K, the Curie-Weiss behavior is cut off by  $T_{vf}$  and  $\chi(T)$  becomes constant. In this model, the value of  $T_{vf}$  can be estimated from the Curie-Weiss behavior of  $\chi(T)$  for  $T \gg T_{vf}$  where it plays the role of the Curie-Weiss temperature. The behavior of  $n_{4f^n}$  and  $n_{4f^{n-1}}$  can also be estimated from measurements of the lattice constant, thermal expansion, "slow" Mössbauer, and "fast" XPS. In some cases, the valence parameters  $n_{4f^n}$  and  $n_{4f^{n-1}}$  evolve as a function of  $T$ , resulting in a weak  $T$  dependence for  $\chi(T)$  below  $T_{vf}$ . This situation is reminiscent of the  $\gamma$ - $\alpha$  transition in elemental Ce, in which the valence undergoes a transition towards 4+ with decreasing  $T$  that is discontinuous (1st order) for pressures  $P < P_c$  where  $P_c$  is the critical point, and continuous (2nd order) for  $P > P_c$ . It is also worth noting that valence fluctuations could produce a narrow resonance near  $E_F$  and thereby give results that might be phenomenologically similar to those seen for Kondo systems [11, 26].

Around the same time as the introduction of the Kondo Hamiltonian, several other theoretical approaches for describing the physics of magnetic impurities in metals were also being developed. One of the most influential of these models has proven to be the well known Anderson Hamiltonian (1961) [27], for which the interaction between a localized spin 1/2  $d$ - or  $f$ -electron ion with a Fermi sea is

given by the expression,

$$H = \sum_{\mathbf{k}, \sigma} \varepsilon_{\mathbf{k}} n_{\mathbf{k}\sigma} + E_0 \sum_{\sigma} n_{f\sigma} + U n_{f\uparrow} n_{f\downarrow} + \sum_{\mathbf{k}, \sigma} (V_{kf} c_{\mathbf{k}\sigma}^* c_{f\sigma} + V_{fk} c_{f\sigma}^* c_{\mathbf{k}\sigma}) \quad (\text{I.14})$$

where  $\varepsilon_{\mathbf{k}}$  is the energy of the conduction electrons with wave vector  $\mathbf{k}$ ,  $n_{\mathbf{k}\sigma}$  is the number operator for conduction electrons with wave vector  $\mathbf{k}$ ,  $E_0$  is the the  $d$ - or  $f$ -electron energy level,  $n_{f\sigma}$  is the number operator for  $d$ - or  $f$ -electrons with spin  $\sigma$ ,  $U$  is the Coulomb repulsion between  $d$ - or  $f$ -electron orbitals, and  $V_{kf}$  is the hybridization parameter. Thus, the first and second terms describe the  $d$ - or  $f$ -electron and the conduction electron states with spin  $\sigma$ , the third term represents the  $d$ - or  $f$ -electron intersite Coulomb repulsion, and the fourth term describes the hybridization interaction between the  $d$ - or  $f$ -electrons and the conduction electrons. Based on this model, it has been shown that the effect of a strong Coulomb interaction is to split the  $d$ - or  $f$ -electron levels into two parts at  $E_0$  and  $E_0 + U$ , according to spin, while the hybridization between the  $d$ - or  $f$ -electrons and the conduction electrons results in a broadening of the  $d$ - or  $f$ -electron levels given by,

$$\Delta = \pi N_c(E_F) V_{fk}^2 \sim \frac{V_{kf}^2}{W} \quad (\text{I.15})$$

where  $N_c(E_F)$  is the density of states of the conduction band at the Fermi energy and  $W$  is the conduction electron bandwidth. Various physical states for the  $d$ - or  $f$ -electrons follow from the Anderson model including, (1) if  $E_0 + U \gg E_F$  and  $E_0 \ll E_F$ , then local magnetic moments are able to form, (2) if  $E_0 \sim E_F$  then the valence fluctuation scenario is realized, and (3) if small admixtures of the  $d$ - or  $f$ -electrons and the conduction electrons occur and  $U$  is taken to be large, then the Schreiffer-Wolff transformation (1966) gives an antiferromagnetic exchange interaction between the  $d$ - or  $f$ -electrons and the conduction electrons described by the expression [28],

$$\mathcal{J} = -\frac{V_{kf}^2 U}{E_F(E_F + U)} \quad (\text{I.16})$$

which provides a route to the negative exchange interaction that was postulated for the Kondo Hamiltonian. It should also be noted that, although the Anderson model and subsequent theoretical developments (such as the Coqblin-Schrieffer model (1969) [29]) have provided a powerful tool to describe several types of systems that include  $d$ - or  $f$ -electron ions, there yet remain significant obstacles to a complete theoretical description of these types of physical situations.

#### I.A.4 Concentrated $d$ - and $f$ -electron ions in a Fermi sea

As mentioned above, the development of the Kondo and Anderson theories for magnetic ions in a Fermi sea was driven, in part, by experimental studies which revealed unusual behavior for metallic alloys containing the elements Ce, Pr, Sm, Eu, Tm, Yb, and U, all of which have partially filled  $f$ -electron shells that can strongly hybridize with conduction electrons. By the mid-70s, it had also become apparent that other remarkable effects are present in compounds with concentrated lattices of these types of ions. As a result, the Kondo picture was soon extended beyond the dilute impurity limit to include materials that have a crystalline sublattice of magnetic ions, i.e. a “Kondo lattice” [20]. It should be noted that intermediate valence ideas were also applied to many of the same systems without invoking the Kondo Hamiltonian. In particular, those that exhibit small energy gap semiconducting behavior were addressed using the intermediate valence picture.

From a conceptual point of view, the Kondo lattice can be realized by increasing the number of magnetic impurities from the dilute impurity limit until a fully occupied sublattice of  $d$ - or  $f$ -electron ions is present in a crystalline lattice. Although this approach implies that the Kondo lattice is related to the single ion Kondo picture, there are several distinct deviations that result in surprising physical behaviors. The first of these differences is that a two peak structure

develops in the Abrikosov-Suhl resonance at the Fermi energy as the result of periodic arrangement of magnetic ions [20]. The second difference is that the Ruderman-Kittel-Kasuya-Yoshida or RKKY interaction [30, 31, 32] gains increased importance in comparison to the dilute limit. The RKKY interaction describes the exchange interaction between local magnetic moments as being mediated by spin polarized conduction electrons, for which  $\mathcal{J}$  is given by the expression,

$$\mathcal{J} \sim -\mathcal{J}_0^2 N(E_F) \frac{\cos(2k_F r)}{|k_F r|^3} \quad (\text{I.17a})$$

where  $\mathcal{J}_0$  quantifies the magnetic exchange interaction strength and  $r$  is the separation between magnetic ions. Depending on the size of  $r$ , magnetic ions that influence one another via the RKKY interaction can exhibit antiferromagnetism, ferromagnetism, no magnetism at all, spin glass behavior, or even more complicated structures. For the RKKY interaction, the characteristic temperature is given by the expression,

$$T_{RKKY} \propto \mathcal{J}^2 N(E_F) \quad (\text{I.18})$$

Thus, it is natural to consider a hypothetical situation in which there is a competition between the Kondo effect and the RKKY interaction, as was done by Doniach in 1977. In the so-called ‘‘Doniach diagram’’ Fig. I.1, the temperatures  $T_K$  and  $T_{RKKY}$  are plotted vs the exchange interaction  $|\mathcal{J}N(E_F)|$  [33]. As shown in this figure, the actual ordering temperature initially increases with increasing  $|\mathcal{J}N(E_F)|$ , as the strength of the RKKY interaction increases. However, as the strength of the Kondo interaction becomes comparable to that of the RKKY interaction, the magnetic ordering temperature is first suppressed and then driven towards  $T = 0$ . Thus, for small  $|\mathcal{J}N(E_F)|$ , the RKKY interaction is strongest, yielding a magnetic ground state and for large values of  $|\mathcal{J}N(E_F)|$ , the Kondo interaction is dominant, leading to a Fermi liquid ground state which shows Pauli paramagnetism. There is also an intermediate region, near  $|\mathcal{J}_c N(E_F)|$  which will be discussed in greater detail below. It should be noted that although the Doniach diagram presents an appealingly simple description for a lattice of magnetic ions, it

represents a simplified subset of possible behaviors that could occur in these types of systems. As such, although some of the discussion given below is in this context, it is not meant to imply that the Doniach picture gives a complete description of the physics.

Several different types of behaviors are possible in the regime where the Kondo interaction is dominant, which depend on the position of  $E_F$  with respect to the two peak (energy gap or pseudogap) structure that develops in the Abrikosov-Suhl resonance. For instance, if  $E_F$  is found outside the energy gap, then metallic behavior is observed and if  $E_F$  is inside the energy gap, then semiconducting behavior occurs. In both cases, the enhanced density of states near  $E_F$  leads to a renormalization of the electron mass, i.e. “heavy fermion” behavior, where  $m^*/m_e = 100-1000$  [34, 35, 36, 37, 38, 39, 40, 41]. For the metallic case, the effect of the heavy fermion quasiparticles is seen experimentally as Fermi liquid behavior at low  $T$ , where the terms  $\gamma$  and  $AT^2$  are greatly enhanced by comparison to those of regular metals. Additionally, the simultaneous screening of the magnetic lattice below a coherence temperature  $T_{coh}$  leads to the formation of Bloch states for the conduction electrons as the result of the equivalence of the screened magnetic ions. Experimentally, the onset of Kondo coherence usually appears in  $\rho(T)$  as an evolution from a weak  $T$  dependence for  $T \gg T_{coh}$  to a rapid decrease in the electrical resistivity near  $T_{coh}$  which evolves into Fermi liquid behavior for  $T \ll T_{coh}$ . The magnetic susceptibility evolves from Curie-Weiss behavior for  $T \gg T_{coh}$  to a nonmagnetic state with an enhanced Pauli susceptibility below  $T_{coh}$ . The low  $T$  electronic specific heat  $\gamma$  and the magnetic susceptibility  $\chi$  are empirically found to scale according to the expression,

$$\frac{\pi^2 k_B^2 \chi}{\mu_{eff}^2 \gamma} \approx 1 \quad (\text{I.19a})$$

which is commonly referred to as the Wilson-Sommerfeld ratio [17]. This relationship reflects the fact that both  $\gamma$  and  $\chi$  scale with  $N(E_F)$ . To put it another way, this expression implies that the electrons involved in the heavy fermion state

are the same ones that contribute to the enhanced Pauli susceptibility. It is also observed that the coefficients  $A$  and  $\gamma$  are related by the expression,

$$A/\gamma^2 = 1 \times 10^{-5} \quad (\text{I.20a})$$

in units of  $\mu\Omega\text{cm}(\text{molK/mJ})^2$ . This expression is called the Kadowaki-Woods ratio [42]. Intense interest in these types of materials was initiated in 1979 when the compound  $\text{CeCu}_2\text{Si}_2$  was reported to be a superconductor with an electronic specific heat coefficient  $\gamma \sim 1100 \text{ mJ/mol-K}^2$  [43, 44, 45], although it should be noted that this compound was not the first to show heavy fermion behavior. Since then, the number of heavy fermion materials has increased dramatically. Some noteworthy examples include  $\text{U}_6\text{Fe}$  [46],  $\text{CeIn}_3$  [47],  $\text{CeCoIn}_5$  [48],  $\text{UBe}_{13}$  [49],  $\text{UPd}_2\text{Al}_3$  [50],  $\text{URu}_2\text{Si}_2$  [51], and  $\text{PrOs}_4\text{Sb}_{12}$  [52].

As mentioned above, hybridization gap semiconducting behavior (Kondo insulator behavior) is also observed in magnetic lattice systems, and is thought to occur when the Fermi level is inside the hybridization energy gap [53]. For these systems, the physical properties are similar to those observed for Kondo lattice metals except that, as  $T$  decreases through  $T_{coh}$ , the conduction electron states are depopulated. As a result, the low  $T$  Pauli-like susceptibility is smaller than that seen for a Kondo lattice metal and the electrical resistivity reveals semiconducting behavior. Additionally, although the effective mass of the charge carriers is enhanced as the result of hybridization, the  $\gamma$  value is small because of the reduction in the number of charge carriers. In some cases, the energy gap can be closed via the Zeeman interaction by the application of a magnetic field and a large  $\gamma$  value is observed. Some compounds that have been described in this way are  $\text{SmB}_6$  [25, 26, 54, 55],  $\text{SmS}$  [22, 23, 24],  $\text{Ce}_3\text{Bi}_4\text{Pt}_3$  [56], several Ce-based filled skutterudites [57, 58, 59], etc. It should also be noted that for several of these compounds, the concept of intermediate valence has also been introduced to describe their physical properties.

### I.A.5 Quantum criticality

A quantum critical point (QCP) is a point in a phase diagram where a second order phase transition has been suppressed to  $T = 0$  by changing a control parameter (e.g. chemical substitution  $x$ , pressure  $P$ , magnetic field  $H$ ). QCPs are similar to classical critical points, except that a QCP is a zero temperature phase transition that influences the finite temperature behavior. To put it another way, the critical order parameter fluctuations for a phase transition at  $T = 0$  are quantum mechanical in nature. For instance, in some materials, it is possible to suppress a magnetic transition to  $T = 0$  with the application of pressure, as is the case for an archetypal QCP material, such as  $\text{CeIn}_3$  [47, 60, 61, 62, 63]. A schematic illustration of how a QCP might occur is given by the Doniach diagram where, with increasing  $|\mathcal{J}|N(E_F)$ , the magnetic ordering due to the RKKY interaction is suppressed towards zero at  $|\mathcal{J}_c|N(E_F)$  due to the screening of the magnetic moments as the result of the Kondo effect, which increases with increasing  $|\mathcal{J}|N(E_F)$ . At  $|\mathcal{J}_c|N(E_F)$ , there is a zero temperature transition between the magnetically ordered RKKY state and the paramagnetic Kondo singlet ground state, i.e. a QCP. There are several ways in which the QCP can influence the finite temperature behavior. In the case of  $\text{CeIn}_3$ , the QCP is hidden by the emergence of an unconventional superconducting state. Similar behavior is seen for the related compounds  $\text{CeRhIn}_5$  [64, 65],  $\text{CeCo}_{1-x}\text{Rh}_x\text{In}_5$  [66, 67],  $\text{CeCu}_2\text{Si}_2$  [43, 44, 45],  $\text{CePd}_2\text{Si}_2$  [47, 60, 68], etc. It is also widely believed that the high temperature superconductivity observed in the cuprate superconductors is the result of a QCP. For all of these materials, it is possible that, instead of the conventional phonon pairing mechanism, the superconductivity is mediated by excitations that are related to the QCP, such as spin fluctuations. In addition to superconductivity, non-Fermi-liquid behavior is often observed in the vicinity of a QCP [69, 70, 71, 72, 73, 74]. In general, non-Fermi-liquid behavior is simply the lack of Fermi liquid behavior and is often seen in electrical resistivity, magnetic susceptibility, and specific heat

as the following types of temperature dependences,

$$\rho(T) = \rho_0 + AT^n \quad (\text{I.21a})$$

$$\chi(T) = -A \ln T, \text{ or } T^{-a} \quad (\text{I.21b})$$

$$C(T)/T = -B \ln T, \text{ or } T^{-b} \quad (\text{I.21c})$$

where  $n < 2$ . It should be noted that, in addition to the QCP scenario, there are several other proposed routes to non-Fermi-liquid behavior including; (1) Kondo disorder, where a range of Kondo temperatures are allowed including  $T_K = 0$  K [75, 76, 77], (2) the Griffiths phase model [78], and (3) the quadrupolar Kondo model [79]. These pictures have been moderately successful in describing numerous non-Fermi-liquid systems [71].

Each of the models that are mentioned in the preceding paragraph require the presence of integral valence  $d$ - or  $f$ -electrons. If the intermediate valence picture is adopted instead, then a different route to a QCP is possible where a transition from an integral valence to intermediate valence state is suppressed to  $T = 0$  and the non-Fermi-liquid behavior would be correlated with quantum valence fluctuations. This possibility has been proposed for several compounds, most notably  $\text{CeCu}_2\text{Si}_2$ ,  $\text{CeCu}_2\text{Ge}_2$ ,  $\text{CePd}_2\text{Si}_2$ , and the alloy  $\text{CeCu}_2(\text{Si}_{1-x}\text{Ge}_x)_2$  [45, 80, 81, 82, 83, 84]. The low pressure region of the  $T$ - $P$  phase diagram for these compounds is similar to that seen for heavy fermion superconductors such as  $\text{CeIn}_3$  and  $\text{CeMIn}_5$  ( $M = \text{Co}, \text{Rh}$ ) where antiferromagnetic order is suppressed with increasing pressure towards a QCP, around which a superconducting dome is observed at low temperatures [61, 64, 66, 67]. Higher pressures then tune the Ce ion from integral to intermediate valence, resulting in a second superconducting dome near a QCP associated with the valence transition. The region surrounding the superconducting dome maximum is also accompanied by non-Fermi-liquid behavior. Thus, although the most commonly described model for a QCP involves the suppression of magnetic order with a tuning parameter, it is worth noting that other types of

QCPs are, in principle, possible including those that involve valence fluctuations, metal-insulator transitions, quadrupolar order, and others.

### I.B Filled skutterudites

The skutterudites are a well known class of compounds that have generated intense activity during the past three decades due to the wide variety of interesting electronic and magnetic phenomena that they have been shown to exhibit including: spin fluctuations, itinerant electron ferromagnetism, local moment ferromagnetism and antiferromagnetism, conventional BCS (Bardeen-Cooper-Schreiffer) superconductivity, unconventional superconductivity, hybridization gap semiconducting behavior, heavy fermion behavior, non-Fermi-liquid behavior, etc. [85, 86, 87, 88, 89]. The term skutterudite originally refers to a naturally occurring mineral with the chemical formula  $\text{CoAs}_3$ , which was mined as a source of cobalt and nickel in Skutterud, Norway. The skutterudite mineral structure was originally characterized in 1928 by I. Oftedal and has the chemical formula  $\text{TX}_3$  where the transition metal  $T = \text{Co, Rh, Ir}$  and the pnictogen  $X = \text{P, As, Sb}$  [90]. The crystal structure of these compounds has two large voids per unit cell which were first exploited in 1977 by W. Jeitschko and D. Braun to accommodate a variety of atoms, thereby introducing the “filled” skutterudite structure and consequently initiating modern interest in the filled skutterudites [91, 92, 93].

Filled skutterudites have the chemical formula  $\text{MT}_4\text{X}_{12}$ . Until recently, it was generally accepted that the “filler” atom  $M = \text{La-Nd, Sm, Eu, Yb, U, and Th}$ , the transition metal  $T = \text{Fe, Ru, Os}$ , and the pnictogen  $X = \text{P, As, Sb}$ . For these compositions, it had been shown that  $T$  can be replaced with transition metals from adjacent rows, such as  $\text{Co}$  [94]. It was subsequently shown that filled skutterudites with  $M = \text{alkali metal and alkaline earth, Hf, Tl}$ ,  $T = \text{Fe, Ru, Os}$ , and  $X = \text{Sb}$  can be formed [95, 96]. Around the same time, filled skutterudites with the small atomic radius rare earth ions  $M = \text{Y, Gd-Lu}$ ,  $T = \text{Fe, Ru, Os}$  and  $X$

= P were also synthesized using a high pressure technique [97, 98, 99], which was also applied to  $\text{La}_x\text{Rh}_4\text{P}_{12}$  [100]. More recently, the filled skutterudite family was expanded to include  $M = \text{Sr}, \text{Ba}, \text{La-Nd}, \text{Eu}, \text{Th}, T = \text{Pt}$ , and  $X = \text{Ge}$  [101, 102].

Filled skutterudites crystallize in the cubic space group  $\text{Im}\bar{3}$  with two formula units per unit cell (Fig.I.2) and are characterized by large lattice constants  $a \sim 7.8\text{-}9.3 \text{ \AA}$ . The rare earth position is  $(0, 0, 0)$ , the transition metal position is  $(0.25, 0.25, 0.25)$  and the pnictogen position is  $(0, y, z)$  where the parameters  $y \sim 0.35$  and  $z \sim 0.16$  are variable depending on the particular chemical composition. It is important to note that the variation in the values of  $y$  and  $z$  is due to the fact that the pnictogen rings are not perfect squares and that the  $\text{MX}_6$  canted octahedra are distorted. This property has important implications for the phenomena that emerge in these systems.

In addition to the wealth of correlated electron phenomena that are observed in these compounds, some of the filled skutterudites show promising thermoelectric properties at elevated temperatures (600-900 K) which generated new excitement in the topic of the filled skutterudites in the mid-1990s. The thermoelectric potential of a material is quantified by the figure of merit  $Z = \sigma S^2 / \lambda$  where  $\sigma$  is the electrical conductivity,  $S$  is the Seebeck coefficient or the thermopower, and  $\lambda$  is the thermal conductivity, which is the sum of an electronic ( $\lambda_e$ ) and a lattice ( $\lambda_l$ ) component. For the filled skutterudites,  $\lambda_l$  is reduced from that of more conventional materials as the result of the motion or “rattling” of the  $M$  filler ions which incoherently scatter phonons as the result of the filler ion’s large amplitude oscillations, in addition to tunneling between equivalent off-center sites within the  $X$  cage. The reader is referred to one of several reviews for more information [85, 103, 104, 105].

### I.B.1 Ce-based filled skutterudites

An interesting sub-class of the filled skutterudites are those that include the element Ce. These compounds are characterized by strong hybridization be-

tween the conduction electron and the localized  $f$ -electron states and the resultant correlated electron behavior is a delicate function of various parameters, including the lattice constant  $a$ , the electronic configuration of the  $T - X$  sublattice, and the presence of impurities which can influence the electronic and magnetic states. For instance, as the lattice constant increases for the series P, As, and Sb, the strength of the hybridization apparently decreases, causing the Ce atoms to behave more like localized  $\text{Ce}^{3+}$  ions, although even for the Sb-based compounds the effects of hybridization are not negligible [57]. The importance of the electronic configuration is most apparent in the differences in behavior for the series Fe, Ru, Os where the arsenides and phosphides appear to traverse quantum critical points that are centered near the Ru members, both of which show non-Fermi-liquid behavior [58, 106]. Currently, the order parameters for the possible quantum critical points remain under investigation. The phenomena that manifest as the result of these competing effects are summarized in Fig.I.3.

For the Ce-based  $X = \text{P}$  and  $\text{As}$  examples, the effects of hybridization are first seen as reductions in  $a$  from the values expected for typical lanthanide contractions for ions with a valence of  $3+$ . The reduced lattice constants are accompanied by unusual magnetic susceptibilities that are strongly suppressed below the values expected for  $\text{Ce}^{3+}$  ions according to Hund's rules (Fig. I.4) [59, 106, 107, 108, 109]. In contrast to the phosphides and arsenides, the antimonides show magnetic behavior that is similar to that expected for  $\text{Ce}^{3+}$  ions at temperatures above 100 K [58, 110, 111]. However, around 100 K, the magnetic susceptibilities of the antimonides go through a broad hump and, with decreasing  $T$ , begin to resemble those seen for the phosphides and arsenides. At low  $T$ , these compounds also show a weak increase in  $\chi(T)$  with decreasing  $T$ , the origin of which remains uncertain but could either be intrinsic, as for non-Fermi-liquid behavior or  $T$ -dependant intermediate valence behavior, or due to the presence of a low concentration of magnetic impurities. For more than half of the Ce-based filled skutterudites, the suppressed magnetic behavior is accompanied by small energy

gap semiconducting behavior ( $\Delta/k_B = 1500\text{-}10\text{ K}$ ) as shown in Fig. I.5, where the gap size is inversely proportional to the lattice constant [57]. The members of this family that are not semiconductors are particularly interesting, showing non-Fermi-liquid behavior for  $\text{CeRu}_4\text{As}_{12}$  [106] and  $\text{CeRu}_4\text{Sb}_{12}$  [58], heavy fermion behavior for  $\text{CeFe}_4\text{Sb}_{12}$  [112], and semimetallic behavior for  $\text{CeFe}_4\text{As}_{12}$  [108]. It is also apparent that sample dependence, i.e. structural or chemical disorder, plays an important role in the correlated electron behavior seen in these compounds. This result makes it necessary to synthesize high quality single crystal specimens in order to study the intrinsic properties of these compounds. In this thesis, and the publications associated with it, results for single crystals of the compounds  $\text{CeRu}_4\text{As}_{12}$  and  $\text{CeOs}_4\text{As}_{12}$ , which were synthesized by a unique high pressure molten metal flux technique, are presented.

### I.B.2 $\text{CeRu}_4\text{As}_{12}$

As discussed in Chapter III,  $\text{CeRu}_4\text{As}_{12}$  shows non-Fermi-liquid behavior and is the second Ce-based filled skutterudite compound, after  $\text{CeRu}_4\text{Sb}_{12}$ , to do so. The non-Fermi-liquid behavior is apparent in the low temperature electrical resistivity data which are described for nearly two decades in temperature ( $65\text{ mK} < T < 3.5\text{ K}$ ) by a power law of the form  $\rho(T) = \rho_0 + AT^n$  where  $n = 1.4$ . This unusual  $\rho(T)$  evolution is complemented by a low temperature divergence in the specific heat divided by temperature  $C(T)/T$  for  $650\text{ mK} < T < 2.6\text{ K}$  that can be described by either a weak power law  $C(T)/T \sim T^{-l}$  where  $l = 0.97$  or a logarithmic function  $C(T)/T \sim -\ln T$ . The  $T$ -dependence of the  $\chi(T)$  data provides further evidence for non-Fermi-liquid behavior and are described, for  $1.9\text{ K} < T < 10\text{ K}$ , by either a power law  $T^{-m}$  where  $m = 0.49$ , or a logarithmic function. Measurements also show that the temperature dependence of the thermoelectric power  $S(T)$  deviates from that expected for a Fermi liquid and has a feature near  $5\text{ K}$  which coincides with the upper limit for non-Fermi-liquid behavior observed in the other measurements. Unusual  $T$  dependences are also observed for  $10\text{ K}$

$< T < 300$  K, and are most pronounced in the  $\chi(T)$  data which decrease with decreasing  $T$  down to  $\sim 90$  K. This behavior is particularly interesting, as it signals a transition to a nonmagnetic state at low  $T$ . As discussed above, there are two well-known models that describe such an evolution in magnetism: (1) the  $T$ -dependent intermediate valence picture and (2) the Kondo lattice picture. If the Kondo lattice picture is adopted, then the single ion Kondo temperature  $T_K$  must be above room  $T$  and coherent magnetic lattice effects must develop with decreasing  $T$ , thereby generating the non-Fermi-liquid behavior at low  $T$ , possibly through a magnetic quantum critical point (QCP) scenario. On the other hand, if the valence fluctuation picture is the correct description of the physics, it is possible that  $\text{CeRu}_4\text{As}_{12}$  is located near a QCP where valence fluctuations on the Ce ions, rather than the more common magnetic fluctuations, give rise to the non-Fermi-liquid state. For this reason,  $\text{CeRu}_4\text{As}_{12}$  represents an interesting new material for the investigation of non-Fermi-liquid behavior in Ce-based compounds [106].

### I.B.3 $\text{CeOs}_4\text{As}_{12}$

As reported in Chapter IV, measurements of x-ray diffraction,  $\rho(T)$ ,  $\chi(T)$ ,  $C(T)/T$ , and  $S(T)$  indicate that strong  $f$ -electron-conduction electron hybridization dominates the physics of  $\text{CeOs}_4\text{As}_{12}$ , yielding a variety of behavior types which can be roughly divided into high ( $T > 135$  K) and low ( $T < 135$  K) temperature regions. For  $T > 135$  K, the unusual behavior is most pronounced in the  $\chi(T)$  data, which deviate from the typical Curie-Weiss  $T$ -dependence expected for  $\text{Ce}^{3+}$  ions and instead decrease with decreasing  $T$  to a broad minimum near  $135 \text{ K} < T < 150$  K. Again, the origin of this  $T$ -dependence is unclear, but possible mechanisms include valence fluctuations and Kondo behavior. The effects of  $f$ -electron-conduction electron hybridization become even more pronounced below 135 K, where  $\rho(T)$  reflects the formation of a gapped semiconducting state which persists to the lowest  $T$  measured ( $\sim 65$  mK). The increase in  $\rho(T)$  is not well described by a simple Arrhenius function, as would be expected for a semiconductor

with a single energy gap. Instead, a phenomenological expression that includes three energy gaps ( $\Delta_1/k_B = 73$  K,  $\Delta_2/k_B = 16$  K,  $\Delta_3/k_B = 2.5$  K) describes the data. A possible interpretation of this picture is that the large gap  $\Delta_1$  represents the intrinsic energy gap for  $\text{CeOs}_4\text{As}_{12}$ , while  $\Delta_2$  and  $\Delta_3$  describe impurity donor or acceptor states in the gap (Kondo holes), although the possibility of a pseudo-gap can not be ruled out. In this situation, it is expected that the application of a magnetic field will act to close the energy gaps through the Zeeman interaction. Experiments show that for  $H = 1.5$  T,  $\rho(T)$  is strongly reduced at low  $T$  from the zero field value, suggesting that Zeeman splitting plays an important role in the low  $T$  behavior. Concurrent with the emergence of the semiconducting behavior,  $\chi(T)$  increases slowly down to  $T^* \sim 45$  K, where it goes through a maximum and then continues to decrease with decreasing  $T$ . Therefore, there is an apparent correlation between the intrinsic energy gap value  $\Delta_1/k_B$  taken from fits to  $\rho(T)$  and the broad maximum in  $\chi(T)$  centered around  $T^* \sim 45$  K. If  $T^*$  is taken to indicate the onset of a coherent nonmagnetic ground state where  $T^* \sim T_{coh} \sim \Delta_1/k_B$ , then the likely description of the ground state is the well-known many body hybridization gap picture, where the magnetic moments of the  $\text{Ce}^{3+}$   $f$ -electron lattice are screened by conduction electron spins via an antiferromagnetic exchange interaction. Additionally, the behavior of  $C(T)/T$  at low  $T$  supports the hybridization gap interpretation, for which the low  $T$  electronic specific heat coefficient  $\gamma = C(T)/T$  is expected to be zero in the fully gapped scenario, or small and finite if a low concentration of donor or acceptor levels are present. For  $\text{CeOs}_4\text{As}_{12}$ ,  $\gamma$  is near  $19$  mJ/mol-K<sup>2</sup> and is somewhat sample dependent. The  $T$  dependence of the thermoelectric power provides further insight into the hybridization gap picture. Since  $S(T)$  remains positive over the entire  $T$  range, it appears that charge carriers excited from the top of the valence band to the conduction band dominate the transport behavior for all  $T$ . However, a single energy gap and charge carrier picture does not adequately describe the  $T$  dependence of the data, and instead features in  $S(T)$  closely correspond to those seen in  $\rho(T)$  [59].

## I.C Thin film filled skutterudites

Chapter V summarizes experimental results for thin film synthesis studies of the filled skutterudite  $\text{YbFe}_4\text{Sb}_{12}$ . In order to produce thin films of filled skutterudites, the appropriate growth conditions for synthesis via the pulsed laser deposition technique were developed in the Maple Group at the University of California, San Diego, as described in Chapter II. This work produced thin films of  $\text{PrFe}_4\text{Sb}_{12}$  and  $\text{YbFe}_4\text{Sb}_{12}$ . Thin films of  $\text{PrFe}_4\text{Sb}_{12}$  were grown under a variety of conditions where substrate temperature, annealing schedule, and laser power were optimized to produce single phase material. Various substrates were used for film growth. X-ray diffraction data indicate that the films are primarily single phase with very small amounts of antimony inclusions. The high quality of the films is reflected in  $\rho(T)$  data, which are consistent with previous results for bulk polycrystalline and single crystal specimens of  $\text{PrFe}_4\text{Sb}_{12}$  [113]. Based on the growth conditions for  $\text{PrFe}_4\text{Sb}_{12}$  films,  $\text{YbFe}_4\text{Sb}_{12}$  films were synthesized where the film thickness ( $t$ ) was varied from 6000 to 300 Å [114, 115]. Thick films ( $t > 1000$  Å) show electrical transport behavior similar to that seen for bulk polycrystal and single crystal specimens. A metal to insulator transition is observed for thin films ( $t < 1000$  Å) in electrical resistivity measurements. Since certain film topologies, such as poor intergrain connectivity, are known to promote metal to insulator transitions in granular systems, scanning electron microscope images were collected to explore the film morphology. These measurements revealed that a continuum of topologies, ranging from almost complete surface filling to the inclusion of large surface voids, are present in these films, suggesting that during sample growth, the lower levels of the film are strongly influenced by small variations in the growth conditions. These results may have implications for the development of filled skutterudite thin films for use in thermoelectric devices. Additionally, the ability to control the granularity of thin film specimens provides as additional tuning parameter which may be useful for understanding the correlated electron behavior seen

in these and other filled skutterudite materials.

## I.D Concluding remarks

A major theme in modern condensed matter physics has been the study of phenomena associated with correlated electrons in solids, for which the filled skutterudites have provided a significant reservoir of new materials. In particular, the Ce-based filled skutterudites have been shown to exhibit several types of behaviors that are characterized by strong hybridization between the conduction electron and the localized  $f$ -electron states. Moreover, the delicate interplay between several types of interactions provides the opportunity to turn several “knobs” such as pressure, chemical doping, and disorder (as for thin films) to reveal the underlying mechanisms for the phenomena that are observed. As such, the filled skutterudites have played an important role in the development and understanding of correlated electron materials and, as new subsets are synthesized, likely hold more exciting phenomena yet to be discovered. Finally, they also remain promising candidates for thermoelectric applications.

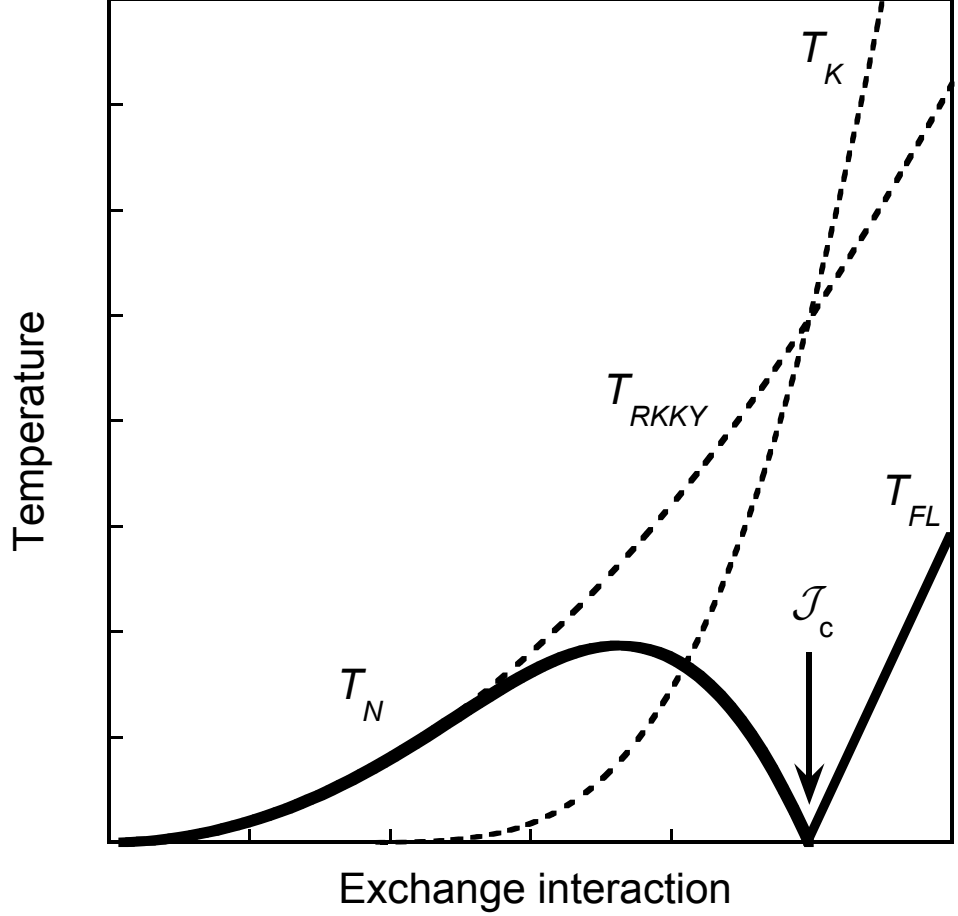


Figure I.1: The Doniach phase diagram, where the temperatures  $T_K \propto \exp(-1/|\mathcal{J}|N(E_F))$  and  $T_{RKKY} \propto \mathcal{J}^2 N(E_F)$  are plotted vs the exchange interaction  $|\mathcal{J}|N(E_F)$  [33], illustrating a hypothetical competition between the RKKY and Kondo interactions. The actual ordering temperature (bold line) initially increases with increasing  $|\mathcal{J}|N(E_F)$ , as the strength of the RKKY interaction increases. However, as the strength of the Kondo interaction becomes comparable to that of the RKKY interaction, the actual magnetic ordering temperature is suppressed, by comparison to the value expected according to the RKKY interaction, and then driven towards  $T = 0$  at  $|\mathcal{J}_c|N(E_F)$ . Thus, for small  $|\mathcal{J}|N(E_F)$ , the RKKY interaction is strongest, yielding a magnetic ground state. For large values of  $|\mathcal{J}|N(E_F)$ , the Kondo interaction is dominant, leading to a paramagnetic (sometimes Fermi liquid) ground state. For real systems,  $|\mathcal{J}|N(E_F)$  is tuned by parameters such as chemical substitution  $x$ , pressure  $P$ , and magnetic field  $H$ .

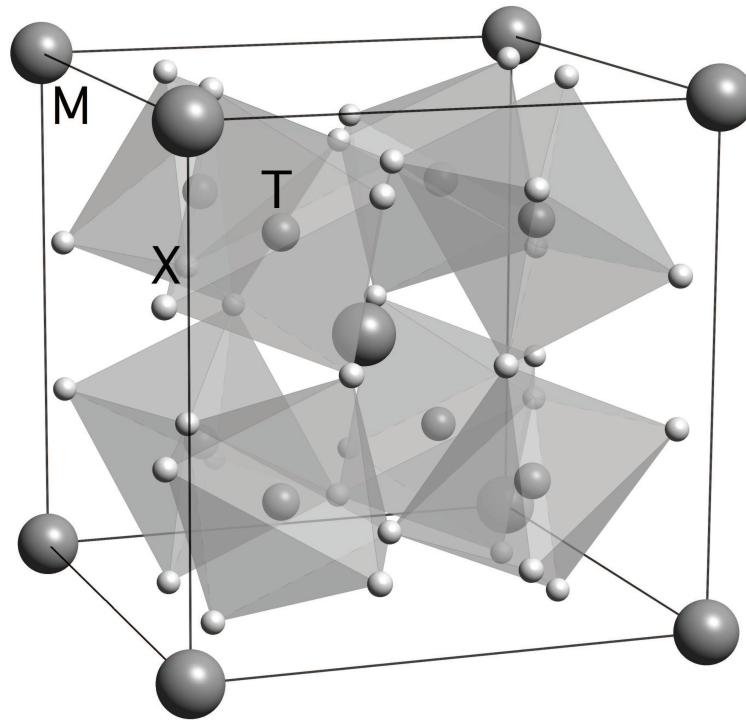


Figure I.2: Filled skutterudites have the chemical formula  $MT_4X_{12}$  and crystallize in the cubic space group  $Im\bar{3}$  with two formula units per unit cell. The lattice constant  $a$  is large  $\sim 7.8-9.3$  Å. The rare earth position is  $(0, 0, 0)$ , the transition metal position is  $(0.25, 0.25, 0.25)$  and the pnictogen position is  $(0, y, z)$  where the parameters  $y \sim 0.35$  and  $z \sim 0.16$  are variable depending on the particular chemical composition.

<b>Ce</b>		<b><i>Fe</i></b>	<b><i>Ru</i></b>	<b><i>Os</i></b>
	<b><i>P</i></b>	Semicond. $\Delta \sim 1500$ K	Semicond. $\Delta \sim 900$ K	Semicond. $\Delta \sim 400$ K
	<b><i>As</i></b>	Weakly magnetic semimetal	NFL	Semicond. $\Delta \sim 50$ K
	<b><i>Sb</i></b>	Heavy fermion $T_{\text{coh}} \sim 150$ K	NFL	Semicond. $\Delta \sim 10$ K

Figure I.3: A grid summarizing the physical behavior observed for  $\text{CeT}_4\text{X}_{12}$ . More than half of these compounds are weakly magnetic semiconductors where the gap size is correlated with the lattice constant. The remaining As-based members of the series are weakly magnetic and show strongly correlated electron behavior. The remaining Sb-based members are similar to their As analogues, except that they show magnetic behavior similar similar to that expected for  $\text{Ce}^{3+}$  ions.

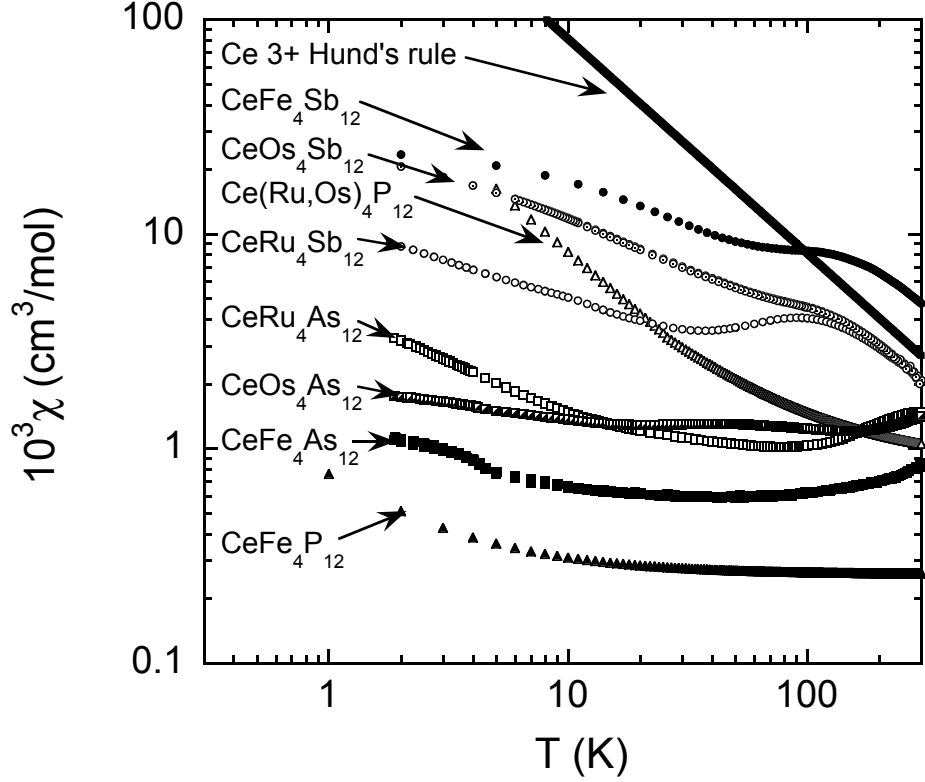


Figure I.4: Magnetic susceptibility  $M/H = \chi(T)$  for the Ce-based filled skutterudites showing that for the P and As-based versions, strong hybridization between the Ce ions and the conduction electron ions results in weakly magnetic or nonmagnetic behavior below room  $T$ . For the Sb-based versions, the magnetic susceptibility is similar to that expected for  $\text{Ce}^{3+}$  ions for  $T > 100$  K, where the development of a Kondo coherent state appears to suppress  $\chi(T)$ . The straight line is the expected  $\chi(T)$  for  $\text{Ce}^{3+}$  ions according to Hund's rules. [58, 59, 106, 107, 108, 109, 110, 111].

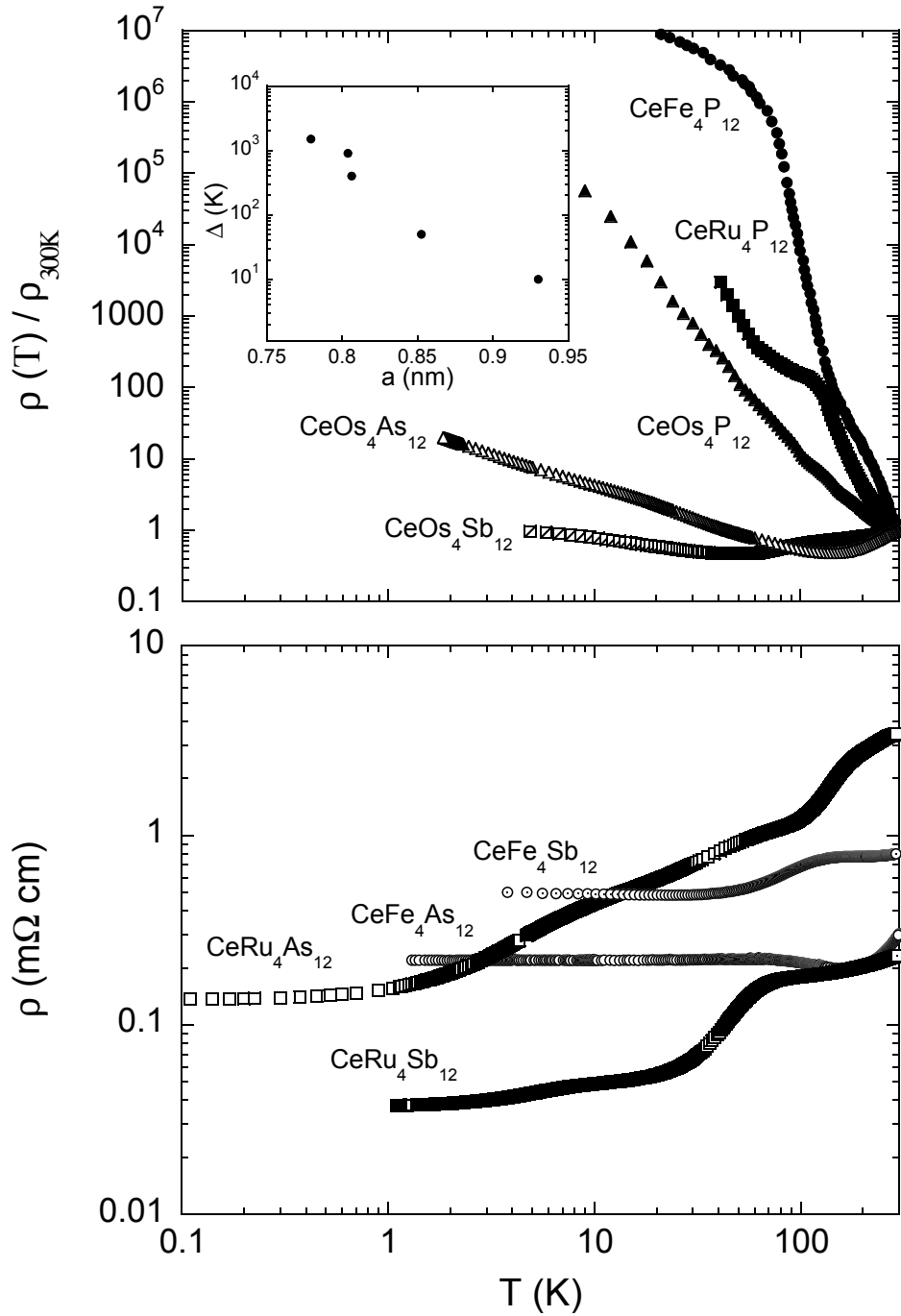


Figure I.5: Electrical resistivity for the Ce-based filled skutterudites showing that, for more than half of these compounds, the transport behavior is semiconducting where the energy gap size decreases with increasing lattice constant. The remaining members of the series exhibit poor metal behavior, with non-Fermi liquid behavior appearing at low  $T$  for  $\text{CeRu}_4\text{As}_{12}$  and  $\text{CeRu}_4\text{Sb}_{12}$  and a Kondo coherent state for  $\text{CeFe}_4\text{Sb}_{12}$ . [57, 106, 108, 112]

## Bibliography

- [1] N. W. Ashcroft and N. D. Mermin, *Solid State Physics*, Harcourt Brace College Publishers, Fort Worth, 1976.
- [2] M. P. Marder, *Condensed Matter Physics*, John Wiley and Sons, INC, New York, 2000.
- [3] L. D. Landau, Sov. Phys. JETP **3**, 920 (1957).
- [4] L. D. Landau, Sov. Phys. JETP **5**, 101 (1957).
- [5] L. D. Landau, Sov. Phys. JETP **8**, 70 (1959).
- [6] A. J. Legget, Rev. Mod. Phys **47**, 331 (1975).
- [7] E. S. R. Gopal, *Specific Heats at Low Temperatures*, Plenum Press, New York, 1966.
- [8] S. Blundell, *Magnetism in Condensed Matter*, Oxford University Press, Oxford, 2001.
- [9] W. J. de Haas, J. H. de Boer, and G. J. van den Berg, Physica **1**, 1115 (1934).
- [10] G. J. V. den Berg and C. J. Gorter, Helvetica Physica Acta **41**, 1230 (1968).
- [11] M. B. Maple, L. E. DeLong, and B. C. Sales in *Handbook on the Physics and Chemistry of Rare Earths Vol 1 - Metals*, eds K. A. Gschneider, Jr. and L. R. Eyring (North-Holland Publishing Company, Amsterdam, 1978), pp. 797-846.
- [12] J. Kondo, Prog. Theor. Phys. (Kyoto) **32**, 37 (1964).
- [13] P. G. deGennes, J. Phys. Rad. **23**, 510 (1962).
- [14] A. A. Abrikosov, Sov. Phys. JETP **23**, 660 (1965).
- [15] H. Suhl, Phys. Rev. **138**, A515 (1965).
- [16] A. A. Abrikosov, Physics **2**, 5 (1965).
- [17] K. G. Wilson, Rev. Mod. Phys. **47**, 773 (1975).
- [18] P. W. Anderson, Journal of Physics C: Solid State Physics **3**, 2436 (1970).
- [19] P. Schlottmann and P. D. Sacramento, Adv. Phys. **42**, 641 (1993).
- [20] A. C. Hewson, *The Kondo Problem to Heavy Fermions*, Cambridge University Press, Cambridge, 1993.
- [21] M. R. MacPherson, G. E. Everett, D. Wohlleben, and M B. Maple, Phys. Rev. Lett. **26**, 20 (1971).

- [22] A. Jayaraman, V. Narayanamurti, E. Bucher, and R. G. Maines, *Phys. Rev. Lett.* **25**, 1430 (1970)
- [23] M. B. Maple and D. Wohlleben, *Phys. Rev. Lett.* **27**, 511 (1971).
- [24] M. B. Maple and D. Wohlleben, *AIP Conference Proceedings* **18**, 447 (1974).
- [25] A. Menth, E. Beuhler, and T. H. Geballe, *Phys. Rev. Lett.* **22**, 295 (1969).
- [26] A. Jayaraman in *Handbook on the Physics and Chemistry of Rare Earths, Vol 2 - Alloys and Intermetallics*, eds K. A. Gschneider, Jr. and L. R. Eyring (North-Holland Publishing Company, Amsterdam, 1979), pp 575-611.
- [27] P. W. Anderson, *Phys. Rev.* **124**, 41 (1961).
- [28] J. R. Schrieffer and P. A. Wolff, *Phys. Rev.* **149**, 491 (1966).
- [29] B. Coqblin and J. R. Schrieffer, *Phys. Rev.* **185**, 847 (1969).
- [30] M. A. Ruderman and C. Kittel, *Phys. Rev.* **96**, 99 (1954).
- [31] T. Kasuya, *Prog. Theoret. Phys.* **16**, 45 (1956).
- [32] K. Yosida, *Phys. Rev.* **106**, 893 (1959).
- [33] S. Doniach, *Physica B* **91**, 231 (1977).
- [34] G. R. Stewart, *Rev. Mod. Phys.* **56**, 755 (1984).
- [35] N. Grewe and F. Steglich, in *Handbook on the Physics and Chemistry of Rare Earths, Vol 14*, edited by K. A. Gschneidner, Jr and L. Eyring (North-Holland, Amsterdam, 1991) pp. 343.
- [36] Z. Fisk, H. R. Ott, T. M. Rice, and J. L. Smith, *Nature* **320**, 124 (1986).
- [37] Z. Fisk, J. D. Thompson, and H. R. Ott, *J. Magn. Magn. Mater.* **76**, 637 (1988).
- [38] H. R. Ott and Z. Fisk, in *Handbook on the Physics and Chemistry of the Actinides, Vol 5*, edited by A. J. Freeman and G. H. Lander (North-Holland, Amsterdam, 1987) pp. 85.
- [39] R. Heffner and M. Norman, *Comments Cond. Mat. Phys.* **17**, 361 (1996).
- [40] D. W. Hess, P. S. Riseborough, and J. L. Smith, in *Encyclopedia of Applied Physics, Vol 7* (VCH, New York, 1993) pp. 435.
- [41] P. Coleman, C. Pepin, Qimiao Si, and R. Ramazashvili, *J. Phys.:Condens. Matter* **13**, R723 (2001).
- [42] K. Kadowaki and S. B. Woods, *Solid State Commun.* **58**, 507 (1986).

- [43] F. Steglich, J. Aarts, C. D. Bredl, W. Lieke, D. Meschede, W. Franz, H Schäfer, Phys. Rev. Lett. **43**, 1892 (1979).
- [44] P. Coleman, C. Pepin, Q. Si, and R. Ramazashvili, Phys. Rev. Lett. **43**, 1892 (1979).
- [45] H. Q. Yuan, F. M. Grosche, M. Deppe, C. Geibel, G. Sparn, and F. Steglich, Science **302**, 2104 (2003).
- [46] L. E. DeLong, J. G. Huber, K. N. Yang, and M. B. Maple, Phys. Rev. Lett. **51**, 312 (1983).
- [47] N. D. Mathur, F. M. Grosche, S. R. Julian, I. R. Walker, D. M. Freye, R. K. W. Haselwimmer, and G. G. Lonzarich, Nature **394**, 39 (1998).
- [48] C. Petrovic, P. G. Pagliuso, M. F. Hundley, R. Movshovich, J. L. Sarrao, J. D. Thompson, Z. Fisk, and P. Monthoux, J. Phys.: Condens. Matter **13**, L337 (2001).
- [49] H. R. Ott, H. Rudigier, Z. Fisk, and J. L. Smith, Phys. Rev. Lett. **50**, 1595 (1983).
- [50] C. Geibel, C. Schank, S. Thies, H. Kitazawa, C. D. Bredl, A. Böhm, M. Pau, A. Grauel, R. Caspary, R. Helfrich, U. Ahlheim, G. Weber, and F. Steglich, Z. Phys. B **84**, 1 (1991).
- [51] W. Schlabitz, J. Baumann, B. Pollit, U. Rauchschwalbe, H. M. Mayer, U. Ahlheim, and C. D. Bredl, Z. Phys B **62**, 171 (1986).
- [52] E. D. Bauer, N. A. Frederick, P.-C. Ho, V. S. Zapf, and M. B. Maple, Phys. Rev. B **65**, 100506(R) (2002).
- [53] P. S. Riseborough, Adv. in Phys. **49**, 257 (2000).
- [54] T. Kasuya, K. Takegahara, T. Fujita, and E. Banai, J. Phys. Coll. **C5**, 308 (1979).
- [55] J. W. Allen, B. Batlogg, and P. Wachter, Phys. Rev. B **20**, 4807 (1979).
- [56] M. F. Hundley, P. C. Canfield, J. D. Thompson, Z. Fisk, and J. M. Lawrence, Phys. Rev. B **42**, 6842 (1990).
- [57] H. Sugawara, S. Osaki, T. Namiki, S. R. Saha, Y. Aoki, and H. Sato, Phys. Rev. B **71**, 125127 (2005).
- [58] E. D. Bauer, A. Slebarski, R. P. Dickey, E. J. Freeman, C. Sirvent, V. S. Zapf, N. R. Dilley, and M. B. Maple, J. Phys.: Condens. Matter **13**, 5183 (2001).
- [59] R. E. Baumbach, P.-C. Ho, T. A. Sayles, M. B. Maple, R. Wawryk, T. Cichorek, A. Pietraszko, and Z. Henkie, Proc. Natl. Acad. Sci. **105**, 17307 (2008).

- [60] F. M. Grosche, I. R. Walker, S. R. Julian, N. D. Mathur, D. M. Freye, M. J. Steiner, and G. G. Lonzarich, *J. Phys.: Condens. Matter* **13**, 2845 (2001).
- [61] I. R. Walker, F. M. Grosche, D. M. Freye, and G. G. Lonzarich, *Physica C* **282**, 303 (1997).
- [62] G. Knebel, D. Braithwaite, P. C. Canfield, G. Lapertot, and J. Flouquet, *Phys. Rev. B* **65**, 024425 (2002).
- [63] S. Kawasaki, T. Mito, Y. Kawasaki, H. Kotegawa, G. q. Zheng, Y. Kitaoka, H. Shishido, S. Araki, R. Settai, and Y. Onuki, *J. Phys. Soc. Jpn.* **73**, 1647 (2004).
- [64] H. Hegger, C. Petrovic, E. G. Moshopoulou, M. F. Hundley, J. L. Sarrao, Z. Fisk and J. D. Thompson, *Phys. Rev. Lett.* **84**, 4986 (2000)
- [65] J. Paglione, P.-C. Ho, M. B. Maple, M. A. Tanatar, L. Taillefer, Y. Lee, and C. Petrovic, *Phys. Rev. B* **77**, 100505(R) (2008).
- [66] V. S. Zapf, E. J. Freeman, E. D. Bauer, J. Petricka, C. Sirvent, N. A. Frederick, R. P. Dickey, and M. B. Maple, *Phys. Rev. B* **65**, 014506 (2001).
- [67] J. R. Jeffries, N. A. Frederick, E. D. Bauer, H. Kimura, V. S. Zapf, K. D. Hof, T. A. Sayles, and M. B. Maple, *Phys. Rev. B* **72**, 024551 (2005).
- [68] F. M. Grosche, S. R. Julian, N. D. Mathur, and G. G. Lonzarich, *Physica B* **223**, 50 (1996).
- [69] J. A. Hertz, *Phys. Rev. B* **14**, 1165 (1973).
- [70] A. J. Millis, *Phys. Rev. B* **48**, 7183 (1993).
- [71] G. R. Stewart, *Rev. Mod. Phys.* **73**, 797 (2001).
- [72] M. B. Maple, C. L. Seaman, D. A. Gajewski, Y. Dalichaouch, V. B. Barbetta, M. C. de Andrade, H. A. Mook, H. G. Lukefahr, O. O. Bernal, D. E. MacLaughlin, *J. Low Temp. Phys* **95**, 225 (1994).
- [73] M. B. Maple, M. C. de Andrade, J. Hermann, Y. Dalichaouch, D. A. Gajewski, C. L. Seaman, R. Chau, R. Movshovich, M. C. Aronson, and R. Osborn, *J. Low Temp, Phys* **99**, 223 (1995).
- [74] C. L. Seaman, M. B. Maple, B. W. Lee, S. Ghamaty, M. S. Torikachvili, J.-S. Kang, L. Z. Liu, J. W. Allen, D. L. Cox, *Phys. Rev. Lett.* **67**, 2882 (1991).
- [75] O. O. Bernal, D. E. MacLaughlin, H. G. Lukefahr, and B. Andraka, *Phys. Rev. Lett* **75**, 2023 (1995).
- [76] E. Miranda, V. Dobrosavljevic, and G. Kotliar, *J. Phys.: Condens. Matter* **8**, 9871 (1996).

- [77] E. Miranda, V. Dobrosavljevic, and G. Kotliar, Phys. Rev. Lett. **78**, 290 (1997).
- [78] A. H. Castro Neto, G. Castilla, and B. A. Jones, Phys. Rev. Lett. **81**, 3531 (1998).
- [79] D. L. Cox, Phys. Rev. Lett. **59**, 1240 (1987).
- [80] A. Holmes, D. Jaccard, and K. Miyake, Phys. Rev. B **69**, 024508 (2004).
- [81] E. Vargoz and D. Jaccard, J. Mag. Mag. Mat. **177-181**, 294-295 (1998).
- [82] S. Raymond and D. Jaccard, Phys. Rev. B **61**, 8679 (2000).
- [83] A. Onodera, S. Tsuduki, Y. Ohishi, T. Watanuki, K. Ishida, Y. Kitaoka, and Y. Onuki, J. Solid State Comm. **123**, 113-116 (2002).
- [84] Y. Onishi and K. Miyake, J. Phys. Soc. Jpn. **69**, 3955 (2001).
- [85] B. C. Sales, in *Handbook on the Physics and Chemistry of the Rare Earths, Vol 33*, edited by K. A. Gschneider, Jr. (Elsevier science publishing Co., New York, New York, 2002) pp. 211.
- [86] M. B. Maple, E. D. Bauer, N. A. Frederick, P.-C. Ho, W. M. Yuhasz, and V. S. Zapf, Physica B **328**, 29 (2003).
- [87] Y. Aoki, H. Sugawara, H. Hisatomo, and H. Sato, J. Phys. Soc. Jpn. **74**, 209 (2005).
- [88] M. B. Maple, Z. Henkie, R. E. Baumbach, T. A. Sayles, N. P. Butch, P.-C. Ho, T. Yanagisawa, W. M. Yuhasz, R. Wawryk, T. Cichorek, and A. Pietraszko, J. Phys. Soc. Jpn. **77**, 7 (2008).
- [89] H. Sato, D. Kikuchi, K. Tanaka, M. Ueda, H. Aoki, T. Ikeno, S. Tatsuoka, K. Kuwahara, Y. Aoki, M. Koghi, H. Sugawara, K. Iwasa, and H. Harima, J. Phys. Soc. Jpn **77**, 1 (2008).
- [90] I. Oftedal, Z. Kristallogr. **A66**, 517 (1928).
- [91] W. Jeitschko and D. Braun, Acta Cryst. **B33**, 3401 (1977).
- [92] D. J. Braun and W. Jeitschko, J. Less Com. Met. **72**, 147 (1980).
- [93] D. J. Braun and W. Jeitschko, J. of Solid State Chem., **32**, 357 (1980).
- [94] V. Keppens, D. Mandrus, B. C. Sales, B. C. Chakoumakos, P. Dai, R. Coldea, M. B. Maple, D. A. Gajewski, E. J. Freeman, and S. Bennington, Nature **395**, 876 (1998).
- [95] G. S. Nolas, G. Yoon, H. Sellingschegg, A. Smalley, D. C. Johnson, Appl. Phys. Lett. **86**, 042111 (2005).

- [96] W. Schnelle, A. Leithe-Jasper, H. Rosner, R. Cardoso-Gil, R. Gumeniuk, D. Trots, J. A. Mydosh, and Y. Grin, *Phys. Rev. B* **77**, 094421 (2008).
- [97] K. Kihou, I. Shirotnani, Y. Shimaya, C. Sekine, and T. Yagi, *Mat. Res. Bul.* **39**, 317-325 (2004).
- [98] I. Shirotnani, N. Araseki, Y. Shimaya, R. Nakata, K. Kihou, C. Sekine, and T. Yagi, *J. Phys.:Condens. Matter* **17**, 4383-4391 (2005).
- [99] C. Sekine, H. Ando, Y. Sugiuchi, I. Shirotnani, K. Matsuhira, M. Wakeshima, *J. Phys. Soc. Jpn. Suppl. A* **77**, 135-141 (2008).
- [100] I. Shirotnani, S. Sato, C. Sekine, T. Keiki, I. Inagawa, T. Yagi, *J. Phys.: Condens. Matter* **17**, 7353-7357 (2005).
- [101] R. Gumeniuk, W. Schnelle, H. Rosner, M. Nicklas, A. Leithe-Jasper, and Y. Grin, *Phys. Rev. Lett.* **100**, 017002 (2008).
- [102] A. Grytsiv, X.-Q. Chen, N. Melnychenko-Koblyuk, P. Rogl, E. Bauer, G. Hilscher, H. Kaldarar, H. Michor, E. Royanian, R. Podlucky, M. Rotter, and G. Geister, *J. Phys. Soc. Jpn.* **77 Suppl.A**, 121-127 (2008).
- [103] B. C. Sales, D. Mandrus, and R. K. Williams, *Science* **272**, 1325 (1996).
- [104] J. P. Fleurial, A. Borshchevsky, T. Caillat, D. T. Morelli, and G. P. Meisner, *Proc. 15<sup>th</sup> International Conference on Thermoelectrics. IEEE Catalogue 96TH8169*, Piscataway, NJ, p. 91 (1996).
- [105] B. C. Sales, *Science* **295**, 1248-1249 (2002).
- [106] R. E. Baumbach, P.-C. Ho, T. A. Sayles, M. B. Maple, R. Wawryk, T. Cichorek, A. Pietraszko, and Z. Henkie, *J. of Phys.: Condens. Matter* **20**, 075110 (2008).
- [107] I. Shirotnani, T. Uchiumi, C. Sekine, M. Hori, and S. Kimura, *J. of Solid State Chem.* **142**, 146 (1999).
- [108] R. E. Baumbach, P.-C. Ho, T. A. Sayles, M. B. Maple, R. Wawryk, T. Cichorek, A. Pietraszko, and Z. Henkie, *Manuscript in preparation*.
- [109] G. P. Meisner, M. S. Torikachvili, K. N. Yang, M. B. Maple, and R. P. Guertin, *J. of Appl. Phys.* **57**, 3073 (1985).
- [110] D. Berardan, E. Alleno, and C. Godart, *Physica B* **359**, 865 (2005).
- [111] E. D. Bauer, A. Slebarski, E. J. Freeman, N. A. Frederick, B. J. Taylor, C. Sirvent, and M. B. Maple, *Physica B* **312**, 230 (2002).
- [112] E. D. Bauer, R. Chau, N. R. Dilley, M. B. Maple, D. Mandrus, and B. C. Sales, *Journal of Physics: Condensed Matter* **12**, 1261 (2000).

- [113] R. E. Baumbach, W. M. Yuhasz, and M. B. Maple, *Applied Physics A* **84**, 227 (2006).
- [114] R. E. Baumbach, W. M. Yuhasz, and M. B. Maple, *Physica B* **403**, 800 (2008).
- [115] R. E. Baumbach, W. M. Yuhasz, and M. B. Maple, *Thin Film Solids* **516**, 3378 (2008).

## II

# Sample Preparation

### II.A Flux growth of As-based filled skutterudites

The majority of studies addressing the filled skutterudites currently focus on the phosphide  $MT_4P_{12}$  and antimonide  $MT_4Sb_{12}$  ( $M=La-Nd, Sm, Eu, Yb$  and  $T=Fe, Ru, Os$ ) families, which are commonly synthesized using low pressure molten metal flux techniques [1, 2, 3, 4]. In contrast, the arsenides  $MT_4As_{12}$  have received considerably less attention; though not for a lack of interesting physical phenomena. The limited research in this direction may be due to materials difficulties related to the elevated vapor pressure of arsenic. Here, a high pressure technique for growing single crystals of the filled skutterudite arsenides, using an As rich Cd : As flux, is described. This section is mostly taken from a recent publication that was written in collaboration with Z. Henkie at the Institute of Low Temperature and Structural Research of the Polish Academy of Sciences [5], who is responsible for the development and implementation of this significant technical achievement. This method was originally applied to the growth of  $PrOs_4As_{12}$  single crystals, although it has been shown to be applicable to the synthesis of  $MT_4As_{12}$  ( $M=La, Ce, Pr$  and  $T=Fe, Ru, Os$ ) single crystals as well.

The  $CeT_4As_{12}$  ( $T=Fe, Ru, Os$ ) single crystals discussed in this dissertation were grown from elements with purities  $> 99.9\%$  by a mineralization process in

a molten Cd : As flux at high temperatures and pressures. The growths occurred over 3 - 4 week periods in carbon coated sealed quartz ampoules at 15 - 40 atm of pressure produced by As<sub>4</sub> vapor and Ar gas at the mineralization temperature 750 - 850 °C. The heating operations occurred in a specially designed pressure cell which is shown schematically in Fig. II.1. Following mineralization, the flux components were removed by sublimation and repeatedly used for subsequent crystallizations. After removing the majority of the flux by sublimation, filled skutterudite single crystals of an isometric form with typical dimensions 0.5 – 2.5 mm were collected and cleaned in acid to remove impurity phases from surface of the crystals prior to measurements. As illustrated in Fig. II.2, As-based filled skutterudite crystals typically have a regular bi-pyramid shape.

Since the vapor pressure of As is high at its melting temperature ( $P_{As}$  (817 °C) = 36 atm), As is difficult to use as a self flux for crystal synthesis. Moreover, small increases in temperature drastically increase  $P_{As}$ . This issue is resolved by inspection of the Cd : As phase diagram (Fig. II.3a) which shows that the metal As liquid phase can be extended to lower temperatures by the introduction of Cd [6]. Based on this observation, a Cd : As flux was chosen for the filled skutterudite arsenide growth experiments. Naturally, a primary question is what Cd : As ratio optimizes the filled skutterudite crystal growth. It was found that when the Cd : As ratio = 1/3 or 1/4 that PrOs<sub>4</sub>As<sub>12</sub> single crystals of size ~ 0.7 mm form at  $T \sim 800$  °C. For the Cd : As ratio > 1/2, single crystals do not form.

The growth experiments were performed in quartz ampoules with the following dimensions; 18 mm inside diameter, 20 cm<sup>3</sup> inner volume, and 2 mm wall thickness. The inside wall of the ampoule was covered with a layer of pyrolytic carbon. The elemental components of the  $MT_4As_{12}$  skutterudite and the flux were taken in the atomic ratio  $M:T:Cd:As = 1:4:12:48$  ( $MT_4As_{12} + 12 CdAs_3$ ), loaded into the quartz ampoule, and sealed in a vacuum environment. The ampoule was heated in a custom built high pressure cell which was filled with Ar of pressure equal to the predicted inner ampoule pressure at the growth temperature (see

calculations below). The heating rate was 20 °C/h from 350 to 650 °C, after which a much higher rate was used up to 730 °C. The ampoule was then heated and cooled down repeatedly between 730 and 800 °C for two weeks with the rate 3 °C/h. Finally, the ampoule was cooled to the ambient temperature at the rate 20 °C/h.

To simplify the growth of the filled skutterudite arsenides, the vapor pressure of CdAs<sub>2</sub> ( $P_{Cd:As}$ ) was estimated in the following way. A two chamber quartz ampoule was prepared where the volume of each chamber was  $\sim 15 \text{ cm}^3$  and the chambers were connected by a 1 cm long capillary with 1.5 mm inside diameter (Fig. II.3b). A 10 g specimen of CdAs<sub>2</sub> was placed in one of the chambers. The ampoule was then sealed with a small amount of Ar ( $P_{Ar} = 0.4 \text{ atm}$  at 293 K) and placed in a two zone furnace with the CdAs<sub>2</sub> located in the higher temperature region ( $T_2$ ) and the empty chamber in the lower temperature region ( $T_1$ ). The possibility of CdAs<sub>2</sub> being transported from chamber 2 to chamber 1 was explored up to  $T_2 = 950 \text{ °C}$  and  $T_1 = 850 \text{ °C}$ . Under these conditions, no material condensed in chamber 1 during 8 hour heating schedules. This result indicates that the vapor pressure of CdAs<sub>2</sub> was insufficient to force all of the Ar out of chamber 2, and thereby allow condensation in chamber 1.

In order to estimate an upper limit for  $P_{Cd:As}$  in chamber 1 for  $T_1 = 850 \text{ °C}$ , the competition between  $P_{Cd:As}$  and  $P_{Ar}$  in chambers 1 and 2 was considered. The temperature dependence of the CdAs<sub>2</sub> vapor pressure  $P_{Cd:As}$  can be approximated using the well known Clausius Clapyron law (CCL),

$$\log P = A/T + B \quad (\text{II.1})$$

where  $A = -7323.5$  and  $B = 8.2751$  are constants determined for arsenic vapor pressure  $P_{As}$  equal to 1 atm and 36 atm at temperature 613 and 817 °C, respectively. In contrast,  $P_{Ar}$  can be treated using the ideal gas law. If the Ar gas is completely displaced into chamber 1 by the CdAs<sub>2</sub> vapor, then the total pressure in chamber 1 will be  $P_1 = P_{Ar} + P_{1,Cd:As}$  where  $P_{Ar} = 3 \text{ atm}$  for  $T = 850 \text{ °C}$  while

the total pressure in chamber 2  $P_2 = P_{2,Cd:As}$ . Thus, in order for condensation to occur in chamber 1, the following must be true.

$$\Delta P_{Cd:As} = P_{2,Cd:As} - P_{1,Cd:As} > 3 \text{ atm} \quad (\text{II.2})$$

However, since no condensation is observed,  $\Delta P_{Cd:As}$  must be less than 3 atm. Moreover, the Clausius Clapyron states that,

$$\log(P_2/P_1) = A(T_1 - T_2)/(T_1T_2) \quad (\text{II.3})$$

and by using Eq. 3, it can be shown that  $P_2/P_1 = 3.41$  for  $T_2 = 950$  °C and  $T_1 = 850$  °C, and therefore  $P_{1,Cd:As} < 1.25$  atm. This value is substantially lower than the vapor pressure expected for an Cd : As liquid solution (for pure As  $\sim 57$  atm) at  $850$  °C, indicating that the CdAs<sub>2</sub> liquid is composed of CdAs<sub>2</sub> molecules.

Therefore, the Raoult law is used to determine the vapor pressure of As over the As-CdAs<sub>2</sub> liquid solution,

$$P_{lAs} = P_{As}[As]/([As] + [CdAs_2]) \quad (\text{II.4})$$

where [As] and [CdAs<sub>2</sub>] are the numbers of moles of dissolved As and solvent CdAs<sub>2</sub>, respectively. This expression yields an inner ampoule pressure that is over 42 atm when CdAs<sub>3</sub> flux is heated to  $880$  °C. Therefore, although this value is smaller than that for pure As, ampoule disintegration remains a concern at high temperatures and the high pressure cell remains a necessity for this type of growth technique.

After growth, the solidified flux with filled skutterudite crystals was placed in a 20 cm long quartz ampoule and sealed under high vacuum. The ampoule was then placed in a two zone furnace where the flux was sublimated from a high temperature zone  $T_2 = 600$  °C to a low temperature zone  $T_1 = 400$  °C. The flux condensed in the cold zone in two spatially separated sections which consisted of As and CdAs<sub>2</sub>. The CdAs<sub>2</sub> condensed just beyond the hot zone while the As con-

densed at the coldest end of the ampoule. The filled skutterudite crystals were then collected and rinsed in acid.

## II.B Pulsed laser deposition of filled skutterudites

The growth of thin films by the pulsed laser deposition (PLD) technique is well known and commonly used to synthesize both oxide and intermetallic materials. As for all thin film synthesis techniques, its main advantages over bulk growth are that precise geometric control is possible and the growth of thin films enables the study of physics at interfaces. There are several excellent reviews of thin film synthesis by PLD which are noted for reference [7, 8, 9]. Here, the details of the PLD apparatus used to synthesize thin films of filled skutterudites are presented, in addition to the growth experiment for the  $\text{PrFe}_4\text{Sb}_{12}$  films. A similar procedure was used to synthesize the  $\text{YbFe}_4\text{Sb}_{12}$  films reported in Chapter V.

The apparatus for growing thin films by PLD is conceptually simple and consists of a pulsed excimer laser, focusing optics, and a high vacuum chamber. There are several excimer lasers that are commercially available, with wavelengths ranging from  $\lambda = 152$  nm ( $\text{F}_2$ ) to  $\lambda = 351$  nm ( $\text{XeF}$ ). The laser used for the synthesis of the filled skutterudite thin films utilizes a KrF gas mixture for which  $\lambda = 248$  nm. When the beam is focused, the energy density reaches a maximum value of  $100$  J/cm<sup>2</sup>.

A schematic for the vacuum chamber is shown in Fig. II.4 where the main components are a turbo pump with backing pump, a home built gas flow system, a heater block, and a target rotator. For intermetallics like the filled skutterudites, it is important that the growth occur in ultraclean atmospheric conditions. This is accomplished by pumping the vacuum chamber to low pressures  $\sim 10^{-8}$ - $10^{-10}$  torr before growth. In order to reach such low pressures, a bakeout procedure is followed where the chamber is evacuated with a turbo pump and baked at  $T = 100$  °C using heater strips. Simultaneously, the heater block is baked at  $200$  °C.

Bakeout times are typically between 24-48 hours. The chamber is subsequently flushed several times with an ultra high purity inert gas, such as Ar. During ablation, the gas flow circuit is used to manage the tendency of elements with high vapor pressure to migrate and thereby cover the inner surfaces of the chamber, including the laser window. This process affects the film growth because, as the laser window is coated, it becomes opaque and the laser intensity at the target rapidly decreases over the course of a single growth. As shown in Fig. II.4, the gas flow system injects ultra high purity Ar near the laser window. The gas then flows back towards the turbo pump, which is at the center of the chamber. As a result, the ablated material that is travelling opposite the gas flow direction is slowed and partially prevented from reaching the laser window. During ablation, the pressure measured at the opposite end of the chamber is maintained near  $10^{-5}$  torr. The gas flow system is assisted by the presence of a metallic barrier that is placed in front of the laser window which allows the laser to enter the chamber through a slit in the barrier, but otherwise covers the interior of the laser window.

In order to prepare thin films using the PLD technique, it is necessary that an appropriate target be used. The target is often prepared by synthesizing a polycrystalline bulk specimen of the material that is to be deposited as a film. This can be done by arc-melting, solid state reaction, molten metal reaction, induction melting, etc. Once the polycrystalline material is prepared, it is either pressed (for powders) or cut (for intermetallic boules) to have two parallel surfaces and is mounted on the target rotator, as shown in Fig. II.4. The rotating target mount is used to uniformly ablate material during the growth. If a carousel with several target mounts is used, then it is possible to synthesize multilayer films. The target is located opposite to the heater block at a distance between 2-10 cm. A substrate, upon which the film will be grown, is mounted on the heater block using an adhesive such as silver paint. Although it is common practice to use polished crystalline substrates with lattice constants similar to that of the desired film, it is also conceivable that other types of materials, such as glass, might be used

as a substrate. Several types of crystalline substrate materials are commercially available, including MgO, Al<sub>2</sub>O<sub>3</sub>, SrTiO<sub>3</sub>, and yttria stabilized zirconia (YSZ). During a growth, the adjustable parameters are the heater block temperature, the chamber pressure, the laser energy density, and the laser pulse rate.

### II.B.1 PrFe<sub>4</sub>Sb<sub>12</sub> growth experiment

A PrFe<sub>4</sub>Sb<sub>12</sub> bulk target was synthesized by first sealing elemental Pr (4N), Fe (3N), and Sb (6N) in a ratio of 1 : 4 : 12.5 in a quartz tube (14 × 16 mm) under 150 torr UHP Ar. The tube was then heated to 1020 °C. At the end of 4 days, the tube was quenched in a centrifuge to prevent the formation of gas pockets and to force the melt to conform to the shape of the quartz tube. X-ray diffraction (XRD) measurements made on powder taken from the top and bottom of the boule indicated that the material in the target was uniformly mixed and consisted of the skutterudite phase in addition to free antimony and binary compounds such as PrFe<sub>2</sub> and FeSb<sub>2</sub>. The boule was then sliced using a diamond wheel saw to form a target. Interestingly, single phase PrFe<sub>4</sub>Sb<sub>12</sub> thin films were readily formed using the mixed phase target.

Polycrystalline PrFe<sub>4</sub>Sb<sub>12</sub> films with thicknesses near 5 μm were synthesized by pulsed laser deposition (PLD) using a Lambda Physik KrF laser with a wavelength of 248 nm. Before ablation, a pump/flush/bakeout procedure was performed in order to minimize background atmosphere in the vacuum chamber. Ablation took place in an atmosphere of 10<sup>-5</sup> torr UHP Ar. During ablation, the target was approximately 1.5 cm from the substrate and was rotated to continuously expose new target material. The estimated energy density of the beam on the target was 3.5 or 4.5 J/cm<sup>2</sup>, depending on the growth sequence, and the beam was pulsed at 15 Hz.

The films were grown on various substrates, each of which has a unique lattice constant  $a$ . Each substrate was chosen because its lattice constant is close to one-half that of PrFe<sub>4</sub>Sb<sub>12</sub> ( $a = 9.14$  Å). The substrates used were c-plane yttria

stabilized zirconia ( $a = 5.13 \text{ \AA}$ ), c-plane magnesium difluoride ( $a = 4.64 \text{ \AA}$ ), c-plane magnesium oxide ( $a = 4.23 \text{ \AA}$ ), c-plane silicon ( $a = 5.40 \text{ \AA}$ ), r-plane alumina ( $a = 4.76 \text{ \AA}$ ,  $b = 15.38 \text{ \AA}$ ), and c-plane strontium titanate ( $a = 3.90 \text{ \AA}$ ). The substrates had surface dimensions 0.25 cm to a side. During growth, they were engulfed by the ablated material that comprises the “plume”. This resulted in uniform film coverage on the substrate.

To determine optimal growth conditions, several films were grown at a variety of different temperatures. The films were then analyzed by XRD using a Rigaku x-ray diffractometer applying Cu K- $\alpha$  radiation. Electrical resistivity  $\rho(T)$  measurements in zero applied magnetic field were also performed using a Quantum Design Physical Properties Measurement System (PPMS) in a four-wire configuration.

Table II.1 summarizes the growth conditions and the quality of the resulting films. The XRD data indicate that films grown below 300 °C are amorphous. For films grown between 300 °C and 400 °C, the XRD data agree with the skutterudite structure reported in previous studies [15, 16, 17]. Films grown above 500 °C show binary phases, mainly FeSb<sub>2</sub>, mixed with the skutterudite phase. It was also found that samples annealed in situ at 500 °C under a vacuum of  $10^{-7}$  torr formed a much firmer bond to the substrate than those that were not annealed. For the remainder of this section, we discuss only those films that were grown at 400 °C and annealed at 500 °C. These films are labeled in Table II.1 as 111705. XRD data (Fig. II.5) for the 111705 samples show that the polycrystalline skutterudite phase forms regardless of the substrate used. For films grown on all substrates, the lattice constant has the value  $9.14 \pm 0.02 \text{ \AA}$ . Thus, there is no correlation between the substrate and the crystallographic quality of the resulting film. XRD data also reveal that there are small antimony inclusions in the films. It is worth noting that films grown on silicon and alumina form cracks that are obvious under low magnification. Since there is no apparent difference in XRD data between films grown on silicon and alumina and those grown on the other substrates, it is likely

that the films grown on silicon and alumina form cracks as a result of poor bonding to the substrate. Cracking is also typical of films that were not annealed at 500 °C.

To further investigate the crystal morphology of samples grown under the same conditions as the 111705 films, scanning electron microscope (SEM) secondary electron images were taken for a film grown on an strontium titanate substrate. As seen in Fig. II.6, the film is composed of a somewhat smooth sub-surface that is covered with a number of “boulders” with a typical size of a few microns. Additionally, some large grains are present. The image reflects the polycrystalline structure that is seen in the XRD data. It is possible that bouldering could be decreased and the crystallinity of the films improved by further fine tuning growth conditions such as growth temperature, annealing schedule, laser power or laser pulse rate, as was done in a previous study of  $\text{Ca}_x\text{Co}_4\text{Sb}_{12}$  thin films [21].

Fig. II.7 reveals that the  $\rho(T)$  data increase monotonically with increasing temperature, exhibit a shoulder near 10 K and become linear above 200 K. The data agree qualitatively with data taken on single crystals grown in a molten flux [16]. However, the residual resistivity of the thin films is nearly twice the value found for single crystal samples. This is not surprising since single crystals typically have fewer defects that can scatter conduction electrons than polycrystals. The inset of Fig. II.7 shows low temperature  $\rho(T)$  data for the films grown on yttria stabilized zirconia, strontium titanate, magnesium difluoride, and magnesium oxide substrates. The similar temperature dependence of  $\rho(T)$  for films grown on different substrates shows that substrate choice is unimportant for these films. Data are not presented for films grown on Si and  $\text{Al}_2\text{O}_3$  because those films tended to form microscopic cracks that make electrical resistivity measurements impossible.

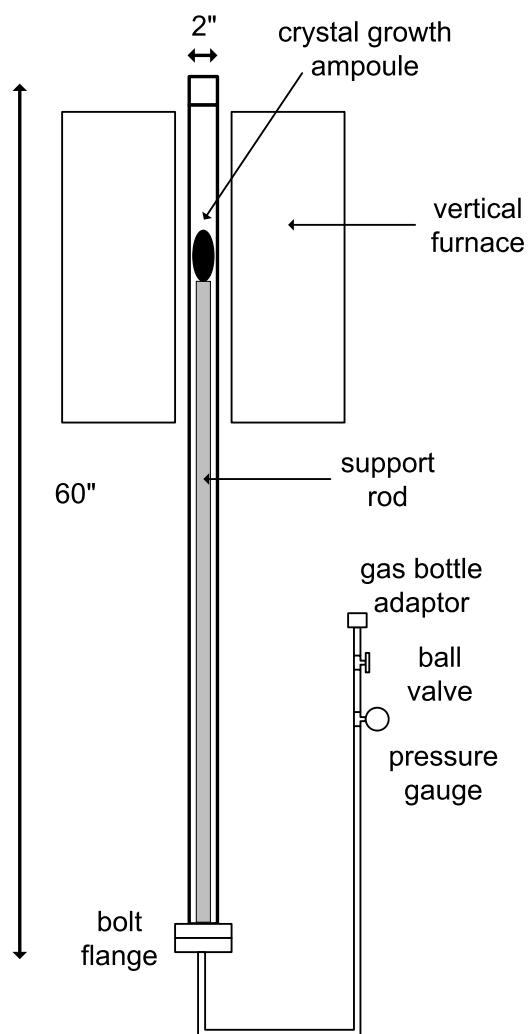


Figure II.1: A schematic of the high pressure cell that was used to synthesize the As-based filled skutterudites.

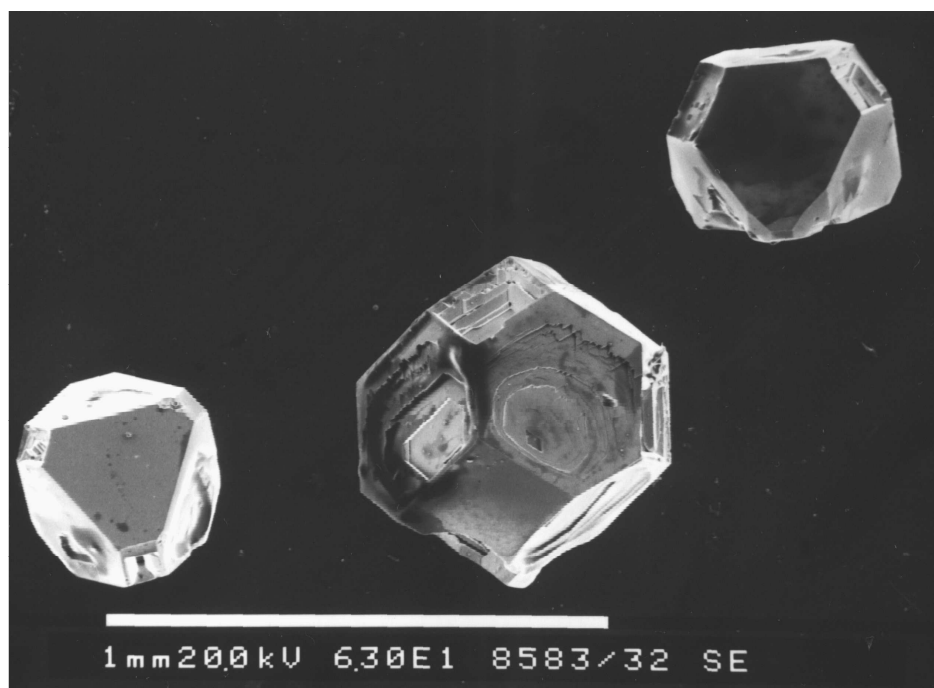


Figure II.2: As shown for these  $\text{PrOs}_4\text{As}_{12}$  specimens, the characteristic form of the filled skutterudite arsenide single crystals is a regular bi-pyramid with summits cut out along the  $[100]$  planes. The crystal in the lower left corner is oriented such that the  $[111]$  direction points out of the page. The central crystal shows interesting macro-defects.

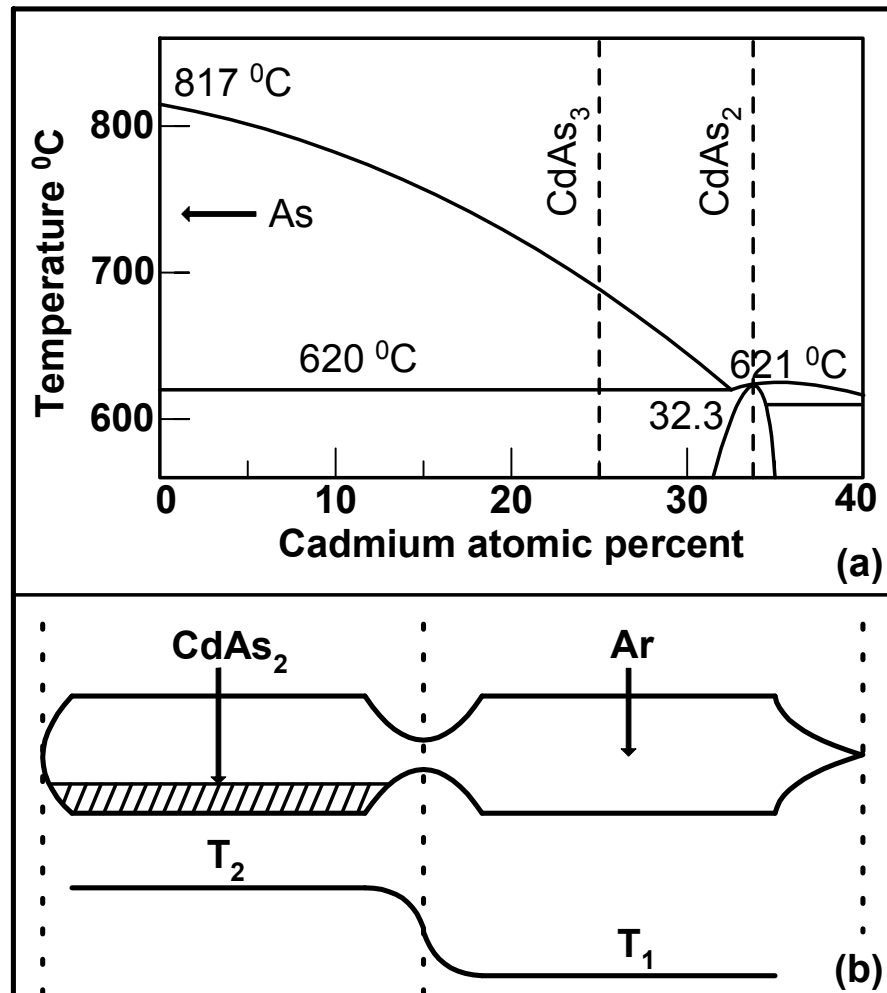


Figure II.3: (a) The arsenic rich part of the Cd - As phase diagram [6] relevant to the flux compositions used for growing crystals of the lanthanide filled skutterudite arsenides. (b) A diagram of the two chamber quartz ampoule used for estimation of the vapor pressure of CdAs<sub>2</sub> as described in the text.

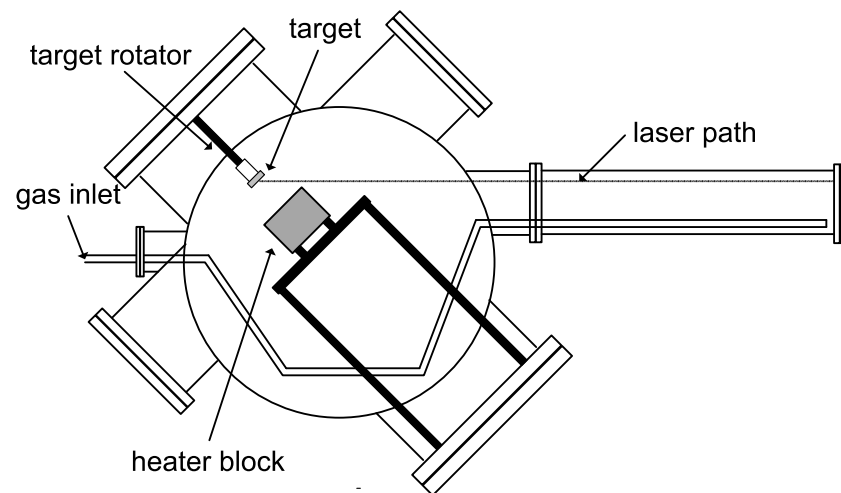


Figure II.4: The schematic for a high vacuum chamber for deposition of thin films using the pulsed laser deposition technique. The main components are the gas flow system, the heater block, the target rotator and the target.

Table II.1: Growth conditions for  $\text{PrFe}_4\text{Sb}_{12}$  thin films.  $T_{abl}$  is the temperature of the substrates during film growth.  $P_{laser}$  is the laser energy density calculated using a beam size at the target of  $2 \text{ mm} \times 1 \text{ mm}$ .  $t_{anneal}(\text{min})/T(^{\circ}\text{C})$  gives the anneal duration in minutes and temperature in  $^{\circ}\text{C}$ .

Film	$T_{abl}$ ( $^{\circ}\text{C}$ )	$P_{laser}$ ( $\text{J}/\text{cm}^2$ )	$t_{anneal}$ (min)/T( $^{\circ}\text{C}$ )	Crystal Morphology
102005	100	3.5	none	amorphous
102405	200	3.5	none	amorphous
102505	300	3.5	none	weakly crystalline
102705	400	3.5	none	crystalline
110105	500	3.5	none	mixed phase
110205	400	4.5	10/400	crystalline
111005	400	4.5	10/400	crystalline
111505	400	4.5	20/600	mixed phase
111705	400	4.5	10/500	crystalline

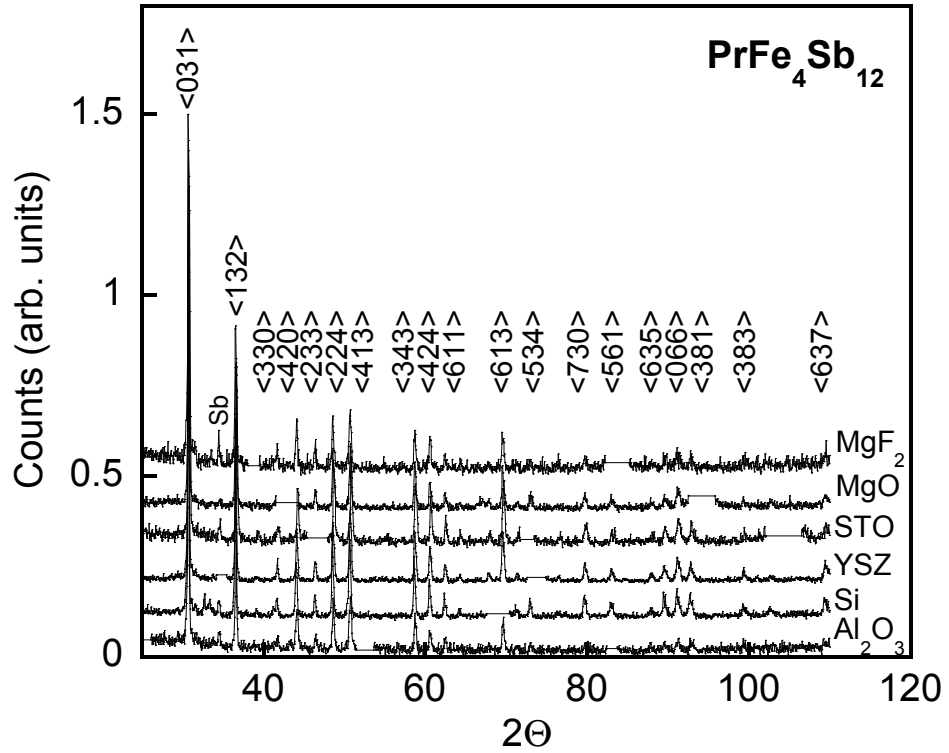


Figure II.5: X-ray diffraction pattern for  $\text{PrFe}_4\text{Sb}_{12}$  grown on various substrates. For clarity, the substrate peaks were removed from the figure. The following abbreviations for substrate names are used : yttria stabilized zirconia (YSZ) and strontium titanate (STO).

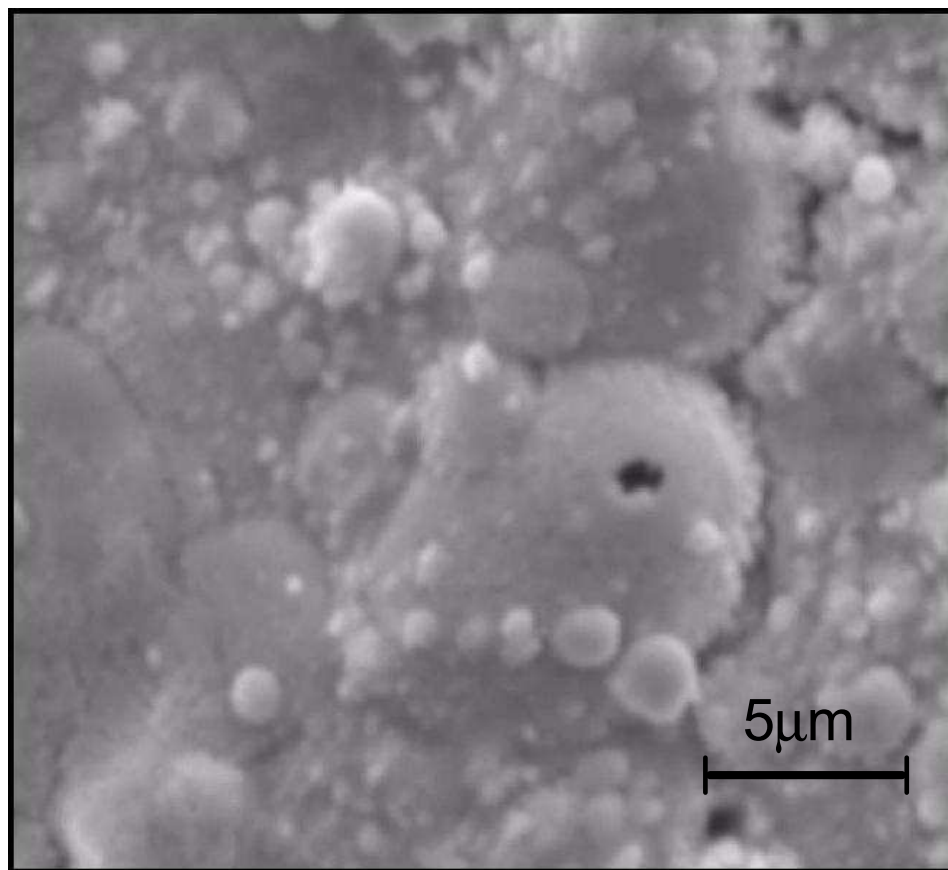


Figure II.6: Scanning electron microscope secondary electron image of a thin film of PrFe<sub>4</sub>Sb<sub>12</sub> grown on a strontium titanate substrate under conditions reported for 111705.

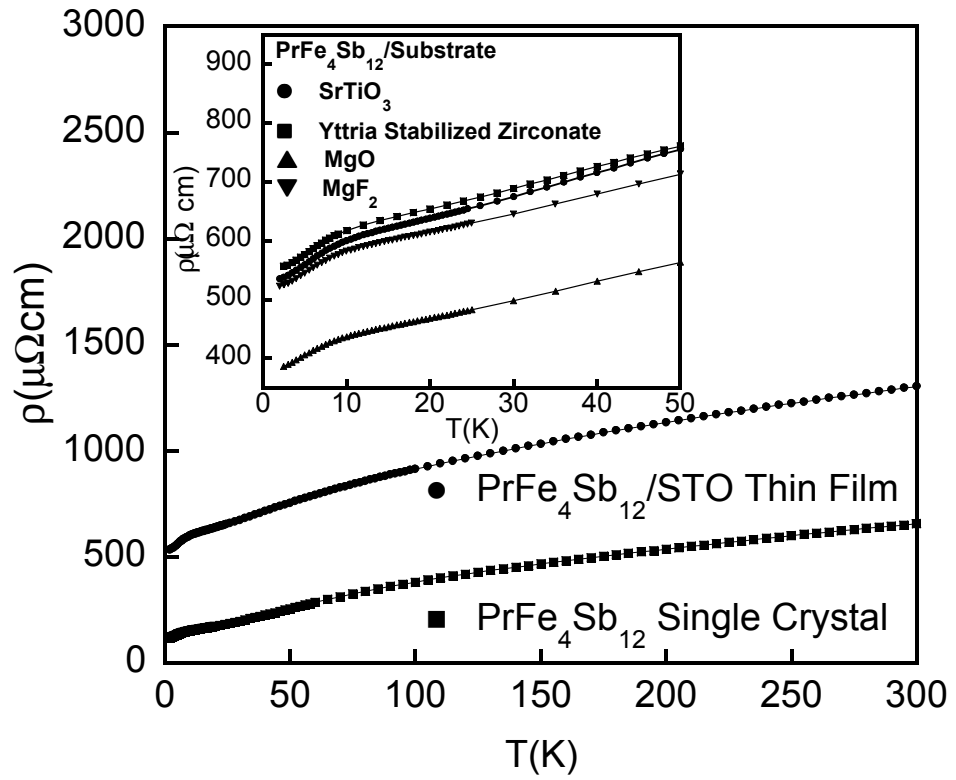


Figure II.7: Electrical resistivity  $\rho$  vs temperature  $T$  data for thin films grown on several different substrates compared to data for single crystals [16].

## Bibliography

- [1] W. Jeitschko and D. Braun, *Acta Cryst.* **B33**, 3401-3406 (1977).
- [2] D. Braun and W. Jeitschko, *J. Less Comm. Met.* **B72**, 147-156 (1980).
- [3] B. C. Sales, D. Mandrus, B. C. Chakoumakos, V. Keppens, and J. R. Thompson: *Phys. Rev. B* **56**, 15081 (1997).
- [4] B. C. Sales, in *Handbook on the Physics and Chemistry of the Rare Earths, Vol 33*, edited by K. A. Gschneider, Jr. (Elsevier Science Publishing Co, New York, New York, 2002) p. 211.
- [5] Z. Henkie, M. B. Maple, A. Pietraszko, R. Wawryk, T. Cichorek, R. E. Baumbach, W. M. Yuhasz, and P.-C. Ho, *J. Phys. Soc. Jpn. Suppl. A* **77** 128-134 (2008).
- [6] T. Massalski, Chief ed.: *Binary Alloy Phase Diagrams*.
- [7] D. B. Chrisey and G. K. Huber, *Pulsed Laser Deposition of Thin Films*. John Wiley and Sons, Inc., New York, 1994.
- [8] D. L. Smith, *Thin Film Deposition*. McGraw-Hill, Inc., 1995.
- [9] M. Ohring, *Materials Science of Thin Films, Deposition and Structure, Second Edition*. Academic Press, 2002.
- [10] J. W. Sharp, E. C. Jones, R. K. Williams, P. M. Martin, and B. C Sales, *J. Appl. Phys.* **78**, 1013 (1995).
- [11] T. Caillat, A. Borshchevsky, and J. Fleurial, *J. Appl. Phys.* **80**, 4442 (1996).
- [12] B. C. Sales, B. C. Chakoumakos, and D. Mandrus, *Phys. Rev. B* **61**, 2475 (2000).
- [13] M. E. Danebrock, C. B. H. Evers, and W. Jeitschko, *J. Phys. Chem. Solids* **57**, 381 (1996).
- [14] E. Bauer, St. Berger, A. Galatanu, Ch. Paul, M. Della Mea, H. Michor, G. Hilscher, A. Grytsiv, P. Rogl, D. Kaczorowski, L. Keller, T. Hermannsdörfer, and P. Fischer, *Phys. B* **312-313**, 840 (2002).
- [15] E. Bauer, St. Berger, Ch. Paul, M. Della Mea, G. Hilscher, H. Michor, M. Reissner, and W. Steiner, *Phys. Rev. B* **66**, 214421 (2002).
- [16] N. P. Butch, W. M. Yuhasz, P.-C. Ho, J. R. Jeffries, N. A. Frederick, T. A. Sayles, X. G. Zheng, and M. B. Maple, *Phys. Rev. B* **71**, 214417 (2005).
- [17] A. Balandin and K. L. Wang, *J. Appl. Phys.* **84**, 6149 (1998).

- [18] D. W. Song, W. L. Liu, T. Zeng, T. Borca-Tasciuc, G. Chen, J. C. Caylor, and T. D. Sands, *Appl. Phys. Lett.* **77**, 3854 (2000).
- [19] J. C. Caylor, A. M. Stacy, R. Gronsky, and T. Sands, *J. Appl. Phys.* **89**, 3854 (2001).
- [20] V. Savchuk, A. Boulouz, S. Chakraborty, J. Schumann, and H. Vinzelberg, *J. Appl. Phys.* **92**, 5319 (2002).
- [21] A. Dauscher, M. Puyet, B. Lenoir, D. Colceag, and M. Dinescu, *Appl. Phys. A* **79**, 1465 (2004).

A portion of the text and data presented in this chapter are reprints of material that appears in “Crystal growth and properties of the filled skutterudite arsenides,” Z. Henkie, M. B. Maple, A. Pietraszko, R. Wawryk, T. Cichorek, R. E. Baumbach, W. M. Yuhasz, and P.-C. Ho, *J. Phys. Soc. Jpn. Suppl. A* 77, 128 (2008) and “Pulsed Laser Deposition of  $\text{PrFe}_4\text{Sb}_{12}$  Thin Films,” R. E. Baumbach, W. M. Yuhasz, and M. B. Maple *Appl. Phys. A* 84, 227-229 (2006). The dissertation author is a coauthor of the first article and the primary investigator and author of the second article.

# III

## Non-Fermi liquid behavior in the filled skutterudite compound

### CeRu<sub>4</sub>As<sub>12</sub>

#### III.A Introduction

The filled skutterudite compounds of the form  $MT_4X_{12}$  ( $M$  = alkali metal, alkaline earth, lanthanide, actinide;  $T$  = Fe, Ru, Os;  $X$  = P, As, Sb) exhibit a wealth of strongly correlated electron phenomena including spin fluctuations, itinerant ferromagnetism, local moment ferromagnetism and antiferromagnetism, conventional BCS superconductivity, unconventional superconductivity, heavy fermion behavior, and non-Fermi liquid behavior [1, 2]. Many of these phenomena depend on hybridization between the rare earth or actinide  $f$ -electron states and the conduction electron states. This trend is evident in the  $CeT_4X_{12}$  systems, most of which are semiconductors where the gap size is correlated with the lattice constant [3, 4, 5]. The effects of hybridization are particularly dramatic for  $CeRu_4Sb_{12}$  which, until now, was the only filled skutterudite known to show non-Fermi liquid (NFL) behavior under regular conditions [6, 7, 8]. In this compound, the NFL behavior is characterized at low  $T$  as follows : resistivity -

$\rho(T) \sim T^{1.4}$ , specific heat divided by temperature -  $C(T)/T \sim -\ln T$  or  $T^{-0.58}$ , and magnetic susceptibility -  $\chi(T) \sim T^{-0.35}$ , all of which suggest that CeRu<sub>4</sub>Sb<sub>12</sub> is located near a quantum critical point (QCP). The value of the lattice constant for CeRu<sub>4</sub>Sb<sub>12</sub> at room temperature indicates that the Ce ions are nearly trivalent, suggesting that a Kondo lattice description is appropriate for this compound.

In this paper, we present measurements of  $\rho(T)$ ,  $C(T)$ , magnetization  $M(H, T)$ , and thermoelectric power  $S(T)$  for CeRu<sub>4</sub>As<sub>12</sub> which show unusual behavior at and below room  $T$ . The  $M(H, T)$  measurements indicate that the Ce ions have a nonmagnetic ground state. We also discuss evidence for NFL behavior at low  $T$  and suggest that this compound may be near a QCP that has been suppressed to 0 K.

### III.B Experimental Details

Single crystals of CeRu<sub>4</sub>As<sub>12</sub> were grown from elements with purities  $\geq 99.9\%$  by a molten metal flux method at high temperatures and pressures, as reported elsewhere [9]. After removing the majority of the flux by distillation, CeRu<sub>4</sub>As<sub>12</sub> single crystals of an isometric form with dimensions up to  $\sim 0.7$  mm were collected and cleaned in acid in an effort to remove any impurity phases from the surfaces of the crystals. The crystal structure of CeRu<sub>4</sub>As<sub>12</sub> was determined by X-ray diffraction on a crystal with dimensions of  $0.17 \times 0.18 \times 0.23$  mm. A total of 5714 reflections (447 unique,  $R_{\text{int}}=0.0772$ ) were recorded and the structure was resolved by the full matrix least squares method using the SHELX-97 program with a final discrepancy factor  $R_1=0.0273$  [for  $I > 2\sigma(I)$ ,  $wR_2=0.0619$ ] [10, 11].

Electrical resistivity  $\rho(T)$  measurements for  $65 \text{ mK} < T < 290 \text{ K}$  were performed in a four-wire configuration in zero magnetic field using a conventional <sup>4</sup>He cryostat and a <sup>3</sup>He - <sup>4</sup>He dilution refrigerator. Magnetization  $M(H, T)$  measurements for  $1.9 \text{ K} < T < 300 \text{ K}$  and  $0 < H < 55 \text{ kOe}$  were conducted using a Quantum Design Magnetic Properties Measurement System on a mosaic of crys-

tals ( $m = 121$  mg) which were mounted on a small Delrin disc using Duco cement. Specific heat  $C(T)$  measurements for  $650 \text{ mK} < T < 10 \text{ K}$  were made using a standard heat pulse technique on a collection of 11 single crystals ( $m = 45$  mg) attached to a sapphire platform with a small amount of Apiezon N grease in a  $^3\text{He}$  semiadiabatic calorimeter. The thermoelectric power  $S(T)$  for  $0.5 \text{ K} < T < 350 \text{ K}$  of  $\text{CeRu}_4\text{As}_{12}$  single crystals with length less than 1 mm was determined by the method described in ref [12].

### III.C Results

Single crystal structural refinement shows that the unit cell of  $\text{CeRu}_4\text{As}_{12}$  has the  $\text{LaFe}_4\text{P}_{12}$ -type structure ( $\text{Im}\bar{3}$ ) space group with two formula units per unit cell, and a lattice constant  $a = 8.5004(4) \text{ \AA}$ , in reasonable agreement with earlier measurements of  $a = 8.4908 \text{ \AA}$  and  $a = 8.4963 \text{ \AA}$  [4, 5, 13]. Other crystal structure parameters are summarized in Table III.1. The displacement parameter  $U_{eq}$  represents the average displacement of an atom vibrating around its lattice position and is equal to its mean-square displacement along the Cartesian axes. The displacement parameters determined for  $\text{CeRu}_4\text{As}_{12}$  exhibit behavior that is typical of the lanthanide filled skutterudites[14, 15]. Table III.1 also indicates that the Ce and As sites in  $\text{CeRu}_4\text{As}_{12}$  may not be fully occupied since there is  $\sim 2\%$  uncertainty in the occupancy factors. The possible incomplete Ce or As occupancy is even more pronounced for some other crystals, not shown in table I, where the Ce and As filling deviates by as much as 3% from 100% occupation.

The  $T$  - dependence of the electrical resistivity is quite unusual (Fig. III.1). The large value of  $\rho \sim 3.5 \text{ m}\Omega\text{cm}$  at room temperature suggests that  $\text{CeRu}_4\text{As}_{12}$  is a semimetal. Below 300 K,  $\rho(T)$  decreases monotonically with decreasing  $T$  with negative curvature between 300 K and  $\sim 150$  K, positive curvature from  $\sim 150$  K to  $\sim 70$  K, negative curvature between  $\sim 70$  K and  $\sim 50$  K, and a semi-linear region from  $\sim 50$  K to  $\sim 10$  K. At the lowest temperatures ( $65 \text{ mK} <$

$T < 3.5$  K),  $\rho(T)$  can be described by a power law of the form,

$$\rho(T) = \rho_0 + AT^n \quad (\text{III.1})$$

where  $n = 1.4$ ,  $A = 19.0 \mu\Omega\text{cmK}^{-n}$ , and  $\rho_0 = 136 \mu\Omega\text{cm}$  for nearly two decades in temperature and is consistent with that seen for other NFL systems [16, 17, 18, 7]. Measurements performed on numerous samples also reveal that the qualitative behavior for  $\rho(T)$  is consistent for all samples, although variation by as much as a factor of 2 in the absolute value of  $\rho$  is observed, possibly due to uncertainty in the geometric factor. It should also be noted that no superconducting transition was detected above 65 mK.

Shown in Fig. III.2 are  $\chi(T) = M(T)/H$  data measured in constant fields  $H = 10$  kOe and 50 kOe. The  $\chi(T)$  data likewise show an unusual  $T$  - dependence in which  $\chi$  decreases with  $T$  down to  $\sim 100$  K, remains roughly constant down to  $\sim 65$  K, and then begins a slow increase down to 1.9 K which depends on the magnitude of the applied field. No part of these curves can be described by a simple Curie - Weiss law, as would be expected for magnetic  $\text{Ce}^{3+}$  ions, nor is any obvious magnetic ordering seen. For fields which fall in the linear portion of low  $T$   $M(H)$  isotherms ( $H \leq 15$  kOe),  $\chi(T)$  increases continuously down to 1.9 K. In contrast, for fields above the linear portion of the low  $T$   $M(H)$  isotherm,  $\chi(T)$  tends to saturate with decreasing  $T$ , approaching a constant value near 1.9 K. The low  $T$  upturn in  $\chi(T)$  is described by various functions, implicit in which is the assumption that the upturn is either intrinsic and due to magnetic fluctuations in the vicinity of a magnetic quantum critical point where a second order magnetic transition has been suppressed to 0 K, or are due to paramagnetic impurities embedded in a nonmagnetic host.

To consider the first viewpoint that the low field behavior of  $\chi(T)$  is intrinsic, the  $\chi(T, H = 10$  kOe) data were fit below  $\sim 10$  K in a manner consistent with the NFL behavior observed in  $\rho(T)$ . Fits show that  $\chi(T)$  is described by either a power law ( $1.9 \text{ K} \leq T \leq 10 \text{ K}$ ) or a logarithmic function ( $1.9 \text{ K} \leq T \leq 6 \text{ K}$ ) of the forms,

$$\chi(T) = aT^{-m} \quad (\text{III.2})$$

$$\chi(T) = b - c \ln(T) \quad (\text{III.3})$$

where  $a = 4.5 \times 10^{-3} \text{ cm}^3\text{K}^m/\text{mol}$  and  $m = 0.49$ , or  $b = 4.1 \times 10^{-3} \text{ cm}^3/\text{mol}$  and  $c = 1.3 \times 10^{-3} \text{ cm}^3/\text{mol}$ , respectively. This analysis assumes that the application of higher fields ( $H = 50 \text{ kOe}$ ) suppresses the low  $T$  divergence in  $\chi(T)$ , consistent with a field induced crossover to a Fermi liquid state.

To address the possibility that the low  $T$  upturn in  $\chi(T)$  is due to magnetic impurities, isothermal  $M$  vs  $H$  measurements were made at low temperatures. As shown in the inset of Fig. III.3, the  $M$  vs  $H$  curve for  $T = 2 \text{ K}$  is linear up to  $\sim 15 \text{ kOe}$ , develops negative curvature, and then becomes linear in higher fields. This field dependence is consistent with the total magnetization  $M$  being a sum of an intrinsic linear contribution  $M_{lin}$  that is linear in  $H$  and an impurity contribution  $M_{imp}$  that saturates at high  $H$ . For  $M(H)$  isotherms at  $T = 2 \text{ K}$ ,  $2.5 \text{ K}$ ,  $3 \text{ K}$ ,  $4 \text{ K}$ ,  $5 \text{ K}$ ,  $10 \text{ K}$ ,  $50 \text{ K}$ ,  $100 \text{ K}$ , and  $\chi(T)$  curves at  $H = 10 \text{ kOe}$  and  $50 \text{ kOe}$ , the impurity contribution was optimized and removed from the total magnetization in the manner described in ref [19]. The resulting curves are shown in Fig. III.3 where the intrinsic susceptibilities  $M_{lin}(T)/H = \chi_{lin}(T)$  for  $H = 10 \text{ kOe}$  and  $50 \text{ kOe}$  as well as those taken from linear fits to the  $M_{lin}(H)$  isotherms are shown to agree and are compared with the total susceptibilities for  $H = 10 \text{ kOe}$  and  $50 \text{ kOe}$ . In the high temperature region,  $\chi$  and  $\chi_{lin}$  are nearly identical since the supposed impurity contribution is small. Near  $100 \text{ K}$ , the deviation between the two quantities is noticeable as  $\chi_{lin}$  becomes constant, while  $\chi$  saturates and then begins a slow increase. Below  $\sim 10 \text{ K}$ ,  $\chi_{lin}$  begins a gradual decrease which becomes much stronger below  $\sim 5 \text{ K}$ , in the range where NFL behavior in  $\rho(T)$  and  $C(T)/T$  occurs. Additionally, the fits to  $M_{imp}$  give an estimate for the impurity concentration. However, since there is no quantitative method for determining the type of magnetic impurity or whether it is of a single species or a mixture, it is

necessary to assume a value for the total angular momentum  $J$ . Fits to the data assuming  $J = 8$  (Ho) and  $J = 2.5$  (Ce) yield impurity concentrations near 1 % with the Landé  $g$  factor  $g = 0.26$  and  $g = 0.71$ , respectively. This concentration is consistent with the amount estimated from XRD measurements.

Displayed in Fig. III.4 are specific heat divided by temperature  $C/T$  vs  $T^2$  data. For  $T < 10$  K, the data decrease with decreasing temperature down to 2.6 K, below which they exhibit an upturn that persists to 650 mK. The strength of the upturn is comparable to that seen for the related NFL compound  $\text{CeRu}_4\text{Sb}_{12}$  [7]. It should be noted that a small feature with a maximum at 2.4 K is also observed. The feature is associated with an impurity component and is not seen in  $C/T$  measurements of all  $\text{CeRu}_4\text{As}_{12}$  specimens, although the other features, such as the low temperature divergence are seen. For temperatures  $2.6 \text{ K} < T < 8 \text{ K}$ , the data can be described by,

$$C/T = \gamma + \beta T^2 \quad (\text{III.4})$$

where  $\gamma$  is the electronic specific heat coefficient and  $\beta \propto \theta_D^{-3}$  describes the lattice contribution. Fits of eq. 6 to  $C(T)/T$  show that  $\gamma \sim 26 \text{ mJ/molK}^2$  and  $\theta_D \sim 156 \text{ K}$ . For  $650 \text{ mK} < T < 2.6 \text{ K}$ ,  $C/T$  diverges from the  $T^2$   $T$  - dependence and increases with decreasing temperature. This low temperature divergence in  $C/T$  can be described by either a weak power law or a logarithmic function (Eqns. III.5 and III.6) where  $\gamma = 26 \text{ mJ/molK}^2$ ,  $\varphi = 74.5 \text{ mJ/mol K}^{2-l}$  and  $l = 0.97$  or  $\phi = 101 \text{ mJ/mol K}^2$  and  $\zeta = 84 \text{ mJ/mol K}^2$ , respectively. Again, the behavior is consistent with typical NFL phenomena.

$$C/T = \gamma + \varphi T^{-l} \quad (\text{III.5})$$

$$C/T = \phi - \zeta \ln T \quad (\text{III.6})$$

Fig. 5 shows the  $T$  - dependence of the thermoelectric power  $S(T)$  for two samples of  $\text{CeRu}_4\text{As}_{12}$ , for which there is a pronounced sample dependence. In the

high temperature region, there is a two peak structure with a broad peak around  ${}^hT_{max} = 250$  K which reaches  ${}^hS_{max} = 67$  V/K for sample 2. The broad peak is followed by a local minimum near  $\sim 150$  K and a sharp peak with a maximum value near  ${}^lS_{max} = 66$   $\mu$ V/K at  ${}^lT_{max} \sim 75$  K for sample 2 and  ${}^lS_{max} = 38$   $\mu$ V/K at  ${}^lT_{max} \sim 100$  K for sample 1. The inset Fig. III.5i displays the  $T$  - dependence of  $S(T)$  below 10 K. The sample with the lower thermoelectric power exhibits an abrupt step in  $S(T)$  by about  $\Delta S_{5K} \sim 2$  V/K near  $T^* = 5.0$  K. The step results in a change of sign from positive above  $T^*$  to negative below. For the sample with higher  $S(T)$ , the jump at  $T^*$  is from one nearly linear  $S(T)$  to another with a slightly lower slope. Additionally, a sign change at 0.9 K is observed for this sample. The  $S(T)$  curves for these two samples converge at an upturn near  $T = 0.47$  K, as shown in Fig. III.5(ii) where the average value of  $S/T$  is equal to - 0.6 V/K<sup>2</sup>.

### III.D Discussion

Taken together, measurements of  $\rho(T)$ ,  $M(H, T)$ ,  $C(T)/T$ , and  $S(T)$  reveal anomalous types of behavior in both the high and low temperature regions. The decreasing magnetic susceptibility with  $T$  is particularly interesting, as it signals a transition to a nonmagnetic state at low  $T$ . There are two well known models which describe such an evolution in magnetism. The first is the intermediate valence picture where the Ce ions have a dynamic temporally fluctuating valence, in this case between 3+ (magnetic) and 4+ (nonmagnetic), which evolves into a nonmagnetic ground state below a characteristic “valence fluctuation” temperature  $T_{vf}$ . The second is a Kondo lattice picture where the magnetic moments of Ce<sup>3+</sup> ions which occupy a sublattice are screened by conduction electrons, resulting in a nonmagnetic ground state, below a characteristic “Kondo” temperature  $T_K$ .

In the intermediate valence picture, the ratios  $n^{3+}(T)$  and  $n^{4+}(T) = 1 - n^{3+}(T)$  describe the fraction of Ce ions in each valence state. The  $4f$ -electron shell

of each Ce ion temporally fluctuates between the configurations  $4f^1$  ( $\text{Ce}^{3+}$ ) and  $4f^0$  ( $\text{Ce}^{4+}$ ) at a frequency  $\omega \approx k_B T_{vf}/\hbar$ , where  $T_{vf}$  separates magnetic behavior at high temperatures  $T \gg T_{vf}$  and nonmagnetic behavior at low temperatures  $T \ll T_{vf}$  [20, 21]. For  $\text{Ce}^{3+}$ , there is one localized  $4f$ -electron and  $\chi(T)$  should behave as a Curie-Weiss law modified by the CEF splitting of the ground state doublet and an excited state quartet by a splitting temperature  $T_{CEF}$  on the order of several hundred K as seen for other Ce filled skutterudite compounds such as  $\text{Ce}_{0.9}\text{Fe}_3\text{CoSb}_{12}$  ( $T_{CEF} \sim 350$  K) [14]. For  $\text{Ce}^{4+}$ , there is no localized  $f$ -electron and  $\chi(T)$  should behave as a Pauli susceptibility. However, for an intermediate valence state involving a temporal admixture of the  $4f^1$  and  $4f^0$  configurations,  $\chi(T)$  is expected to be intermediate between  $\chi(T)$  of the  $\text{Ce}^{3+}$  and  $\text{Ce}^{4+}$  integral valence states for  $T \gg T_{vf}$  and to exhibit an enhanced Pauli-like susceptibility for  $T \ll T_{vf}$ . Magnetic ordering can also occur if the characteristic temperature for the RKKY interaction is comparable to the valence fluctuation temperature  $T_{vf}$ .

Thus, down to 90 K,  $\chi(T)$  and  $\chi_{lin}(T)$  are consistent with an intermediate valence scenario, and one in which the intermediate valence shifts in the direction of 4+ with decreasing  $T$  as indicated by the decrease in  $\chi(T)$  with decreasing  $T$ . Comparison to other known intermediate valence compounds such as  $\text{SmS}$ ,  $\text{SmB}_6$ , or  $\text{La}_{1-x}\text{Th}_x$  doped with Ce impurities where the Ce valence evolves from 3+ to an intermediate value as a function of Th concentration supports this perspective [20, 21, 22, 23]. Moreover, the intermediate valence picture is consistent with the depressed room temperature lattice constant, as compared to the expected trivalent lanthanide contraction (LC) value for the  $\text{MRu}_4\text{As}_{12}$  series where  $M = \text{La} - \text{Pr}$  [4, 5]. To emphasize this point, a comparison can be made to the related compounds  $\text{MT}_4\text{Sb}_{12}$  and  $\text{MT}_4\text{P}_{12}$  where  $M = \text{La} - \text{Nd}$  and  $T = \text{Fe}, \text{Ru}, \text{and Os}$ . For  $\text{MT}_4\text{Sb}_{12}$ , there is no deviation from the expected LC value at room temperature and, therefore, the Ce ions appear to have a valence near 3+, although this does not preclude the possibility of an intermediate valence state below room temperature. To probe this viewpoint, XANES measurements were recently made

to directly measure the Ce valence in  $\text{CeRu}_4\text{As}_{12}$ . Contrary to the above discussion, the Ce ions in  $\text{CeRu}_4\text{As}_{12}$  appeared to be in the 3+ state, indicating an alternative description. These results will be discussed in detail in an upcoming publication [24].

It is also possible that the Kondo lattice picture is the appropriate description of the physics, if the Ce ions are trivalent and carry localized magnetic moments. In this case, the decrease of the magnetic susceptibility with decreasing temperature indicates that the Kondo temperature  $T_K$  is above room temperature. Thus, the decrease of the resistivity with decreasing temperature could be due to a decrease in the magnetic exchange scattering consistent with the formation of the coherent Kondo lattice ground state. This scenario is expected to lead to a non-magnetic Fermi liquid ground state. Thus, the formation of an NFL ground state would be surprising and not in agreement with the typical picture where NFL behavior is seen in the vicinity of a magnetically ordered ground state. However, there are some  $f$ -electron systems such as  $\text{Y}_{1-x}\text{U}_x\text{Pd}_3$  and  $\text{U}_{1-x}\text{Th}_x\text{Pd}_2\text{Al}_3$  in which the physical properties exhibit NFL behavior at temperatures much lower than the  $T_K$  and far away from any magnetic quantum critical points [25, 26, 17, 18]. It should also be noted that if a Kondo picture is adopted, the reduced lattice constant could be explained by a Kondo - like volume collapse [27].

The high temperature behavior is further complicated by the two peak structure in the  $S(T)$  data. Similar two peak structures have been observed for various other cerium systems including the heavy fermion system  $\text{Ce}_x\text{Y}_{1-x}\text{Cu}_{2.05}\text{Si}_2$ , [28] where  $x = 0.3, 0.5$ . In that case, the low- $T$  peak is ascribed to electron scattering by the ground state doublet of the  $\text{Ce}^{3+}$  ion while the high temperature peak is due to electronic scattering from the entire sextet of CEF levels of the  $\text{Ce}^{3+}$  ion. A more general description of  $S(T)$  for the Ce-based intermetallic systems is given by a theoretical model that takes into account the CEF splitting of the  $\text{Ce}^{3+}$  4*f* Hund's rule ground state multiplet and strong Coulomb repulsion of the 4*f*-electrons [29].

Measurements of  $\rho(T)$ ,  $M(H, T)$ , and  $C(T)/T$  also reveal an anomalous NFL state for CeRu<sub>4</sub>As<sub>12</sub> at low  $T$ . The NFL behavior is characterized by sub-quadratic power law behavior in  $\rho(T)$ , weak power law or logarithmic divergences in  $C(T)/T$ , and either weak power law or logarithmic divergences in  $\chi(T)$  or a strong depression in  $\chi_{lin}(T)$  near 5 K. To roughly quantify the NFL state, a temperature scale  $T_0$  may be derived from the low temperature fits to  $\rho(T)$ ,  $\chi(T)$  and  $C(T)/T$  using the scaled equations,[20, 17, 18]

$$\rho(T) = \rho_0[1 + (T/T_{0\rho})^n] \quad (\text{III.7})$$

$$\chi(T) = -B \ln(T/T_{0\chi}) \quad (\text{III.8})$$

$$C(T)/T = -\lambda R/T_{0K} \ln(T/bT_{0K}) \quad (\text{III.9a})$$

$$\partial(C(T)/T)/\partial(\ln T) = -\lambda R/T_{0K} \quad (\text{III.9b})$$

which yield the values  $T_{0\rho} \sim 4$  K,  $T_{0\chi} \sim 23$  K, and  $T_{0K} \sim 25$  K. For the fit to  $C(T)/T$  (eq. 12), the parameters  $\lambda = 0.251$  and  $b = 0.41$  are taken from the two channel Kondo model which has proven to be a useful phenomenological description that yields reasonable values of the scaling temperature  $T_{0K}$  for many NFL systems, although it is not strictly applicable to the present situation from a theoretical point of view. The unusual behavior seen in  $S(T)$  below 5 K also supports the viewpoint that  $T_0$  is in this temperature range. Although the values for  $T_0$  seem to span a wide range of temperatures, this phenomenological scaling analysis provides a rough estimate of the temperature range through which the system makes a gradual transition into the NFL state.

The low  $T$   $S(T)$  data also imply an unusual state below 5 K. In this measurement,  $T^*$  coincides with the upper limit of the temperature range for NFL behavior. Behnia et al. [30] have argued that, in the zero temperature limit, the thermoelectric power should obey the relation,

$$q = \frac{SN_A e}{T\gamma} \quad (\text{III.10})$$

where  $N_A$  is Avogadro's number,  $e$  is the electron charge and the constant  $N_A e = 9.65 \times 10^4 \text{ Cmol}^{-1}$  is the Faraday number. The dimensionless quantity  $q$  corresponds to the density of carriers per formula unit for the case of a free electron gas with an energy independent relaxation time. In our case,  $q = -2.2$  and differs by sign from all eight cerium compounds considered in Ref [30]. This unusual result may also be related to the possible NFL state at low temperatures.

A comparison to typical heavy fermion systems may be made by computing an effective Wilson-Sommerfield ratio  $R_W = (\pi^2 k_B^2 / 3 \mu_{eff}^2) (\chi_0 / \gamma)$ . Since unambiguous choices for  $\chi_0$  and  $\gamma$  are not obvious, the values  $\chi(H = 10 \text{ kOe})$ ,  $\chi_{lin}$ , and  $\gamma$  are taken at 1.9 K to probe the low temperature state. Also, the Hund's rule effective magnetic moment  $\mu_{eff} = 2.54 \mu_B$  for  $\text{Ce}^{3+}$  ions is used. From these values,  $R_W$  is calculated to be  $\sim 0.46$  and  $\sim 0.06$ , for  $\chi(H = 10 \text{ kOe})$  and  $\chi_{lin}$ , respectively. The first value is similar to those found in  $f$ -electron materials that exhibit Fermi liquid behavior with heavy quasiparticles while the second value seems far too low to be physically meaningful. This result suggests that the behavior of  $\chi(T)$  in low fields is intrinsic and the curvature in the isothermal  $M(H)$  curves at low temperatures is not due to paramagnetic impurities.

In typical discussions of NFL physics in  $f$ -electron materials, the phenomena are described in terms of interactions between the itinerant electrons and the magnetic rare earth ions. Examples include; (1) nearness to various types of magnetic quantum critical points where a second-order phase transition is suppressed to 0 K and quantum fluctuations govern the physical properties, [31, 32] (2) Kondo disorder where a range of Kondo temperatures are allowed including  $T_K = 0 \text{ K}$ , [33, 34, 35] (3) the Griffiths phase model, [36] and (4) the quadrupolar Kondo model [37]. These pictures have been moderately successful in describing numerous NFL systems [16]. If the viewpoint is taken that the Ce ions are in the magnetic 3+ valence state, then one of these models may be appropriate for describing the low  $T$  behavior. In such a picture, it must be assumed that the anomalous  $\chi(T)$  behavior is due to some unusual phenomena, such as a high  $T_K$ .

However, if the intermediate valence picture is adopted, then Kondo scenarios are unlikely to describe the NFL behavior since they require the presence of  $\text{Ce}^{3+}$  ions. As such, the possibility of a QCP where valence fluctuations on the Ce ions give rise to the incipient NFL state is considered. The existence of a QCP due to a quantum phase transition from integral to intermediate valence has been conjectured in a few other compounds, most notably  $\text{CeCu}_2\text{Si}_2$ ,  $\text{CeCu}_2\text{Ge}_2$ ,  $\text{CePd}_2\text{Si}_2$ , and the alloy  $\text{CeCu}_2(\text{Si}_{1-x}\text{Ge}_x)_2$  [39, 40, 41, 38, 42, 43]. The low pressure region of the  $T - P$  phase diagram for these compounds is similar to that seen for heavy fermion superconductors such as  $\text{CeIn}_3$  and  $\text{CeMIn}_5$  ( $M = \text{Co}, \text{Rh}$ ) where antiferromagnetic order is suppressed with increasing pressure towards a QCP, around which a superconducting dome is observed at low temperatures [44, 45, 46]. Higher pressures then tune the Ce ion from integral to intermediate valence, resulting in a second superconducting dome near a QCP which is associated with the valence transition. The region surrounding the superconducting dome maximum is also accompanied by NFL behavior. By comparison, an analogous description may be applicable for  $\text{CeRu}_4\text{As}_{12}$  where pressure, magnetic field, or chemical substitution tune the dynamic intermediate valence state.

Finally, it is noteworthy that a recent study shows that  $\rho(T)$  for polycrystalline specimens of  $\text{CeRu}_4\text{As}_{12}$  exhibit thermally activated behavior  $\rho \sim \exp(\Delta/T)$  where  $\Delta = 50$  K, while  $\chi(T)$  and  $C(T)/T$  are similar to those reported here [13]. The transition from a weakly insulating state for polycrystalline samples to poor metal NFL behavior for single crystal samples signals that the electronic state of  $\text{CeRu}_4\text{As}_{12}$  is highly sensitive to perturbations, such as Ce filling or structural disorder, that are affected by sample growth technique or degree of crystallinity. We also make a comparison to  $\text{CeOs}_4\text{As}_{12}$ , for which  $\rho(T)$  shows semiconducting behavior [47, 48]. A similar situation is seen for  $\text{CeRhSb}_{1-x}\text{Sn}_x$ , where  $\text{CeRhSb}$  is a Kondo semiconductor and  $\text{CeRhSn}$  exhibits NFL behavior [49]. In this system, it is possible to tune through a Kondo insulator - NFL quantum critical point as a function of dopant  $x$ . An analogous study would be of interest for the doping

series  $\text{Ce}(\text{Ru}_{1-x}\text{Os}_x)_4\text{As}_{12}$ .

### III.E Summary

Measurements of  $\rho(T)$ ,  $M(H, T)$ ,  $C(T)/T$ , and  $S(T)$  for single crystals of  $\text{CeRu}_4\text{As}_{12}$  reveal anomalous behavior, most notably a nonmagnetic or weakly magnetic behavior, which evolves into NFL phenomena at low temperatures. As such,  $\text{CeRu}_4\text{As}_{12}$  may be a member of the class of materials whose close proximity to a QCP precipitates NFL behavior. However, the lack of any readily identifiable magnetic quantum critical point suggests that the behavior is due to another type of transition such as a valence or metal - insulator transition that has been suppressed to 0 K. Measurements of the electrical resistivity, thermoelectric power, specific heat, and magnetization as a function of pressure, magnetic field, and chemical substitution may yield insight into the nature of the anomalous behaviors that are seen in this compound.

Table III.1: Atomic coordinates, displacement parameters, and occupancy factors for  $\text{CeRu}_4\text{As}_{12}$ .  $U_{eq}$  is defined as one-third of the trace of the orthogonalized  $U_{ij}$  tensor.

atom	$x$	$y$	$z$	$U_{eq}(\text{\AA}^2 \times 10^{-3})$	Occupancy Factor
Ru	0.25	0.25	0.25	3(1)	1.00(2)
As	0.1495(1)	0.3499(1)	0	4(1)	0.99(2)
Ce	0	0	0	11(1)	0.99(2)

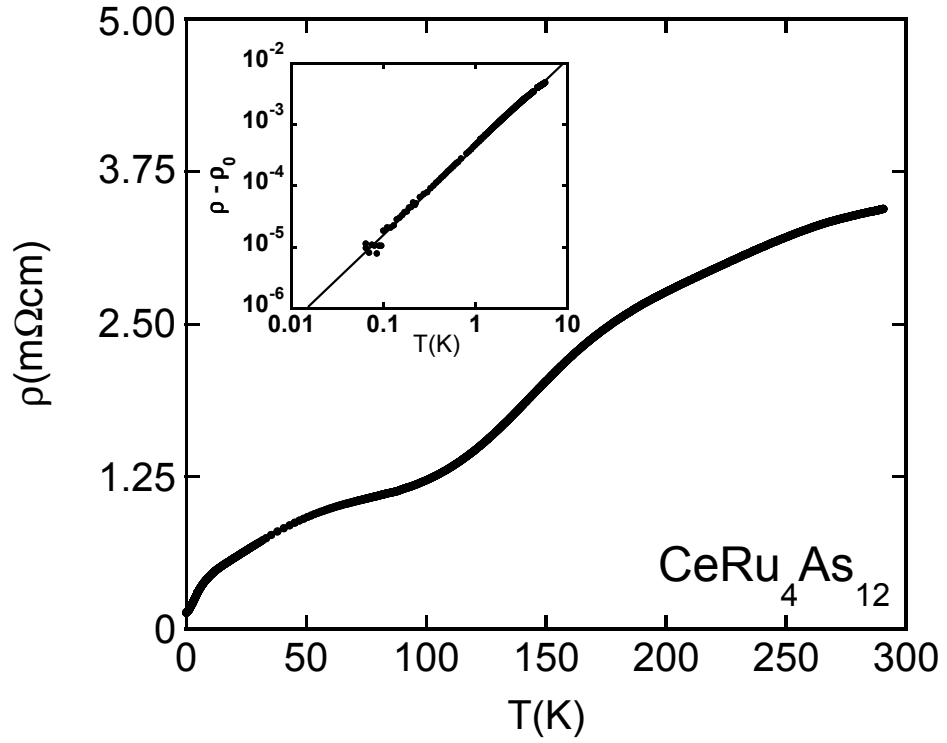


Figure III.1: Electrical resistivity  $\rho$  vs temperature  $T$  for  $\text{CeRu}_4\text{As}_{12}$ . Inset : log - log plot of  $\rho - \rho_0$  vs  $T$  between 65 mK and 10 K, where  $\rho_0$  is the residual resistivity. The data can be described by the expression  $\rho(T) = \rho_0 + AT^n$  where  $\rho_0 = 136 \mu\Omega\text{cm}$ ,  $A = 19.0 \mu\Omega\text{cmK}^{-n}$  and  $n = 1.4$  (straight line in the figure).

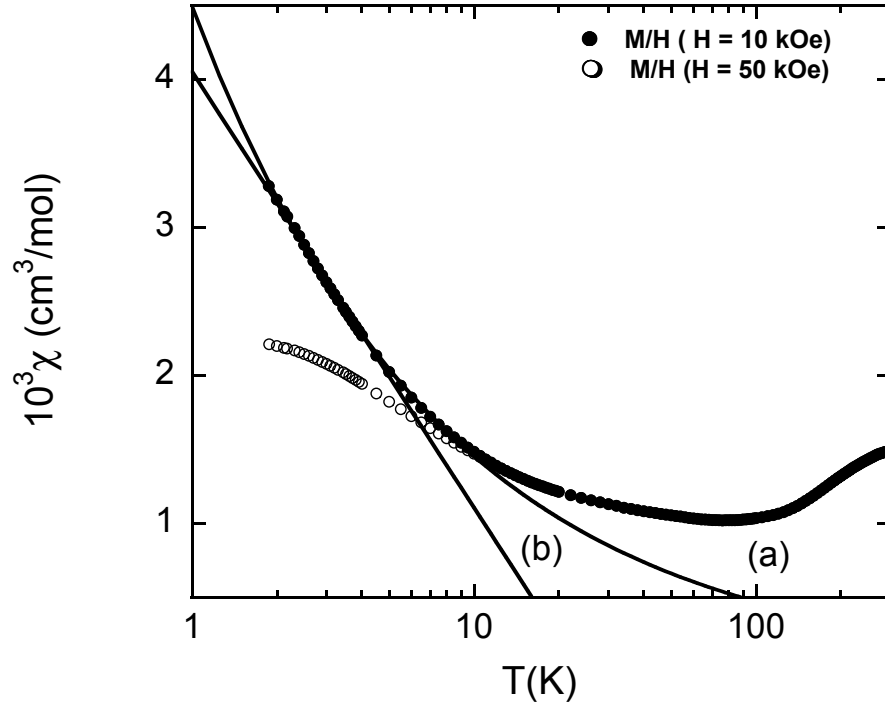


Figure III.2: Magnetic susceptibility  $\chi$  vs temperature  $T$  for  $\text{CeRu}_4\text{As}_{12}$  between 2 K and 300 K. The magnetic susceptibility is defined as  $\chi = M/H$ , where  $M$  is the magnetization and  $H$  is the magnetic field, and was measured in fields of 10 kOe (filled circles) and 50 kOe (unfilled circles). For  $2 \text{ K} < T < 10 \text{ K}$ ,  $\chi(T)$  measured in a 10 kOe field is described by either a power law (curve a) or a logarithmic (curve b) function (see text).

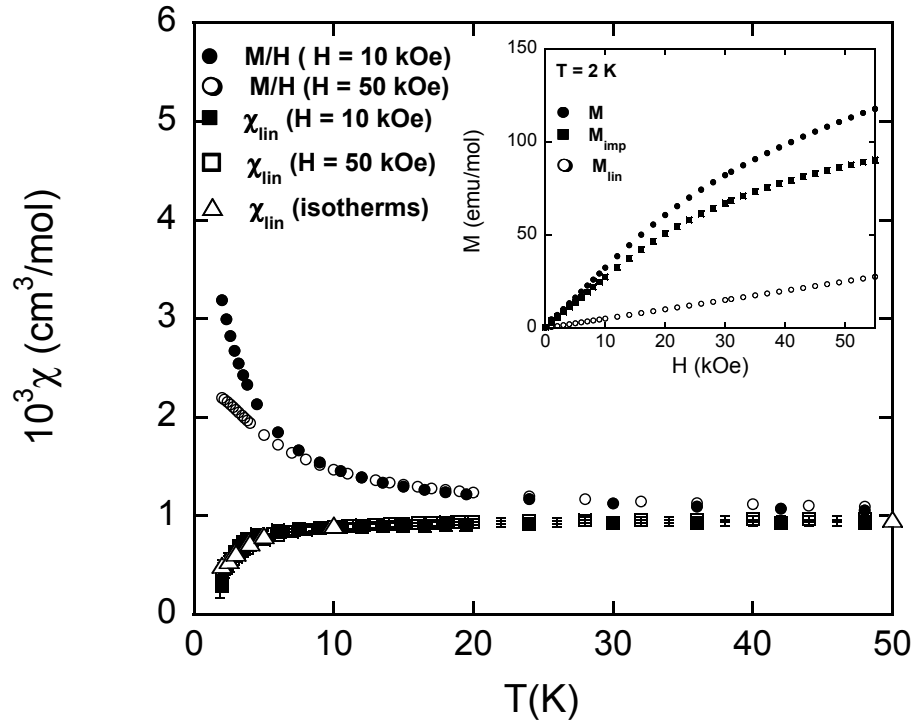


Figure III.3: Total magnetic susceptibility  $\chi$  and intrinsic susceptibility  $\chi_{lin}$  (see text) vs temperature  $T$  for CeRu<sub>4</sub>As<sub>12</sub> between 2 K and 300 K. Inset: Magnetization  $M$  vs applied field  $H$  at  $T = 2$  K. The total magnetization  $M$  is treated as a sum of a linear intrinsic magnetization  $M_{lin}$  and an impurity Brillouin function  $M_{imp}$ .

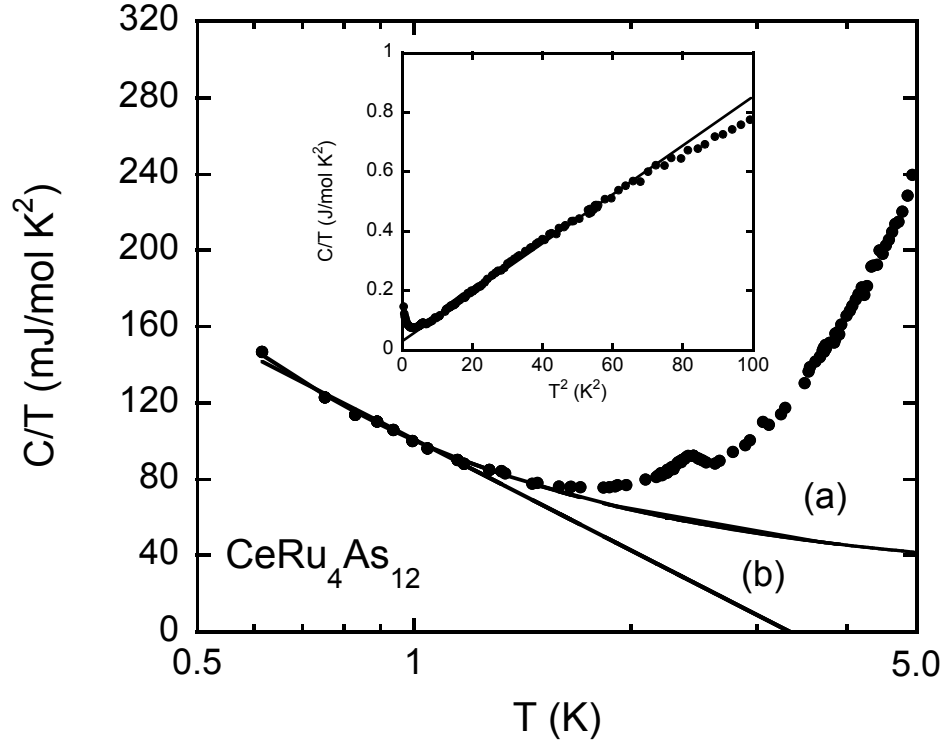


Figure III.4: Specific heat  $C$  divided by temperature  $T$  vs  $T$  for  $\text{CeRu}_4\text{As}_{12}$ . For  $T < 2.6$  K, an upturn is observed which persists to 650 mK. The divergence conforms to a weak power law (curve a) or logarithmic function (curve b) (see text). It should be noted that a small feature is observed with a maximum at 2.4 K which appears to be related to an impurity phase. Shown in the inset is a plot of  $C/T$  vs  $T^2$  between 0.5 K and 10 K. The straight line is a fit of Eqn. III.4 which yields  $\gamma = 26$   $\text{mJ/mol K}^2$  and  $\theta_D = 156$  K.

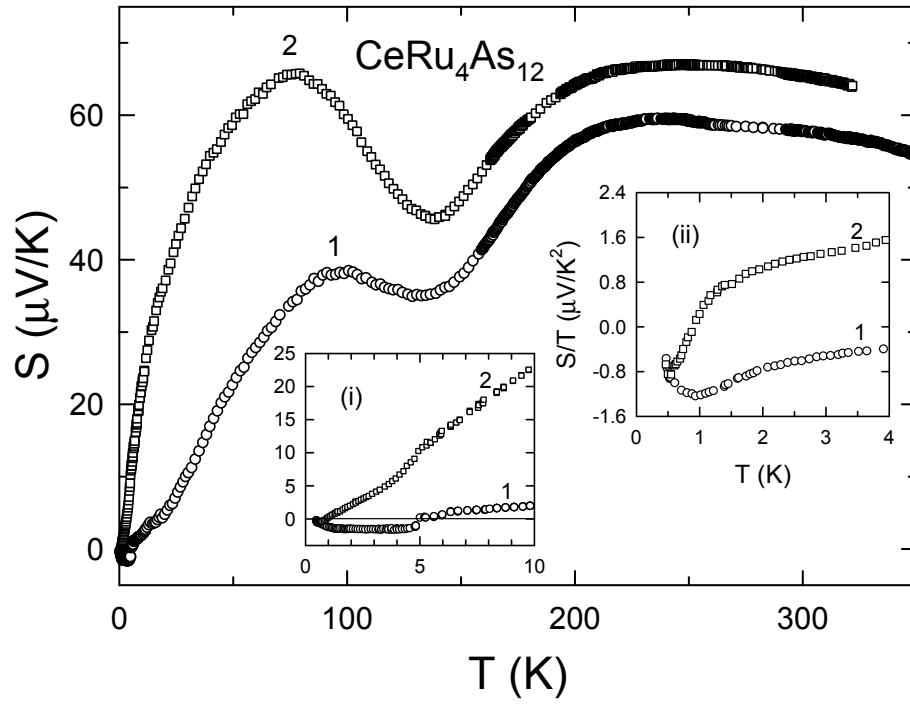


Figure III.5: Thermoelectric power  $S$  vs temperature  $T$  for two different crystals of  $\text{CeRu}_4\text{As}_{12}$  from the same batch. Inset (i) shows  $S$  vs  $T$  between 0.47 K and 10 K while inset (ii) displays  $S/T$  vs  $T$  between 0.47 K and 4 K.

## Bibliography

- [1] M. B. Maple, E. D. Bauer, N. A. Frederick, P.-C. Ho, W. M. Yuhasz, and V. S. Zapf, *Physica B* **328**, 29 (2003).
- [2] Y. Aoki, H. Sugawara, H. Harima, and H. Sato, *J. Phys. Soc. Jpn.* **74**, 209 (2005).
- [3] H. Sugawara, S. Osaki, M. Kobayashi, T. Namiki, S. R. Saha, Y. Aoki, and H. Sato, *Phys. Rev. B* **71**, 125127 (2005).
- [4] D. J. Braun and W. Jeitschko, *J. Solid State Chem.* **32**, 357 (1980).
- [5] D. J. Braun and W. Jeitschko, *J. Less Comm. Met.* **72**, 147 (1980).
- [6] M. Takeda and M. Ishikawa, *J. Phys. Soc. Jpn.* **69**, 868 (2000).
- [7] E. D. Bauer, A. Slebarski, R. P. Dickey, E. J. Freeman, C. Sirvent, V. Zapf, N. R. Dilley, and M. B. Maple, *J. Phys.: Condens. Matter* **13**, 5183 (2001).
- [8] S. V. Dordevic, K. S. D. Beach, N. Takeda, Y. J. Wang, M. B. Maple, and D. N. Basov, *Phys. Rev. Lett.* **96**, 017403 (2006).
- [9] Z. Henkie, M. B. Maple, A. Pietraszko, R. Wawryk, T. Cichorek, R. E. Baumbach, W. M. Yuhasz, and P.-C. Ho, *J. Phys. Soc. Jpn. Suppl. A* **77** 128-134 (2008).
- [10] G. M. Sheldrick, in *Program for the Solution of Crystal Structures* (University of Göttingen, Germany, 1985).
- [11] G. M. Sheldrick, in *Program for Crystal Structure Refinement* (University of Göttingen, Germany, 1987).
- [12] R. Wawryk and Z. Henkie, *Phil. Mag. B* **81**, 223 (2001).
- [13] C. Sekine, N. Hoshi, K. Takeda, T. Yoshida, I. Shirovani, K. Matsuhira, M. Wakeshima, and Y. Hinatsu, *J. Magn. Magn. Matter* **310**, 260 (2007).
- [14] B. C. Sales, D. Mandrus, B. C. Chakoumakos, V. Keppens, and J. R. Thompson, *Phys. Rev. B* **56**, 15081 (1997).
- [15] B. C. Sales, B. C. Chakoumakos, D. Mandrus, J. W. Sharp, N. R. Dilley, and M. B. Maple, *Mater. Res. Soc. Symp. Proc.* **545**, 13 (1999).
- [16] G. R. Stewart, *Rev. Mod. Phys.* **73**, 797 (2001).
- [17] M. B. Maple, C. L. Seaman, D. A. Gajewski, Y. Dalichouch, V. B. Barbetta, M. C. deAndrade, H. A. Mook, H. G. Lukefahr, O. O. Bernal, and D. E. MacLaughlin, *J. Low Temp. Phys.* **95**, 225 (1994).

- [18] M. B. Maple, M. C. deAndrade, J. Herrmann, Y. Dalichouch, D. A. Gajewski, C. L. Seaman, R. Chau, R. Movshovich, M. C. Aronson, and R. Osborn, *J. Low Temp. Phys.* **99**, 224 (1995).
- [19] H. G. Lukefahr, O. O. Bernal, D. E. MacLaughlin, C. L. Seaman, M. B. Maple, and B. Andraka, *Phys. Rev. Lett.* **52**, 3038 (1995).
- [20] M. B. Maple and D. Wohlleben, *Phys. Rev. Lett.* **27**, 511 (1971).
- [21] M. B. Maple and D. Wohlleben, *AIP Conference Proceedings* (No. 18), *Magnetism and Magnetic Materials - 1073*, eds. C. D. Graham, Jr., and J. J. Rhyne, 1974; p. 447.
- [22] J. G. Huber, W. A. Fertig, and M. B. Maple, *Solid State Comm.* **15**, 453 (1974).
- [23] J. G. Huber, J. Brooks, D. Wohlleben, and M. B. Maple, *AIP Conference Proceedings* (No. 24), *Magnetism and Magnetic Materials*; p. 475.
- [24] Unpublished.
- [25] C. L. Seaman, M. B. Maple, B. W. Lee, S. Ghamaty, M. S. Torikachvili, J.-S. Kang, L. Z. Liu, J. W. Allen, and D. L. Cox, *Phys. Rev. Lett.* **67**, 2882 (1991).
- [26] R. P. Dickey, A. Amann, E. J. Freeman, M. C. de Andrade, and M. B. Maple, *Phys. Rev. B* **62**, 3979 (2000).
- [27] J. W. Allen and R. Martin, *Phys. Rev. Lett.* **49**, 1106 (1982).
- [28] M. Ocko, C. Geibel and F. Steglich, *Phys. Rev. B* **64**, 195107 (2001).
- [29] V. Zlatic and R. Monnier, *Phys. Rev. B* **71**, 165109 (2005).
- [30] K. Behnia, D. Jaccard and J. Flouquet, *J. Phys.: Condens. Matter* **16**, 5187 (2004).
- [31] J. A. Hertz, *Phys. Rev. B* **14**, 1165 (1976).
- [32] A. J. Millis, *Phys. Rev. B* **48**, 7183 (1993).
- [33] O. O. Bernal, D. E. MacLaughlin, H. G. Lukefahr, and B. Andraka, *Phys. Rev. Lett.* **75**, 2023 (1995).
- [34] E. Miranda, V. Dobrosavljevic, and G. Kotliar, *J. Phys.: Condens. Matter* **8**, 9871 (1996).
- [35] E. Miranda, V. Dobrosavljevic, and G. Kotliar, *Phys. Rev. Lett.* **78**, 290 (1997).
- [36] A. H. Castro Neto, G. Castilla, and B. A. Jones, *Phys. Rev. Lett.* **81**, 3531 (1998).

- [37] D. L. Cox, Phys. Rev. Lett. **59**, 1240 (1987).
- [38] H. Q. Yuan, F. M. Grosche, M. Deppe, C. Geibel, G. Sparn, and F. Steglich, Science **302**, 2104 (2003).
- [39] A. Holmes, D. Jaccard, and K. Miyake, Phys. Rev. B **69**, 024508 (2004).
- [40] E. Vargoz and D. Jaccard, J. Mag. Mag. Mat. **177-181**, 294-295 (1998).
- [41] S. Raymond and D. Jaccard, Phys. Rev. B **61**, 8679 (2000).
- [42] A. Onodera, S. Tsuduki, Y. Ohishi, T. Watanuki, K. Ishida, Y. Kitaoka, and Y. Onuki, J. Solid State Comm. **123**, 113-116 (2002).
- [43] Y. Onishi and K. Miyake, J. Phys. Soc. Jpn. **69**, 3955 (2001).
- [44] I. R. Walker, F. M. Grosche, D. M. Freye, and G. G. Lonzariach, Physica C **282-287**, 303 (1997).
- [45] H. Hegger, C. Petrovic, E. G. Moshopoulou, M. F. Hundley, J. L. Sarrao, Z. Fisk, and J. D. Thompson, Phys. Rev. Lett. **84**, 4986 (2000).
- [46] J. R. Jeffries, N. A. Frederick, E. D. Bauer, H. Kimura, V. S. Zapf, K. -D. Hof, and T. A. Sayles, Phys. Rev. B **72**, 024551 (2005).
- [47] M. B. Maple, Z. Henkie, R. E. Baumbach, T. A. Sayles, N. P. Butch, P.-C Ho, T. Yanagisawa, W. M. Yuhasz, R. Wawryk, T. Cichorek, and A. Pietraszko, J. Phys. Soc. Jpn. Suppl. A **77**, 7-13 (2008).
- [48] R. E. Baumbach, P.-C. Ho, T. A. Sayles, M. B. Maple, R. Wawryk, T. Cichorek, T. Pietraszko, and Z. Henkie, Proc. Natl. Acad. Sci. **105**, 17307 (2008).
- [49] A. Slebarski and J. Spalek, Phys. Rev. Lett. **95**, 046402 (2005).

The text and data presented in this chapter are reprints of material that appears in “Non Fermi liquid behavior in the filled skutterudite compound  $\text{CeRu}_4\text{As}_{12}$ ,” R. E. Baumbach, P.-C. Ho, T. A. Sayles, M. B. Maple, R. Wawryk, T. Cichorek, A Pietraszko, and Z. Henkie, *J. Phys.: Condens. Matter* 20, 075110 (2008). The dissertation author is the primary investigator and author of this article.

## IV

# The filled skutterudite $\text{CeOs}_4\text{As}_{12}$ : a hybridization gap semiconductor

### IV.A Introduction

The ternary transition metal pnictides with the chemical formula  $MT_4X_{12}$  ( $M$  = alkali metal, alkaline earth, lanthanide, actinide;  $T$  = Fe, Ru, Os;  $X$  = P, As, Sb) which crystallize in the filled skutterudite structure (space group  $\text{Im}\bar{3}$ ) exhibit a wide variety of strongly correlated electron phenomena [1, 2, 3, 4]. Many of these phenomena depend on hybridization between the rare earth or actinide  $f$ -electron states and the conduction electron states which, in some filled skutterudite systems, leads to the emergence of semiconducting behavior. This trend is evident in the cerium transition metal phosphide and antimonide filled skutterudite systems, most of which are semiconductors where the gap size is correlated with the lattice constant [5, 6, 7]. While these systems have been studied in detail, the arsenide analogues have received considerably less attention, probably due to materials difficulties inherent to their synthesis. In this paper, we present new measurements of electrical resistivity  $\rho$ , magnetization  $M$ , specific heat  $C$ , and thermoelectric

power  $S$  which show that  $\text{CeOs}_4\text{As}_{12}$  has a nonmagnetic or weakly magnetic semiconducting ground state with an energy gap  $\Delta$  in the range  $45 \text{ K} \leq \Delta/k_B \leq 73 \text{ K}$  and a small electronic specific heat coefficient  $\gamma \sim 19 \text{ mJ/mol K}^2$ . Thus, we suggest that  $\text{CeOs}_4\text{As}_{12}$  may be a member of the class of compounds, commonly referred to as hybridization gap semiconductors or, in more modern terms, Kondo insulators. In these materials the localized  $f$ -electron states hybridize with the conduction electron states to produce a small gap ( $\sim 1 - 10 \text{ meV}$ ) in the electronic density of states. Depending on the electron concentration, the Fermi level can be found within the gap, yielding semiconducting behavior, or outside the gap, giving metallic heavy fermion behavior. For a more complete discussion of the topic, we refer the reader to several excellent reviews [8, 9]. For comparison purposes, we also report results for the weakly magnetic analogue material  $\text{LaOs}_4\text{As}_{12}$ .

## IV.B Experimental Details

Single crystals of  $\text{CeOs}_4\text{As}_{12}$  and  $\text{LaOs}_4\text{As}_{12}$  were grown from elements with purities  $\geq 99.9 \%$  by a molten metal flux method at high temperatures and pressures, as reported elsewhere [10]. After removing the majority of the flux by distillation,  $\text{CeOs}_4\text{As}_{12}$  single crystals with dimensions up to  $\sim 0.7 \text{ mm}$  and  $\text{LaOs}_4\text{As}_{12}$  single crystals with dimensions up to  $\sim 0.3 \text{ mm}$  were collected and cleaned in acid in an effort to remove any impurity phases from the surfaces of the crystals. The crystal structure of  $\text{CeOs}_4\text{As}_{12}$  was determined by X-ray diffraction on a crystal with dimensions of  $0.28 \times 0.25 \times 0.23 \text{ mm}$ . A total of 5757 reflections (454 unique,  $R_{\text{int}}=0.1205$ ) were recorded and the structure was resolved by the full matrix least squares method using the SHELX-97 program [11, 12]. A similar measurement was made for the  $\text{LaOs}_4\text{As}_{12}$  crystals.

Electrical resistivity  $\rho(T)$  measurements for temperatures  $T = 65 \text{ mK} - 300 \text{ K}$  and magnetic fields  $H = 0 - 9 \text{ T}$  were performed on the  $\text{CeOs}_4\text{As}_{12}$  crystals in a four-wire configuration using a conventional  $^4\text{He}$  cryostat and a  $^3\text{He} - ^4\text{He}$  dilution

refrigerator. Magnetization  $M(T)$  measurements for  $T = 1.9$  K - 300 K and  $H = 0$  - 5.5 T were conducted using a Quantum Design Magnetic Properties Measurement System on mosaics of both  $\text{CeOs}_4\text{As}_{12}$  ( $m = 154.2$  mg) and  $\text{LaOs}_4\text{As}_{12}$  ( $m = 138.9$  mg) crystals, which were mounted on a small Delrin disc using Duco cement. Specific heat  $C(T)$  measurements for  $T = 650$  mK - 18 K and  $H = 0$  and 5 T were made using a standard heat pulse technique on a collection of 116 single crystals ( $m = 65$  mg) of  $\text{CeOs}_4\text{As}_{12}$  which were attached to a sapphire platform with a small amount of Apiezon N grease in a  $^3\text{He}$  semiadiabatic calorimeter. Thermoelectric power  $S(T)$  measurements for  $T = 0.5$  K - 350 K for  $\text{CeOs}_4\text{As}_{12}$  single crystals was determined by a method described elsewhere [13].

### IV.C Results

Single crystal structural refinement shows that the unit cells of  $\text{CeOs}_4\text{As}_{12}$  and  $\text{LaOs}_4\text{As}_{12}$  have the  $\text{LaFe}_4\text{P}_{12}$  - type structure ( $\text{Im}\bar{3}$  space group) with two formula units per unit cell, and room temperature lattice constants  $a = 8.519(2)$  Å and  $a = 8.542(1)$  Å, respectively, in reasonable agreement with earlier measurements of  $a = 8.5249(3)$  Å and  $a = 8.5296$  Å for  $\text{CeOs}_4\text{As}_{12}$  and  $a = 8.5437(2)$  Å for  $\text{LaOs}_4\text{As}_{12}$  [6, 14]. Other crystal structure parameters for these compounds are summarized in Table IV.1. The displacement parameter  $D$  represents the average displacement of an atom vibrating around its lattice position and is equal to its mean-square displacement along the Cartesian axes. The displacement parameters determined for  $\text{CeOs}_4\text{As}_{12}$  and  $\text{LaOs}_4\text{As}_{12}$  are typical of the lanthanide filled skutterudites [15, 16]. Table IV.1 also indicates that the Ce sites in  $\text{CeOs}_4\text{As}_{12}$  may not be fully occupied, as is often the case for filled skutterudite materials. By comparison to other lanthanide filled skutterudite arsenides, the lattice constant of  $\text{CeOs}_4\text{As}_{12}$  is reduced from the expected lanthanide contraction value, indicating that the  $\text{Ce}^{3+}$  4*f*-electron states are strongly hybridized with the conduction electron states of the surrounding Os and As ions.

Electrical resistivity data for a typical  $\text{CeOs}_4\text{As}_{12}$  single crystal specimen for  $T = 65 \text{ mK} - 300 \text{ K}$  and  $H = 0$  and a polycrystalline  $\text{LaOs}_4\text{As}_{12}$  reference specimen [17] are shown in Fig. IV.1. For  $H = 0 \text{ T}$ ,  $\rho(T)$  for  $\text{CeOs}_4\text{As}_{12}$  decreases weakly with  $T$  from a value near  $1 \text{ m}\Omega\text{cm}$  at  $300 \text{ K}$  to  $0.5 \text{ m}\Omega\text{cm}$  at  $135 \text{ K}$ , below which  $\rho(T)$  increases continuously to low  $T$ . An extremely broad hump centered around  $\sim 15 \text{ K}$  is superimposed on the increasing  $\rho(T)$  which saturates below  $300 \text{ mK}$  towards a constant value near  $100 \text{ m}\Omega\text{cm}$ . Above  $135 \text{ K}$ ,  $\rho(T)$  for  $\text{CeOs}_4\text{As}_{12}$  is similar to that of polycrystalline  $\text{LaOs}_4\text{As}_{12}$ . However, below  $135 \text{ K}$ ,  $\text{LaOs}_4\text{As}_{12}$  continues to exhibit metallic behavior, wherein  $\rho(T)$  saturates near  $0.1 \text{ m}\Omega\text{cm}$  before undergoing an abrupt drop at the superconducting transition near  $3.2 \text{ K}$ . With the application of a magnetic field (left Fig. IV.1 inset),  $\rho(T)$  for  $\text{CeOs}_4\text{As}_{12}$  increases for  $3 \text{ K} \leq T \leq 300 \text{ K}$  by a small and nearly temperature independent amount and the broad hump moves towards lower  $T$ . Below  $\sim 3 \text{ K}$ ,  $\rho(T)$  for  $\text{CeOs}_4\text{As}_{12}$  is drastically affected by  $H$ , where the residual resistivity,  $\rho_0$ , is reduced by more than a factor of 10 with  $H = 5 \text{ T}$ . For fields greater than  $5 \text{ T}$ , the relative effect of increasing magnetic field on  $\rho(T)$  is less pronounced, as  $\rho_0$  saturates near  $6 \text{ m}\Omega\text{cm}$ . Finally, it should be noted that the residual resistivity for  $H = 9 \text{ T}$  is slightly larger than that for  $H = 7 \text{ T}$ .

DC magnetization data,  $\chi(T) = M(T)/H$ , collected in a small constant field  $H = 0.5 \text{ kOe}$ , are shown in Fig. IV.2 for  $\text{CeOs}_4\text{As}_{12}$  and  $\text{LaOs}_4\text{As}_{12}$ . For  $\text{CeOs}_4\text{As}_{12}$ ,  $\chi(T)$  shows a weak and unusual  $T$  dependence. Below  $300 \text{ K}$ ,  $\chi(T)$  decreases with decreasing  $T$ , suggesting a maximum above  $300 \text{ K}$ . Below a first minimum at  $T \sim 135 \text{ K}$ ,  $\chi(T)$  increases with decreasing  $T$  down to  $T_{\chi,0} \sim 45 \text{ K}$ , where it again decreases with decreasing  $T$  down to  $\sim 20 \text{ K}$ . Near  $20 \text{ K}$ ,  $\chi(T)$  show a second minimum, below which a weak upturn persists down to  $1.9 \text{ K}$  with a small feature between  $2$  and  $4 \text{ K}$ . The minimum in  $\chi(T)$  near  $135 \text{ K}$  roughly corresponds to the temperature where  $\rho(T)$  begins to increase with decreasing  $T$ . The low  $T$  upturn in  $\chi(T)$  is weakly suppressed in field, as reflected in the low temperature  $M$  vs  $H$  isotherms (not shown) which have weak negative curvature, and only begin

to show a tendency towards saturation above  $\sim 30$  kOe. No hysteretic behavior is observed. Similar measurements for  $\text{LaOs}_4\text{As}_{12}$  at  $T = 1.9$  K reveal that the low  $T$  magnetic isotherm is linear in field up to 55 kOe. The magnetic susceptibility of  $\text{LaOs}_4\text{As}_{12}$  is of comparable magnitude to that of  $\text{CeOs}_4\text{As}_{12}$ , and shows a weak increase with decreasing  $T$  down to the superconducting transition temperature  $T_c \sim 3.2$  K, as is typical for many La based compounds for which  $\chi(T)$  often has a weak temperature dependence [18].

Displayed in Fig. IV.3 are specific heat divided by temperature  $C(T)/T$  vs  $T^2$  data for  $T = 650$  mK - 18 K in magnetic fields  $H = 0$  and 5 T. For  $650$  mK  $< T < 7$  K,  $C(T)/T$  is described by the expression,

$$C(T)/T = \gamma + \beta T^2 \quad (\text{IV.1})$$

where  $\gamma$  is the electronic specific heat coefficient and  $\beta \propto \theta_D^{-3}$  describes the lattice contribution. Fits of Eqn. IV.1 to the zero field  $C(T)/T$  data show that  $\gamma(H = 0) \sim 19$  mJ/mol K<sup>2</sup> and  $\theta_D(H = 0) \sim 264$  K. In contrast to  $\rho(T)$ , the application of a 5 T magnetic field has only a modest affect on  $C(T)/T$ , for which  $\gamma$  remains constant while  $\theta_D$  increases to  $\sim 287$  K. It should also be noted that a small deviation from the linear behavior is seen at  $T^2 \sim 40$  K<sup>2</sup> ( $T \sim 6$  K), as shown in the Fig. IV.3 inset.

The thermoelectric power  $S(T)$  data for  $\text{CeOs}_4\text{As}_{12}$  and  $\text{LaOs}_4\text{As}_{12}$  are shown in Fig. IV.4. Near 300 K,  $S(T)$  for  $\text{CeOs}_4\text{As}_{12}$  is positive and one order of magnitude larger than that for metallic  $\text{LaOs}_4\text{As}_{12}$ , which is shown here for reference and studied in greater detail elsewhere [18]. From room  $T$ , the thermoelectric power for  $\text{CeOs}_4\text{As}_{12}$  increases with decreasing  $T$  to a maximum value  $S_{MAX} = 83$   $\mu\text{V}/\text{K}$  at  $T_{MAX} = 135$  K, close to the  $T$  where semiconducting behavior is first observed in the  $\rho(T)$  data. The  $S(T)$  data then decrease with decreasing  $T$  down to a minimum  $S_{min} = 31$   $\mu\text{V}/\text{K}$  at  $T_{min} = 12$  K, close to the maximum of the broad hump in  $\rho(T)$ . Additionally, there is a broad peak superimposed on the decreasing  $S(T)$  for  $T = 12$  K - 60 K. Below 12 K, the  $S(T)$  data go through a

second maximum  $S_{max} = 46 \mu\text{V/K}$  at  $T_{max} = 2 \text{ K}$  and finally continue to decrease down to 0.5 K, but remain positive.

#### IV.D Discussion

When viewed globally, measurements of x-ray diffraction,  $\rho(T)$ ,  $M(T)$ ,  $C(T)/T$ , and  $S(T)$  indicate that strong  $f$ -electron - conduction electron hybridization dominates the physics of  $\text{CeOs}_4\text{As}_{12}$ , yielding a variety of types of behavior which can be roughly divided into high ( $T \geq 135 \text{ K}$ ) and low ( $T \leq 135 \text{ K}$ ) temperature regions. For  $T > 135 \text{ K}$ , the unusual behavior is most pronounced in the  $\chi(T)$  data, which deviate from the typical Curie - Weiss  $T$ -dependence expected for  $\text{Ce}^{3+}$  ions and instead decrease with decreasing  $T$  to a broad minimum near  $135 \text{ K} \leq T \leq 150 \text{ K}$ . Although it is difficult to definitively determine the origin of this  $T$ -dependence, possible mechanisms include valence fluctuations and Kondo behavior. In the valence fluctuation picture, which was introduced to account for the nonmagnetic behavior of  $\alpha$  - Ce [19], SmS in its collapsed “gold” phase [20], and  $\text{SmB}_6$  [21], the  $4f$ -electron shell of each Ce ion temporally fluctuates between the configurations  $4f^1$  ( $\text{Ce}^{3+}$ ) and  $4f^0$  ( $\text{Ce}^{4+}$ ) at a frequency  $\omega \approx k_B T_{vf}/\hbar$ , where  $T_{vf}$  separates magnetic behavior at high temperatures  $T \gg T_{vf}$  and nonmagnetic behavior at low temperatures  $T \ll T_{vf}$ . In this phenomenological model, the decrease in  $\chi(T)$  with decreasing  $T$  can be accounted for in terms of an increase in the Ce ion valence  $v(T)$  with decreasing  $T$  towards 4+, corresponding to a decrease in the average  $4f$ -electron shell occupation number  $n_{4f}(T)$  towards zero. At  $T = 0 \text{ K}$ ,  $\chi(T)$  should be approximately,

$$\chi(0) \approx \frac{n_{4f^0}(T)\mu_{eff}^2(4f^0) + n_{4f^1}(T)\mu_{eff}^2(4f^1)}{3k_B(T + T_{vf})} \Big|_{T=0} \quad (\text{IV.2a})$$

$$= \frac{n_{4f^1}(0)\mu_{eff}^2(4f^1)}{3k_B(T_{vf})} \quad (\text{IV.2b})$$

since  $\mu_{eff}(4f^0) = 0$ . In this model, the value of  $T_{sf}$  can be estimated from the Curie - Weiss behavior of  $\chi(T)$  for  $T \gg T_{sf}$  where it plays the role of the Curie -

Weiss temperature, and  $n_{4f^1}(0)$  can be inferred from  $\chi(0)$ . Since the Curie - Weiss behavior would be well above room  $T$  for this case, it is not possible to estimate  $T_{sf}$  and  $n_{4f^1}(T)$ . The behavior of  $n_{4f^1}(0)$  can also be deduced from measurements of the lattice constant  $a$  as a function of  $T$ , by x - ray diffraction or thermal expansion measurements. The increase in valence with decreasing  $T$  is reminiscent of the  $\gamma - \alpha$  transition in elemental Ce, in which the valence undergoes a transition towards 4+ with decreasing  $T$  that is discontinuous (1st order) for pressures  $P < P_c$  where  $P_c$  is the critical point, and continuous (2nd order) for  $P > P_c$ . According to this picture, it would appear that the critical point for CeOs<sub>4</sub>As<sub>12</sub> is at a negative pressure and the valence is increasing with decreasing  $T$ . A great deal of effort has been expended to develop a microscopic picture of the intermediate valence state, and the reader is referred to two of many review articles on the subject [22, 23].

In contrast to the intermediate valence picture, it is possible that the Ce ions remain in the 3+ state at all  $T$ , and the Ce<sup>3+</sup> magnetic moments are screened by the conduction electron spins below a characteristic temperature  $T_K$ . This scenario is commonly called the Kondo picture [24], and may be appropriate for CeOs<sub>4</sub>As<sub>12</sub> if  $T_K > 300$  K, leading to Curie - Weiss behavior for  $T > T_K$  and the observed  $\chi(T)$  behavior for  $135 \text{ K} < T < T_K$ . A rough approximation of  $T_K$  can be made using the expression,

$$T_K = N_A \mu_{eff}^2 / 3 \chi_0 k_B \quad (\text{IV.3})$$

where  $\mu_{eff} = 2.54 \mu_B$  is the Hund's rule value for Ce<sup>3+</sup> ions and  $\chi_0 \sim 1.2 \times 10^{-3} \text{ cm}^3 / \text{mol}$  is the saturated value of  $\chi(T)$  at  $T \sim 135$  K, representing the magnetic susceptibility of a screened Kondo ion singlet [25]. Using this rough expression,  $T_K$  is found to be near 670 K, supporting the notion of a high Kondo temperature. Moreover, if the Kondo interpretation with a high  $T_K$  is correct, the decrease of  $\rho(T)$  with decreasing  $T$  may reflect the onset of Kondo coherence above 300 K, in addition to the freezing out of phonons. Finally, it is worth noting that the  $\chi(T)$  data for LaOs<sub>4</sub>As<sub>12</sub> indicate that spin fluctuations associated with

the transition metal atoms do not account for the unusual  $\chi(T)$  behavior seen for  $\text{CeOs}_4\text{As}_{12}$ .

The affects of  $f$ -electron - conduction electron hybridization become even more pronounced below 135 K, where  $\rho(T)$  evolves into a gapped semiconducting state which persists to the lowest  $T$  measured. The increase in  $\rho(T)$  is not well described by a simple Arrhenius function, as would be expected for a semiconductor with a single energy gap. Instead, the following phenomenological expression [26],

$$\rho^{-1}(T) = \sum_{i=0}^3 A_i \exp(-\Delta_i/k_B T) \quad (\text{IV.4})$$

where  $A_1 = 2.7 \text{ (m}\Omega\text{cm)}^{-1}$ ,  $\Delta_1/k_B = 73 \text{ K}$ ,  $A_2 = 0.44 \text{ (m}\Omega\text{cm)}^{-1}$ ,  $\Delta_2/k_B = 16 \text{ K}$ ,  $A_3 = 0.18 \text{ (m}\Omega\text{cm)}^{-1}$  and  $\Delta_3/k_B = 2.51 \text{ K}$ , describes the data for  $1 \text{ K} \leq T \leq 135 \text{ K}$ , as shown in the right Fig. IV.1 inset. A possible interpretation of this fit is that the large gap  $\Delta_1$  describes the intrinsic energy gap for  $\text{CeOs}_4\text{As}_{12}$  while  $\Delta_2$  and  $\Delta_3$  describe impurity donor or acceptor states in the gap (Kondo holes) [27, 28, 29], or, possibly, a pseudogap. In this situation, it is naively expected that the application of a magnetic field will act to close the energy gaps ( $\Delta_1, \Delta_2, \Delta_3$ ) through the Zeeman interaction,

$$\Delta_n(H) = \Delta_n(H = 0) - g_J |J_z| \mu_B H \quad (\text{IV.5})$$

where  $\Delta_n(H = 0)$  are the zero field gaps,  $g_J = 6/7$  is the Landé  $g$  factor for  $\text{Ce}^{3+}$  ions,  $J_z = 5/2$  is the  $z$  component of the total angular momentum for  $\text{Ce}^{3+}$  ions, and  $\mu_B$  is the Bohr magneton. According to this expression, it is expected that a field  $H = \Delta_n(H = 0)/g_J |J_z| \mu_B \sim 1.74 \text{ T}$  is sufficient to close the low  $T$  gap. This behavior is qualitatively shown in the left Fig. IV.1 inset where the low  $T$  resistivity is reduced by nearly 70 % for  $H = 1.5 \text{ T}$ .

Concurrent with the emergence of the semiconducting behavior,  $\chi(T)$  increases slowly down to  $T_{\chi,0} \sim 45 \text{ K}$ , where it goes through a maximum and then continues to decrease with decreasing  $T$ . Therefore, there is an apparent correlation between the intrinsic energy gap value  $\Delta_1 \sim 73 \text{ K}$  taken from fits to

$\rho(T)$  and the broad maximum in  $\chi(T)$  centered around  $T_{\chi,0} \sim 45$  K. If  $T_{\chi,0}$  is taken to indicate the onset of a coherent nonmagnetic ground state where  $T_{\chi,0} \sim T_{coh} \sim \Delta_1/k_B$ , then the likely description of the ground state is the well known many body hybridization gap picture, where the magnetic moments of the  $Ce^{3+}$   $f$ -electron lattice are screened by conduction electron spins via an antiferromagnetic exchange interaction.

In the context of this model, the weak upturn in  $\chi(T)$  for  $T < 20$  K is unexpected. For this reason, it is necessary to consider whether it is intrinsic or extrinsic to  $CeOs_4As_{12}$ . As shown in the inset to Fig. IV.2, various functions describe the  $T$ -dependence of the upturn below  $\sim 10$  K, including both power law and logarithmic functions of the forms,

$$\chi(T) = aT^{-m} \quad (IV.6)$$

and

$$\chi(T) = b - c \ln(T) \quad (IV.7)$$

where  $a = 1.96 \times 10^{-3}$  cm<sup>3</sup>K <sup>$m$</sup> /mol and  $m = 0.16$ , or  $b = 1.92 \times 10^{-3}$  cm<sup>3</sup>/mol and  $c = 0.25 \times 10^{-3}$  cm<sup>3</sup>/mol, respectively. These weak power law and logarithmic divergences in  $T$  of physical properties are often associated with materials that exhibit non-Fermi liquid behavior due to the proximity of a quantum critical point [30, 31, 32]. On the other hand, it is also possible that the upturn is the result of paramagnetic impurities, as is often found for hybridization gap semiconductors [9, 33]. To address this possibility, the low  $T$  upturn in  $\chi(T)$  was fitted using a Curie - Weiss function of the form,

$$\chi(T) = \chi_0 + C_{imp}/(T - \Theta) \quad (IV.8)$$

where  $\chi_0 = 1.13 \times 10^{-3}$  cm<sup>3</sup>/mol,  $C_{imp}(T) = 3.12 \times 10^{-3}$  cm<sup>3</sup>K/mol, and  $\Theta = -3$  K. Although it is not possible, by means of this measurement, to quantitatively determine the origin of such an impurity contribution, a rough estimate of the

impurity concentration can be made by assuming that it is due to paramagnetic impurity ions, such as rare earth ions like  $\text{Ce}^{3+}$  or  $\text{Gd}^{3+}$ , which give impurity concentrations near 0.4 % and 0.04% respectively. Finally, to elucidate the significance of an impurity contribution of this type, the hypothetical intrinsic susceptibility  $\chi_{int}(T) = \chi(T) - \chi_{imp}(T)$  is shown in Fig. IV.2. The resulting  $\chi_{int}(T)$  remains nearly identical to  $\chi(T)$  down to  $\sim 100$  K, where the affect of  $\chi_{imp}(T)$  becomes apparent. Near 55 K,  $\chi_{int}(T)$  goes through a weak maximum and then saturates towards a value near  $1.1 \times 10^{-3} \text{ cm}^3/\text{mol}$  with decreasing  $T$ , consistent with the onset of Kondo coherence leading to a weakly magnetic or nonmagnetic ground state.

Additionally, the behavior of  $C(T)/T$  at low  $T$  supports the hybridization gap interpretation, for which the low  $T$  electronic specific heat coefficient  $\gamma = C/T$  is expected to be zero in the fully gapped scenario, or small and finite if a low concentration of donor or acceptor levels are present or if there is a pseudogap [34]. Similar results were seen for the archetypal hybridization gap semiconductor  $\text{Ce}_3\text{Bi}_4\text{Pt}_3$ , for which  $\gamma \sim 3.3 \text{ mJ}/(\text{mol Ce K}^2)$ . For hybridization gap semiconductors, this value is expected to be sample dependent and to correlate with the number of impurities in the system [9, 35]. Similar sample dependence has been observed in both  $\rho(T)$  and  $C(T)/T$  measurements for  $\text{CeOs}_4\text{As}_{12}$  specimens. Moreover, a comparison to other systems where large effective masses are seen as the result of many body enhancements can be made by computing an effective Wilson-Sommerfeld ratio  $R_W = (\pi^2 k_B^2 / 3\mu_{eff}^2)(\chi/\gamma)$ . The values  $\chi$ ,  $\chi_{int}$ , and  $\gamma$  are taken at 1.9 K to probe the low temperature state. Also, the Hund's rule effective magnetic moment  $\mu_{eff} = 2.54 \mu_B$  for  $\text{Ce}^{3+}$  ions is used. From these values,  $R_W$  is calculated to be  $\sim 1.04$  and  $\sim 0.67$ , for the  $\chi$  and  $\chi_{int}$  cases. As expected, these values are similar to those found in  $f$ -electron materials where the low  $T$  transport and thermodynamic properties are due to conduction electrons with or without enhanced masses.

The  $T$  dependence of the thermoelectric power provides further insight

into the hybridization gap picture. Since  $S(T)$  remains positive over the entire  $T$  range, it appears that charge carriers excited from the top of the valence band to the conduction band dominate the transport behavior for all  $T$ . However, a single energy gap and charge carrier picture does not adequately describe the  $T$  dependence of the data. Instead, there are several unusual features which include, (1)  $T_{MAX} = 135$  K, which corresponds to the high  $T$  transition in  $\rho(T)$  from semimetallic to metallic behavior, (2)  $T_{min} = 12$  K, which is close to the low  $T$  portion of the extremely broad hump superimposed on  $\rho(T)$ , and (3)  $T_{max} = 2$  K, which is close to  $\Delta_3/k_B$ . Thus, there is a close correspondence between the deviations from a single energy gap picture between  $S(T)$  and  $\rho(T)$ , although the deviations are more pronounced in  $S(T)$  since electrons and holes make contributions of opposite sign to the total  $S(T)$ . To further characterize  $S(T)$ , it is useful to consider the expression [36],

$$S(T) = -P(\mu_n, \mu_p)(k_B/e)(\Delta/2k_B T) + Q \quad (\text{IV.9})$$

which describes intrinsic effects in  $S(T)$  for a gapped system, such as activation of electrons from the lower band to the higher one, which creates both hole and electron charge carriers. For this expression, the coefficients  $P(\mu_n, \mu_p) = (\mu_n - \mu_p)/(\mu_n + \mu_p)$  and  $Q = - (k_B/e)[(a/2k_B) - 2] - (3/4)\ln(m_n/m_p)$ , are defined by the electron mobility  $\mu_n$ , hole mobility  $\mu_p$ , the temperature coefficient  $a$  of  $\Delta$  vs  $T$ , the electron effective mass  $m_n$ , and the hole effective mass  $m_p$ . Since the quantity  $Q(a, m_n, m_p)$  is expected to be weakly  $T$  dependent, this expression is a useful tool for identifying energy gap behavior, as was the case for the semiconductor  $\text{Th}_3\text{As}_4$  [37]. However, as shown in the left Fig. IV.4 inset, there is only one  $T$  range,  $6.5 \text{ K} \leq T \leq 15 \text{ K}$ , where this type of behavior is observed. A linear fit to  $S(T)$  in this  $T$  range yields  $\Delta/k_B = 2.2 \text{ K}$ , which is of the order of  $\Delta_3/k_B$  found by fits to  $\rho(T)$ . To further characterize  $S(T)$ , it is also of interest to consider  $dS/dT$  vs  $\log T$  (not shown), which was used previously to analyze the compound  $\text{Ce}_x\text{Y}_{1-x}\text{Cu}_{2.05}\text{Si}_2$  [38], where a change in the slope was interpreted as evidence for

a change of dominant electronic transport mechanism. For  $\text{CeOs}_4\text{As}_{12}$ , inspection of  $dS/dT$  vs  $\log T$  yields a characteristic temperature  $T^* = 32$  K.

Behnia et al. [39] have argued that, in the zero temperature limit, the thermoelectric power should obey the relation,

$$q = (S/T)(N_A e/\gamma) \quad (\text{IV.10})$$

where  $N_A$  is Avogadro's number,  $e$  is the electron charge and the constant  $N_A e = 9.65 \times 10^4$  C mol<sup>-1</sup> is the Faraday number. The dimensionless quantity  $q$  corresponds to the density of carriers per formula unit for the case of a free electron gas with an energy independent relaxation time. Taking the values  $S/T = 17.5$  V/K<sup>2</sup> and  $\gamma = 19$  mJ/mol K<sup>2</sup> at  $T = 0.5$  K and 0.65 K, respectively, the quantity  $q = 89$  is calculated. This value is nearly two orders of magnitude larger than that seen for most of the correlated electron metals analyzed by Behnia et al., but is similar to that found for the Kondo insulator CeNiSn ( $q = 107$ ), for which the Hall carrier density was found to be 0.01/f.u. at 5 K [39]. Thus, the  $q$  determined for  $\text{CeOs}_4\text{As}_{12}$  is consistent with a related hybridization gap insulator and may be indicative of a low charge carrier density in  $\text{CeOs}_4\text{As}_{12}$  at low  $T$ .

## IV.E Summary

The compound  $\text{CeOs}_4\text{As}_{12}$  is considered in the context of a simple picture where valence fluctuations or Kondo behavior dominates the physics down to  $T \sim 135$  K. The correlated electron behavior is manifested at low temperatures as a hybridization gap insulating state, or using modern terminology, as a Kondo insulating state. The size of the energy gap  $\Delta_1/k_B \sim 73$  K, is deduced from fits to electrical resistivity data and the evolution of a weakly magnetic or nonmagnetic ground state, which is evident in the magnetization data below a coherence temperature  $T_{coh} \sim 45$  K. Additionally, the low temperature electronic specific heat coefficient is small,  $\gamma \sim 19$  mJ/mol K<sup>2</sup>, as is expected for hybridization gap insu-

lators. The thermoelectric power and electrical resistivity data also indicate that either impurity states in the energy gap or the presence of a pseudogap strongly perturbs the physical behavior away from that of an ideal hybridization gap insulator.

Table IV.1: Crystal structure data for  $\text{LaOs}_4\text{As}_{12}$  and  $\text{CeOs}_4\text{As}_{12}$ . The atomic coordinates  $x$ ,  $y$ , and  $z = 0.25$  for  $T$  atoms and 0 for  $M$  atoms. The listed quantities are the following;  $a$  ( $\text{\AA}$ ) is the unit cell parameter,  $x$ ,  $y$ , and  $z$  are the atomic coordinates for the As atoms,  $O$  are the occupancy factors for the  $T$ , As, and  $M$  atoms,  $l_{M,T:As}$  ( $\text{\AA}$ ) are the chemical bond lengths  $M$  - As and  $T$  - As,  $D$  ( $\text{\AA}^2 \times 10^3$ ) are the displacement parameters for atoms  $T$ , As,  $M$ , and  $R1/wR2$  are the final discrepancy factors in %.

	$\text{LaOs}_4\text{As}_{12}$	$\text{CeOs}_4\text{As}_{12}$
$a$	8.542(1)	8.519(2)
$x$	0.1488	0.1485
$y$	0.3491	0.3485
$z$	0	0
$O_T$	1.00	1.00
$O_{As}$	1.00	1.00
$O_M$	1.00	0.99
$l_{M,As}$	3.2416	3.2350
$l_{T,As}$	2.4544	2.4470
$D$	6; 7; 14	3; 4; 12
$R1/wR2$	3.49/8.55	4.02/11.0

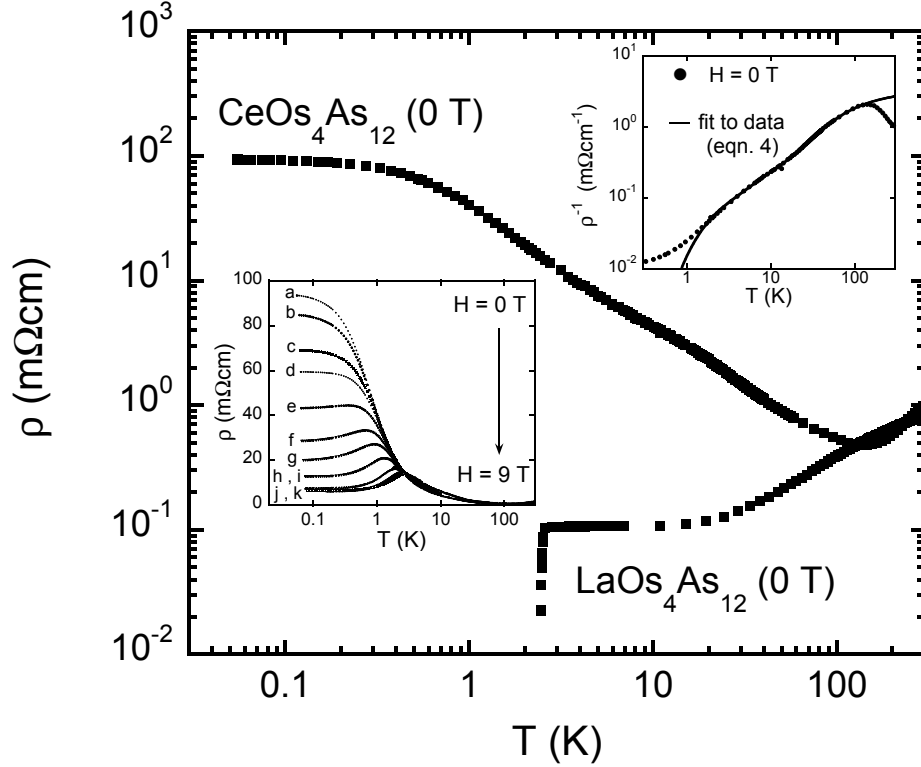


Figure IV.1: Electrical resistivity  $\rho$  vs temperature  $T$  data for  $\text{LaOs}_4\text{As}_{12}$  [17] and  $\text{CeOs}_4\text{As}_{12}$  for  $T = 65$  mK - 300 K. Right inset close up: The zero field  $\rho(T)$  data for  $\text{CeOs}_4\text{As}_{12}$  are not described well by an Arrhenius equation which would be appropriate for a simple single gap semiconductor. Instead, the data are described by a three gap expression (Eqn. IV.4). Left inset close up:  $\rho(T)$  data for  $\text{CeOs}_4\text{As}_{12}$  for  $T = 65$  mK - 300 K and magnetic fields (a) 0 T, (b) 0.3 T, (c) 0.5 T, (d) 0.7 T, (e) 1.0 T, (f) 1.5 T, (g) 2.0 T, (h) 3.0 T, (i) 5.0 T, (j) 7.0 T, and (k) 9.0 T.

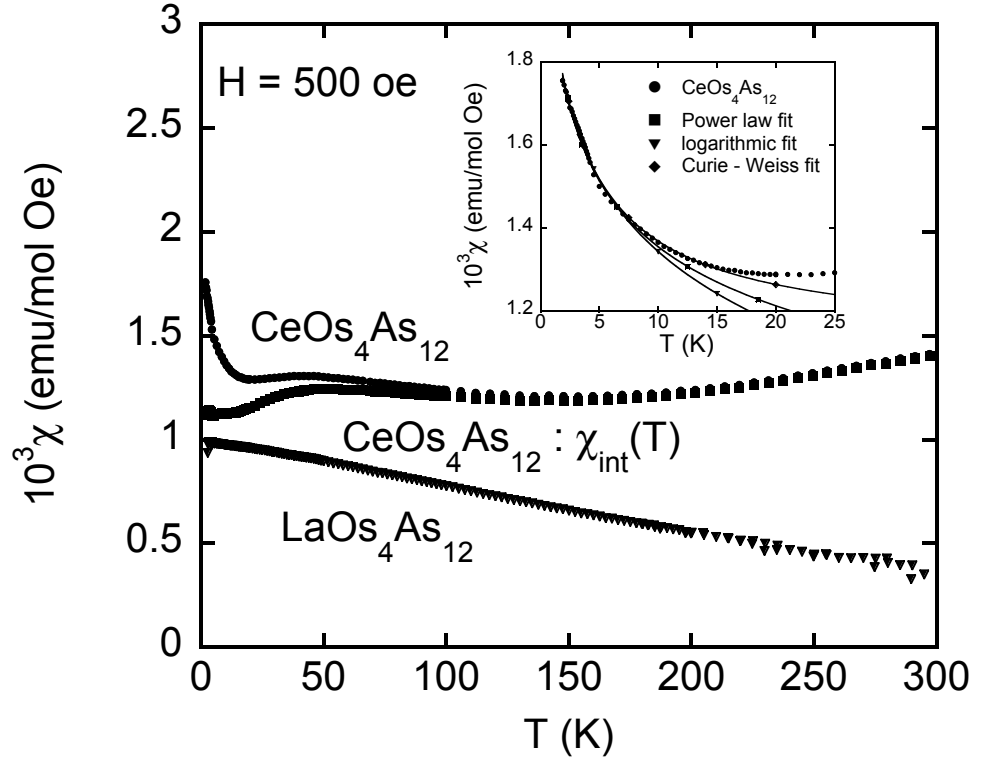


Figure IV.2: Magnetic susceptibility  $M/H = \chi$  vs temperature  $T$  data for  $\text{CeOs}_4\text{As}_{12}$  and  $\text{LaOs}_4\text{As}_{12}$  for  $T = 1.9$  K - 300 K and  $H = 500$  Oe. Also shown is the intrinsic magnetic susceptibility  $\chi_{int}(T)$ , as defined in the text, for which a Curie - Weiss (CW) impurity contribution has been subtracted. Inset close up: The low  $T$  fits to  $\chi(T)$  are described by Eqns. IV.6, IV.7, and IV.8.

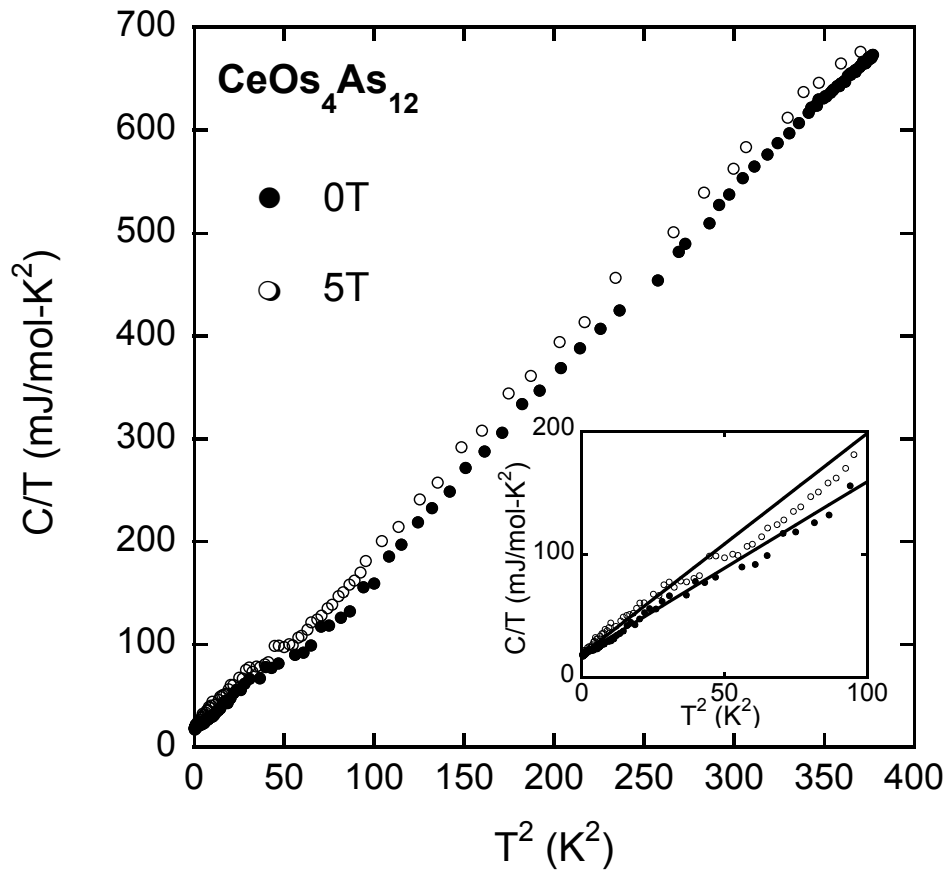


Figure IV.3: Specific heat divided by temperature  $C(T)/T$  vs temperature squared  $T^2$  data for  $\text{CeOs}_4\text{As}_{12}$  for  $T = 650$  mK - 18 K and in magnetic fields of 0 and 5 T. Inset close up:  $C(T)/T$  vs  $T^2$  data for  $T = 650$  mK - 10 K and in magnetic fields of 0 and 5 T. The straight lines are the fits to the data as described in the text by Eqn. IV.1.

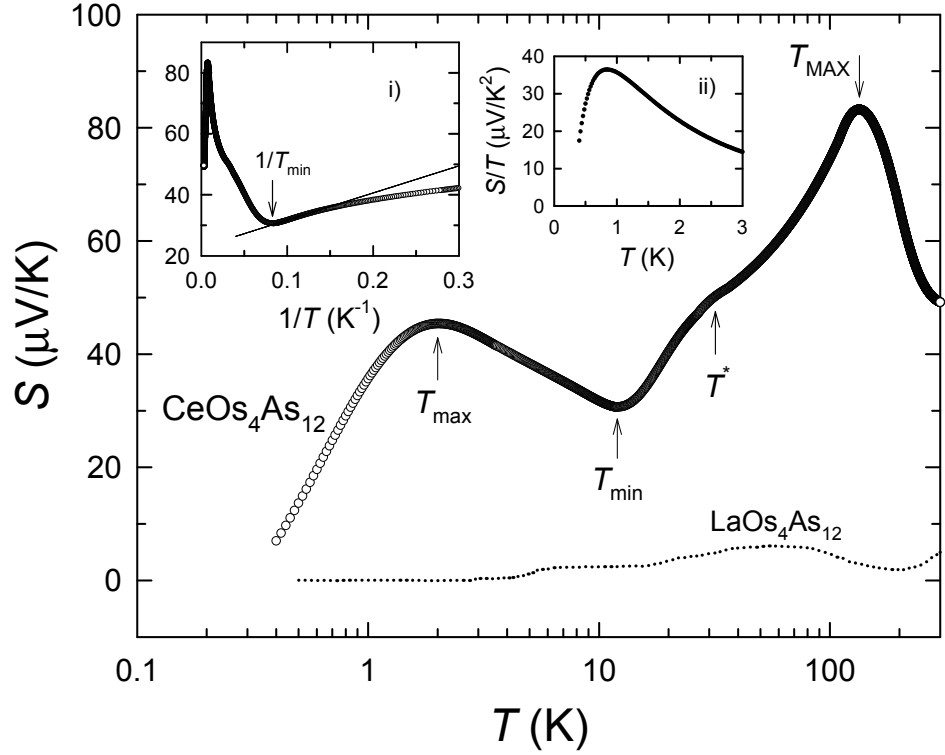


Figure IV.4: Thermoelectric power  $S$  vs temperature  $T$  for  $\text{CeOs}_4\text{As}_{12}$  and  $\text{LaOs}_4\text{As}_{12}$  for  $T = 0.5 \text{ K} - 300 \text{ K}$ . Near  $300 \text{ K}$ ,  $S(T)$  for  $\text{CeOs}_4\text{As}_{12}$  is positive and one order of magnitude larger than that for metallic  $\text{LaOs}_4\text{As}_{12}$ . Left inset close up:  $S$  vs  $1/T$  is used in the text to identify an energy gap. Right inset close up:  $S/T$  vs  $T$  is used to characterize the charge carrier density at low  $T$ , as discussed in the text.

## Bibliography

- [1] M. B. Maple, E. D. Bauer, N. A. Frederick, P.-C. Ho, W. M. Yuhasz, and V. S. Zapf, *Physica B* **328**, 29 (2003).
- [2] Y. Aoki, H. Sugawara, H. Harima, and H. Sato, *J. Phys. Soc. Jpn.* **74**, 209 (2005).
- [3] M. B. Maple, Z. Henkie, R. E. Baumbach, T. A. Sales, N. P. Butch, P.-C. Ho, T. Yanagisawa, W. M. Yuhasz, R. Wawryk, T. Cichorek, and A. Pietraszko, *J. Phys. Soc. Jpn. Suppl. A* **77**, 7 (2008).
- [4] H. Sato, D. Kikuchi, K. Tanaka, M. Ueda, H. Aoki, T. Ikeno, S. Tatsuoka, K. Kuwahara, Y. Aoki, M. Koghi, H. Sugawara, K. Iwasa, and H. Harima, *J. Phys. Soc. Jpn. Suppl. A* **77**, 1 (2008).
- [5] H. Sugawara, S. Osaki, M. Kobayashi, T. Namiki, S. R. Saha, Y. Aoki, and H. Sato, *Phys. Rev. B* **71**, 125127 (2005).
- [6] D. J. Braun and W. Jeitschko, *J. Solid State Chem.* **32**, 357 (1980).
- [7] D. J. Braun and W. Jeitschko, *J. Less Comm. Met.* **72**, 147 (1980).
- [8] Z. Fisk, P. C. Canfield, J. D. Thompson, and M. F. Hundley, *J. Alloys and Comp.* **181**, 369 (1992).
- [9] P. S. Riseborough, *Adv. Phys.* **49**, 257 (2000).
- [10] Z. Henkie, M. B. Maple, A. Pietraszko, R. Wawryk, T. Cichorek, R. E. Baumbach, W. M. Yuhasz, and P.-C. Ho, *J. Phys. Soc. Jpn. Suppl. A* **77**, 128.
- [11] G. M. Sheldrick, In Program for the Solution of Crystal Structures. University of Göttingen, Germany (1985).
- [12] G. M. Sheldrick, In Program for Crystal Structure Refinement. University of Göttingen, Germany (1987).
- [13] R. Wawryk and Z. Henkie, *Phil. Mag. B* **81**, 223 (2001).
- [14] C. Sekine, R. Abe, K. Takeda, K. Matsuhira, and M. Wakeshima, *Physica B* **403**, 856 (2007).
- [15] B. C. Sales, D. Mandrus, B. C. Chakoumakos, V. Keppens, and J. R. Thompson, *Phys. Rev. B* **56**, 15081 (1997).
- [16] B. C. Sales, B. C. Chakoumakos, D. Mandrus, J. W. Sharp, N. R. Dilley, and M. B. Maple, *Mater. Res. Soc. Symp. Proc.* **545**, 13 (1999).
- [17] I. Shirovani, K. Ohno, C. Sekine, T. Yagi, T. Kawakami, T. Nakanishi, H. Takahashi, J. Tang, A. Matsushita, and T. Matsumoto, *Physica B* **281**, 1021 (2000).

- [18] R. Wawryk, O. Zogal, A. Pietraszko, S. Paluch, T. Cichorek, W.M. Yuhasz, T. A. Sayles, P.-C. Ho, T. Yanagisawa, N. P. Butch, M. P. Maple, and Z. Henkie, *J. Alloys and Comp.* **451**, 454 (2008).
- [19] M. R. MacPherson, G. E. Everett, D. Wohlleben, and M B. Maple, *Phys. Rev. Lett.* **26**, 20 (1971).
- [20] M. B. Maple and D. Wohlleben, *AIP Conference Proceedings* **18**, 447 (1974).
- [21] A. Menth, E. Beuhler, and T. H. Geballe, *Phys. Rev. Lett.* **22**, 295 (1969).
- [22] M. B. Maple, L. E. DeLong, and B. C. Sales, in *Handbook on the Physics and Chemistry of Rare Earths Vol 1 - Metals*, eds K. A. Gschneider, Jr. and L. R. Wyring (North-Holland Publishing Company, Amsterdam, 1978), pp. 797-846.
- [23] A. Jayaraman, in *Handbook on the Physics and Chemistry of Rare Earths Volume 2 - Alloys and Intermetallics*, eds K. A. Gschneider, Jr. and L. R. Wyring (North-Holland Publishing Company, Amsterdam, 1979), pp. 575-611.
- [24] A. C. Hewson (1993) *The Kondo Problem to Heavy Fermions* (Cambridge University Press).
- [25] D. A. Gajewski, N. R. Dilley, E. D. Bauer, E. J. Freeman, R. Chau, M. B. Maple, D. Mandrus, B. C. Sales, and A. Lacerda, *J. Phys: Cond. Mat.* **10**, 6973 (1998).
- [26] N. F. Mott and W. D. Twose, *Adv. Phys.* **10**, 107 (1961).
- [27] R. Sollie and P. Schlottmann, *J. Appl. Phys.* **69**, 5478 (1991).
- [28] R. Sollie and P. Schlottmann, *J. Appl. Phys.* **70**, 5803 (1991).
- [29] P. Schlottmann, *Phys. Rev. B* **46**, 998 (1992).
- [30] M. B. Maple, C. L. Seaman, D. A. Gajewski, Y. Dalichouch, V. B. Barbetta, M. C. deAndrade, H. A. Mook, H. G. Lukefahr, O. O. Bernal, and D. E. MacLaughlin, *J. Low Temp. Phys.* **95**, 225 (1994).
- [31] M. B. Maple, M. C. de Andrade, J. Herrmann, Y. Dalichouch, D. A. Gajewski, C. L. Seaman, R. Chau, R. Movshovich, M. C. Aronson, and R. Osborn, *J. Low Temp. Phys* **99**, 224 (1995).
- [32] G. R. Stewart, *Rev. Mod. Phys.* **73**, 797 (2001).
- [33] M. F. Hundley, P. C. Canfield, J. D. Thompson, and Z. Fisk, *Phys. Rev. B* **42**, 6842 (1990).
- [34] P. Schlottmann, *Physica B* **186-188**, 375 (1993).
- [35] M. F. Hundley, P. C. Canfield, J. D. Thompson, and Z. Fisk, *Phys. Rev. B* **50**, 18142 (1994).

- [36] G. Busch and U. Winkler (1956) Bestimmung der Charakteristischen Grssen eines Halbleiters. Edited by Ergebnisse der Exakten Naturwissenschaften, Zürich.
- [37] Z. Henkie and P. J. Markowski, J. Phys. Chem. Solids **39**, 39 (1978).
- [38] M. Ocko, C. Gaibel, and F. Steglich, Phys. Rev. B **64**, 195107 (2001).
- [39] K. Behnia, D. Jaccard and J. Flouquet, J. Phys.: Condens. Matter **16**, 5187 (2004).

The text and data presented in this chapter are reprints of material that appears in “The filled skutterudite  $\text{CeOs}_4\text{As}_{12}$ : a hybridization gap semiconductor,” R. E. Baumbach, P.-C. Ho, T. A. Sayles, M. B. Maple, R. Wawryk, T. Cichorek, T. Pietraszko, and Z. Henkie, *Proc. Natl. Acad. Sci.* 105, 17307 (2008). The dissertation author is the primary investigator and author of this article.

# V

## A metal insulator transition in $\text{YbFe}_4\text{Sb}_{12}$ granular thin films

### V.A Introduction

The ternary filled skutterudite compounds  $\text{MT}_4\text{X}_{12}$  ( $\text{M}$  = alkali metal, alkaline earth, actinide, or rare earth,  $\text{T}$  = Fe, Ru, Os, and  $\text{X}$  = P, As, Sb) have attracted attention, in part, because they often show correlated electron behavior. The compound  $\text{YbFe}_4\text{Sb}_{12}$  is an interesting example because the Yb ions appear to have an intermediate valence [1, 2], the electronic specific heat coefficient (electron effective mass) is moderately large [1], and the electrical resistivity displays Kondo lattice coherence [1, 3, 4].

In general, the evolution of novel electronic states can also be driven by material granularity. A granular material is usually an artificial structure composed of a large number of granules with sizes ranging from the nanometer to the hundreds of nanometers scale. In particular, electronic states can be tuned as a function of limiting scales such as grain size or intergrain conductance. The physics of these systems is mediated by quantum effects, disorder, electronic and magnetic fluctuations, and electron confinement. In many instances, the granule sizes and the associated physical phenomena can be precisely controlled by sample growth

conditions [5, 6, 7]. As such, pulsed laser deposition provides an ideal method for the production of tunable granular materials.

In this study, results for  $\text{YbFe}_4\text{Sb}_{12}$  thin films grown by pulsed laser deposition are reported. Film thicknesses ( $t$ ) are varied from 6000 to 300 Å. Thick films ( $t > 1000$  Å) universally show electrical transport behavior similar to results for bulk polycrystal and single crystal specimens. Surprisingly, a metal to insulator transition for thin films ( $t < 1000$  Å) is observed. It is shown that the metal to insulator transition is correlated with film topology and from that result it is inferred that the intergrain connectivity mediates the metal to insulator transition. Besides being of fundamental interest, this observation may provide a new approach to engineering filled skutterudite materials for use in devices.

## V.B Experimental Details

A bulk target with stoichiometry 1 Yb : 4 Fe : 12.5 Sb was synthesized by sealing elemental Yb (4N), Fe (3N), and Sb (6N) in a quartz tube ( $14 \times 16$  mm) under 150 torr ultra high purity Ar and heating the material to 1050 °C. After annealing the material for 2 days, the tube was quenched in a centrifuge to prevent the formation of gas pockets and to force the melt to conform to the shape of the quartz tube. X-ray diffraction measurements indicate that the target consisted of multiple phase material with a uniform distribution of Yb, Fe, and Sb. Based on a previous study of  $\text{PrFe}_4\text{Sb}_{12}$  thin films grown by pulsed laser deposition, it was expected that single phase films would result from the mixed phase target [8].

Polycrystalline  $\text{YbFe}_4\text{Sb}_{12}$  films were synthesized by pulsed laser deposition using a Lambda Physik KrF laser with a wavelength of 248 nm. The details of the growth are nearly identical to those reported previously for  $\text{PrFe}_4\text{Sb}_{12}$  thin films grown by pulsed laser deposition with the exception that the films reported here were grown at  $T = 350$  °C, a laser energy density at the target near 4 J/cm<sup>2</sup>, and with a post-growth anneal at  $T = 435$  °C for five minutes. The growth rate

was found to be roughly  $r_g \sim 20 \text{ \AA/s}$ . Similar to  $\text{PrFe}_4\text{Sb}_{12}$ ,  $\text{YbFe}_4\text{Sb}_{12}$  films form on various substrates including c-plane yttria stabilized zirconia, c-plane magnesium oxide, and c-plane magnesium aluminate. In this study, only films grown on MgO substrates are discussed. The samples discussed in the text are summarized in Table V.1.

The films were characterized by x-ray diffraction, scanning electron microscopy, and electrical resistivity  $\rho(T)$ . X-ray diffraction measurements were performed using a Rigaku D-MAX diffractometer with applied Cu K- $\alpha$  radiation in a  $\theta$ - $2\theta$  configuration. Powdered Si was applied to each sample to measure the intrinsic goniometer  $2\theta$  offset. Scanning electron microscope measurements were performed using a typical apparatus. Electrical resistivity measurements were performed in a four-wire configuration in zero applied magnetic field using a Quantum Design Physical Properties Measurement System and a conventional  $^4\text{He}$  cryostat.

## V.C Results

X-ray diffraction data (Fig. V.1) show that polycrystalline films of  $\text{YbFe}_4\text{Sb}_{12}$  form under the reported growth conditions. Since the signal to noise ratio worsens as  $t$  decreases, the diffraction data are smoothed using Lorentzian and Gaussian fitting functions, both of which give comparable results. There are no observable impurity or amorphous components in the data. Moreover, there is no variation in the lattice constant ( $9.155 \pm 0.01 \text{ \AA}$ ) as a function of  $t$ .

Scanning electron microscope (SEM) images were collected to explore film morphology (Fig. V.2). It is assumed that dark spots are voids in the film and grey and white spots are filled. The images show that thick samples are nearly completely connected across the entire film surface ( $t > 1000 \text{ \AA}$ ). In contrast, thin samples that were grown under similar conditions have a continuum of topologies ranging from almost complete surface filling to the inclusion of large surface voids as for samples “a” - “h”. This result suggests that, during sample growth, the

lower levels of the film are strongly influenced by small variations in the growth conditions. The variations do not influence thick films because with increased growth time, topological variations are averaged out. To quantify the topological variation, the ratio of the empty space surface area to the total surface area ( $V/A$ ) is defined.  $V/A$  is a rough quantity since it treats a complicated three dimensional surface in two dimensions. Regardless, it provides a reasonable method for comparing samples if a consistent definition is used. The dark spots were traced by hand and the software package ImageJ [9] was used to measure their surface area. The results of this analysis are summarized in Table V.1.

Electrical resistivity data are presented in Fig. V.3 where  $\rho(T)$  smoothly evolves from insulating to metallic behavior for samples “a” - “h”. When  $\rho(T)$  is considered with  $V/A$ , it is evident that the metal to insulator transition is correlated with  $V/A$ . This trend is emphasized in the Fig. V.3 inset where residual resistivity at 3 K is shown to increase logarithmically with  $V/A$ . Based on this observation, the data are organized into three categories : metallic (samples “f” - “h”), weakly insulating (samples “e” - “c”), and strongly insulating (samples “b” and “a”).

For the metallic samples,  $\rho(T)$  decreases monotonically with decreasing temperature, exhibits a pronounced downturn near 70 K, and becomes constant at lowest temperatures. As the void density increases to  $V/A \sim 0.05$ ,  $\rho(T)$  decreases with temperature weakly compared to bulk-like samples, shows the expected downturn near 70 K, and exhibits an upturn at lowest temperatures. Samples that show this behavior are intermediate between the metallic and weakly insulating states. When the void density is greater than  $V/A \sim 0.05$  the electrical resistivity data increase slowly with decreasing temperature, show the expected shoulder near 70 K, and continue to increase to the lowest temperatures. The strength of the weakly insulating state increases with increasing  $V/A$  until a transition is made into the strongly insulating state for  $V/A > 0.09$ . The qualitative temperature dependence of  $\rho(T)$  for the strongly insulating samples is similar to weakly insulating samples

except that the resistivity is much higher. It is also interesting to note that the knee at 70 K is preserved in all samples, supporting the notion that the metal to insulator transition is driven by topological rather than chemical changes such as Yb depletion or a change in the Yb valence.

To address the possibility that oxidation causes the insulating behavior,  $\rho(T)$  measurements were performed on a thin sample that was carefully isolated from exposure to atmosphere before measurement. The sample was exposed to air for no more than ten seconds while being transferred into the  $^4\text{He}$  bath for  $\rho(T)$  measurements. The electrical resistivity data for this sample are comparable to results for weakly insulating samples that were exposed to air for an extended period of time before measurement. While this procedure may have reduced the affect of oxidation, it remains uncertain whether oxidation plays a role in the metal to insulator transition. In addition, it should be noted that Yb depletion, the formation of secondary binary phases, or a Yb valence transition could, in principle, be responsible for the metal to insulator transition. However, x-ray diffraction measurements indicate that all samples have the same crystal structure. Moreover, the shoulder in the electrical resistivity data is preserved for all samples. This result strongly indicates that the  $\text{YbFe}_4\text{Sb}_{12}$  stoichiometry and structure are preserved and that all variations away from bulk behavior are driven by granularity.

## V.D Analysis

(i) Metallic state : The electrical resistivity for films with small  $V/A$  is in good agreement with results for bulk polycrystal and single crystal specimens. It should be noted that the residual resistivity for metallic thin film specimens is greater than the residual resistivity for bulk specimens. This result indicates that the metallic films are more disordered than bulk specimens. Detailed discussions of the metallic state are given elsewhere [1, 2, 3, 4].

(ii) Weakly and strongly insulating states : To gain a detailed under-

standing of the insulating states, the quantity  $W(T)$  is defined (Eqn. V.1) and calculated for samples “a” - “e” (Fig. V.4).  $W(T)$  is constant up to near 10 K for the weakly insulating samples. In contrast,  $W(T)$  increases with decreasing temperature for the strongly insulating samples at temperatures below 10 K.

$$W(T) = -\frac{\partial \ln \rho(T)}{\partial \ln T} = -T \frac{\partial \ln \rho(T)}{\partial T} \quad (\text{V.1})$$

Since  $W(T)$  is constant at low temperatures for the weakly insulating samples, it can be inferred that their  $\rho(T)$  data follow a weak power law function where  $W(T) = \beta$  (Eqns. V.2a, V.2b). Furthermore, the data show that the strength of the power law divergence increases with  $V/A$  (Table V.1).

$$\rho(T) = AT^{-\beta} \quad (\text{V.2a})$$

$$W(T) = \beta \quad (\text{V.2b})$$

In contrast, samples “a” and “b” are best described by the well known “stretched” exponential function seen in a variety of semiconductor and granular systems (Eqn. V.3a). As shown in Eqns. V.3b and V.3c, the behavior of such a system is quantified by plotting  $\ln W$  vs  $\ln T$  where a linear function with slope  $x$  is expected to result. It is also possible to extract a characteristic temperature  $T_1$  from such plots. The fit results are summarized in Table V.1.

$$\rho(T) = \rho_0 \exp\left[\frac{T_1}{T}\right]^x \quad (\text{V.3a})$$

$$W = x \left(\frac{T_1}{T}\right)^x \quad (\text{V.3b})$$

$$\ln W = \ln x + x \ln T_1 - x \ln T \quad (\text{V.3c})$$

A similar strategy is adopted to address  $\rho(T)$  data for samples “a” - “e” at temperatures above 100 K. On this temperature range,  $\rho(T)$  data conform

to the Arrhenius equation (Eqn. V.3a,  $x = 1$ ). To distinguish between the low temperature “stretched” exponential and the high temperature pure exponential behavior,  $T_1$  is renamed  $T_\Delta$  for fits in the high temperature region. The fits show that  $T_\Delta$  is roughly constant at a value of 85 K for the weakly insulating samples and increases to a constant value near 133 K for strongly insulating samples (Table V.1).

## V.E Discussion

The metal to insulator transition in granular media is fundamentally driven by the strength of electrical conductance between granules. Recent theoretical advances have been made that expand on the seminal work by Mott and Anderson [10, 11, 12] to describe the evolution in a granular system from a metallic state to an insulating state. To summarize, it is expected that a granular system will evolve from the metallic state to a weakly insulating state where  $\rho(T) \sim \ln T$  or  $T^{-\beta}$  and then to a strongly insulating state where  $\rho(T) \sim \exp[T_0/T]^x$  as intergrain conductance decreases. The theoretical advances are supported by a variety of experimental systems including such varied materials as the polymer poly(p-phenylenevinylene) [13] and the superconducting Al-Ge amorphous granular matrix [14].

The weakly insulating state occurs in the case of weak electron confinement where both electron-electron interactions and quantum interference can increase the electrical resistivity at low temperatures. According to Efetov and Tschersich [15, 16], a logarithmic correction to the classical conductivity due to electron-electron interactions is uniquely expected for granular metals. A similar prediction was made by Larkin and Khmel'nitskii [17], where weak power law behavior is expected. The key feature in these models is that when electrons are localized due to granularity, screening is inhibited and electron-electron interactions are enhanced. A logarithmic correction to the conductivity is also predicted

by Beloborodov et al. [5] as the result of quantum interference between electrons scattering from the grain surface. For the case of the strongly insulating state, the electrical resistivity is dominated by the weak tunneling conductivity between grains. At low temperatures, electron tunnelling occurs over distances that far exceed the average granule size. This process occurs as the result of tunnelling through virtual electron levels in long series of grains and is relevant only as long as the hopping length  $\zeta$  exceeds the average granule size. This effect appears in  $\rho(T)$  as the “stretched” exponential function [5].

It is interesting to note that while the theory of Efros and Shklovskii [18] predicts  $x = 0.5$  and Mott predicts  $x = 0.25$  [12], fits to the data presented here for samples “a” and “b” yield intermediate values. A similar result was reported in the case of polymer poly(p-phenylenevinylene) where  $x$  increases towards 0.5 with increasing disorder [10]. By analogy it may be reasonable to expect that  $x$  for  $\text{YbFe}_4\text{Sb}_{12}$  could be increased to 0.5 with increased disorder.

It is also expected that  $\zeta$  will decrease with increasing temperature. When  $\zeta$  is similar to the average grain size, conduction electrons tunnel only to the nearest granules. Thus, a decaying exponential (Eqn. V.3a :  $x = 1$ ) is expected where the gap defines the Coulomb repulsion energy [5]. As discussed above, the high temperature electrical resistivity data for samples “a”-“e” are fit well by such a curve.

## V.F Summary

The data reported here can be interpreted in the context of theories for granular metals. As  $V/A$  grows, electrons become more localized and large corrections due to electron-electron interactions or quantum interference effects enhance the low temperature resistivity. When  $V/A$  exceeds a critical value, all conductivity occurs as the result of long range hopping. The results of this experiment are not only of fundamental interest but may also indicate a new direction for engi-

neering functional filled skutterudite devices. Since it has been shown here that the electronic state of  $\text{YbFe}_4\text{Sb}_{12}$  can be tuned by granularity, it is expected that similar tunability will be observed in other thin film filled skutterudites produced by pulsed laser deposition.

Table V.1: Summary of results.  $V/A$  is the void surface area to total surface area ratio calculated from SEM images as defined above,  $t$  ( $\text{\AA}$ ) is the film thickness,  $A$  is the coefficient for the power law fit Eqn. V.2a where the error is  $\sim 0.01A$ ,  $\beta$  is the power law exponent described in Eqn. V.2a where the error is  $\sim 0.005$ ,  $\rho_0$  is the coefficient for the stretched exponential fit Eqn. V.3a where the error is  $\sim 0.25\rho_0$ ,  $x$  is the power of the stretched exponential as described in Eqn. V.3a where the error is  $\sim 0.05$ ,  $T_1$  is the fit parameter described in Eqn. V.3a where the error is  $\sim 10$  K, and  $T_\Delta$  is the gap size as defined in Eqn. V.3a when  $x = 1$  with error  $\sim 5$  K.

sample	$V/A$	$t$ ( $\text{\AA}$ )	$A$ ( $\mu\Omega cm K^{-\beta}$ )	$\beta$	$\rho_0$ ( $\mu\Omega cm$ )	$x$	$T_1$ (K)	$T_\Delta$ (K)
a	0.18	800	NA	NA	30400	0.40	40	136
b	0.12	600	NA	NA	3850	0.27	30	129
c	0.09	600	8310	0.175	NA	NA	NA	80
d	0.08	300	4580	0.120	NA	NA	NA	96
e	0.07	300	2240	0.075	NA	NA	NA	79
f	0.05	300	NA	NA	NA	NA	NA	NA
g	0.05	500	NA	NA	NA	NA	NA	NA
h	0.00	600	NA	NA	NA	NA	NA	NA

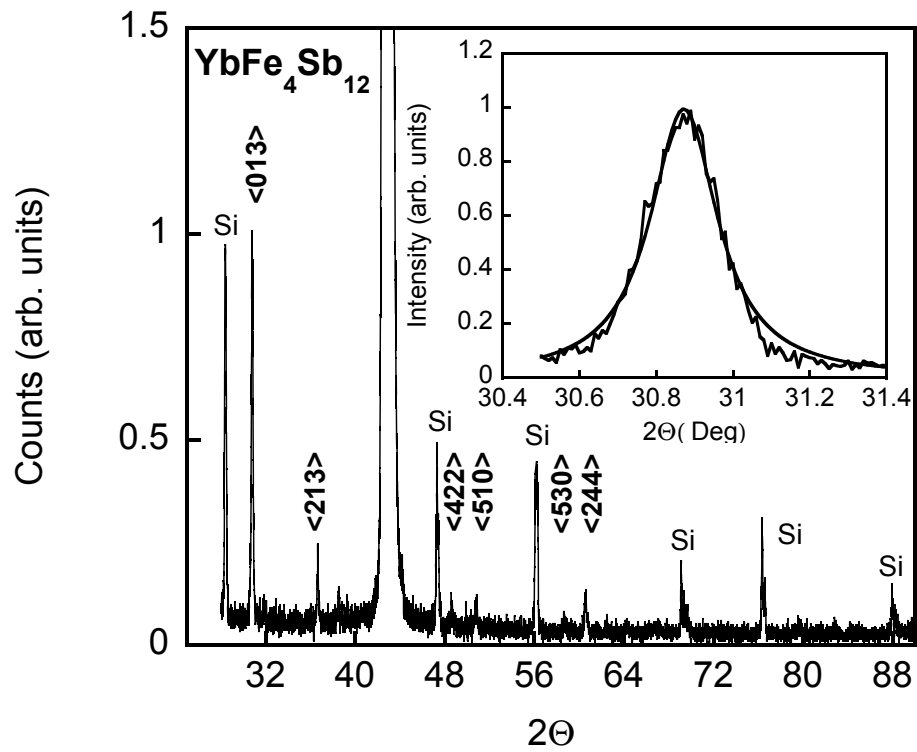


Figure V.1: X-ray diffraction data for a  $\text{YbFe}_4\text{Sb}_{12}$  film ( $t = 6000 \text{ \AA}$ ) grown on an MgO substrate. Filled skutterudite peaks are apparent and show the film is polycrystalline. The inset displays the main peak width at half maximum.

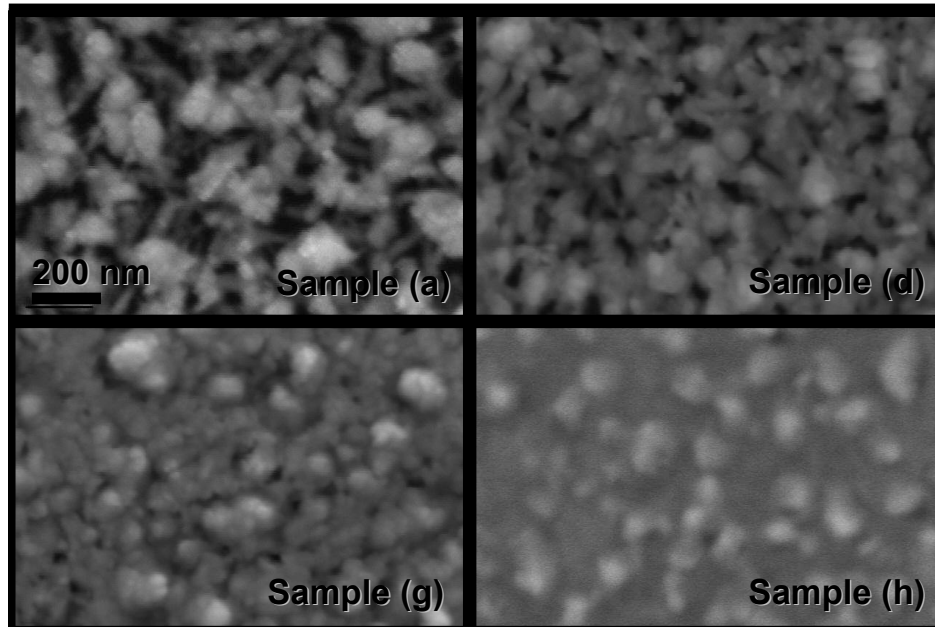


Figure V.2: SEM images for samples “a”, “d”, “g”, and “h”, show some of the different topologies found for thin film specimens of  $\text{YbFe}_4\text{Sb}_{12}$ . It is assumed that dark spots are voids in the film and grey and white spots are filled. To quantify the topological variation, the ratio of the empty space surface area to the total surface area ( $V/A$ ) is defined. The dark spots were traced by hand and the software package ImageJ [9] was used to measure their surface area. The results, summarized in Table I, show that  $V/A$  decreases systematically for samples “a”-“h”.

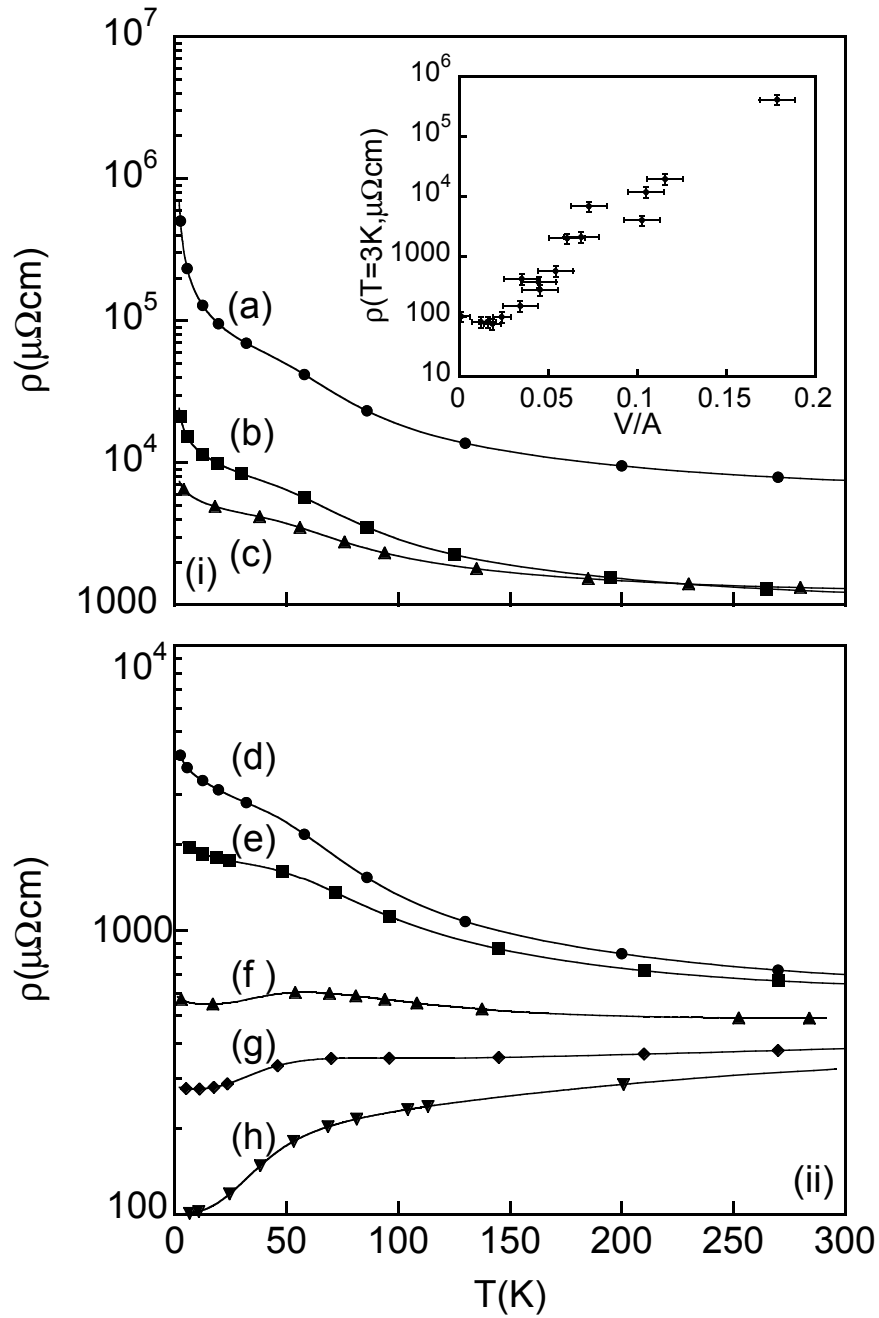


Figure V.3: (i,ii) Electrical resistivity vs temperature for samples “a” - “h” illustrating the smooth evolution from the insulating to metallic state. (inset) Residual resistivity at  $T = 3$  K vs void density ( $V/A$ ) for various samples. The correlation between the electronic state and  $V/A$  is evident as residual resistivity increases logarithmically with  $V/A$ .

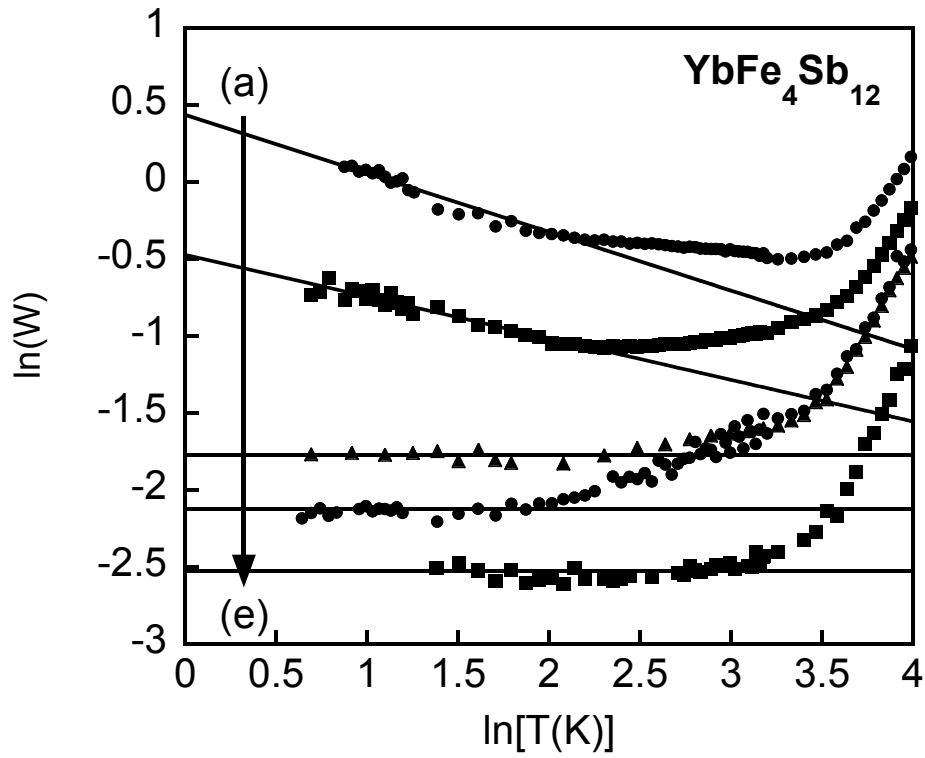


Figure V.4: Linear fits to  $\ln W$  vs  $\ln T$  at low temperatures for samples “a” - “e” show that samples “a” and “b” conform to a stretched exponential function (Eqn. V.3a) while samples “c” - “e” are described by a power law function (Eqn. V.2a).

## Bibliography

- [1] N. R. Dilley, E. J. Freeman, E. D. Bauer, and M. B. Maple, *Phys. Rev. B* **58**, 6287 (1998).
- [2] A. Leithe-Jasper, D. Kaczorowski, P. Rogl, J. Bogner, M. Reissner, W. Steiner, G. Wiesinger, and C Godart, *Solid State Commun.* **109**, 395 (1999).
- [3] E. D. Bauer, R. Chau, N. R. Dilley, M. B. Maple, D. Mandrus, and B. C. Sales, *J. Phys.: Condens. Matter* **12**, 1261 (2000).
- [4] S. V. Dordevic, D. N. Basov, N. R. Dilley, E. D. Bauer, and M. B. Maple, *Phys. Rev. Lett.* **86**, 684 (2001).
- [5] I. S. Beloborodov, A. V. Lopatin, V. M. Vinokur, and K. B. Efetov, *Rev. Mod. Phys.* **79**, 469 (2007).
- [6] D. Belitz and T. R. Kirkpatrick, *Rev. Mod. Phys.* **66**, 261 (1994).
- [7] P. A. Lee, and T. V. Ramakrishnan, *Rev. Mod. Phys.* **57**, 287 (1985).
- [8] R. E. Baumbach, W. M. Yuhasz, and M. B. Maple, *Appl. Phys. A: Mater. Sci. Process.* **84**, 227 (2006).
- [9] W. S. Rasband, ImageJ, U. S. National Institutes of Health, Bethesda, Maryland, USA, <http://rsb.info.nih.gov/ij/>, 1997-2006.
- [10] N. F. Mott, *Rev. Mod. Phys* **40**, 688 (1968).
- [11] P. W. Anderson, *Phys. Rev.* **109**, 1492 (1958).
- [12] N. S. Mott and E. A. Davis, *Electronic Processes in Noncrystalline Materials*, Clarendon Oxford, (1979).
- [13] M. Ahlskog, R. Menon, A. J. Heeger, T. Noguchi, and T. Ohnishi, *Phys. Rev. B* **55**, 6777 (1997).
- [14] A. Gerber, A. Milner, G. Deutscher, M. Karpovsky, and A. Gladkikh, *Phys. Rev. Lett.* **78**, 4277 (1997).
- [15] K. B. Efetov and A. Tscherisich, *Europhys. Lett.* **59**, 114 (2002).
- [16] K. B. Efetov and A. Tscherisich, *Phys. Rev. B* **67**, 174205 (2003).
- [17] A. I. Larkin and D. E. Khmel'nitskii, *Sov. Phys. JETP* **56**, 647 (1982).
- [18] A. L. Efros and B. I. Shklovskii, *J. Phys. C* **L49** (1975).

The text and data presented in this chapter are reprints of material that appears in “A metal insulator transition in  $\text{YbFe}_4\text{Sb}_{12}$  thin films,” R. E. Baumbach, W. M. Yuhasz, and M. B. Maple, *Thin Solid Films* 516, 3378 (2008). The dissertation author is the primary investigator and author of this article.